NTNU

Norwegian University of
Science and Technology

Identification of EEG-based signature produced by visual exposure to the primary colors RGB

Lars-Erik Notevarp Bjørge

Trond Hübertz Emaus

Master of Science in Cybernetics and Robotics

Submission date: July 2017

Supervisor: Marta Maria Cabrera Molinas, ITK

Co-supervisor: Geir Kulia, ITK

Norwegian University of Science and Technology

Department of Engineering Cybernetics

Preface

This is a Master Thesis carried out during the spring semester of 2017 in cooperation with the Department of Engineering Cybernetics at Norwegian University of Science and Technology as a part of the study program Cybernetics and Robotics. The idea of the project was brought up by our supervisor Professor Marta Molinas. This thesis assumes that the reader has some background in mathematics and a bit understanding of signal analysis.

Trondheim, 4/7-17

Lars-Erik Notevarp Bjørge Trond Hübertz Emaus

Acknowledgment

First, we would like to thank Marta Molinas for being an outstanding supervisor, and for providing us with support and advices whenever needed. She has been a great mentor, and always pointing us in the right direction. We would like to acknowledge the contributions and give thanks to Signal Analysis Lab for providing us with algorithms which we utilized for data analysis in this master thesis. A big thanks to all of the test subjects for taking the time and participating in the experiments. Last we would like to thank our friends and family for the support they have given along the way.

Lars-Erik Notevarp Bjørge & Trond Hübertz Emaus

Abstract

In this thesis we have presented results for experiments regarding identification of electroencephalograph (EEG) signatures, produced by the visual exposure of primary colors i.e. red, green and blue (RGB) to the subject. The experiments are conducted with an open-source Brain-Computer Interface (BCI) called OpenBCI with the help of 10 healthy participants doing 2 types of experiments, short pulse exposure and steady-state exposure. The reason for the study is to see if there are any clear brain-wave patterns in the EEG data by looking at characteristics between the different colors and individuals.

Regarding data analysis, a well-known signal analysis technique called Hilbert-Huang Transform (HHT) has been applied to the EEG data. The algorithm uses Empirical Mode Decomposition (EMD) to break the signal into meaningful Intrinsic Mode Functions (IMFs). By executing Hilbert Transform (HT) on the IMFs, instantaneous frequency and amplitude is obtained. These instantaneous frequencies are examined by using Hilbert Spectral Analysis (HSA), to get a qualitative visual representation of the data. As for the steady-state experiment, Fourier transform has been applied to acquire spatial information.

A significant difference was found between exposure to the different colors. Exposure to the color blue seems elicit a considerably narrower frequency band with a larger amplitude than that of the color red and green. Moreover, the frequency response for color green showed a frequency shift towards higher frequency compared to that of the red and blue color. The individual differences were quite significant, and it seems that the brain responses varies a lot across all of the subjects. From these results, we can conclude that OpenBCI is well-suited for recording complex EEG data, and may be utilized for several applications without the need of more expensive equipment for recording EEG data.

Sammendrag

I denne masteroppgaven blir det presentert resultater fra eksperimenter som omhandler identifikasjon av EEG-signaturer, produsert av visuell eksponering av primærfargene rød, grønn og blå. Eksperimentene er utført med en Brain-Computer Interface (BCI) kalt OpenBCI med hjelp av 10 friske deltakere som utførte to typer eksperiment, kort puls eksponering og langvarig stasjonær eksponering. Bakgrunnen for denne studien er å se om det finnes et klar hjernebølge mønster i EEG-data ved å se på forskjeller mellom farger og individer.

Dataanalysen ble utført ved å bruke en velkjent metode for signalanalyse, kalt Hilbert-Huang Transform (HHT). Algoritmen bruker Empirical Mode Decomposition (EMD) til å splitte signalet opp og ekstrahere Instrinsic Mode Functions (IMFs). Ved å kjøre Hilbert Transform (HT) på IMFene, får man momentan frekvens og amplitude. Momentanverdiene blir deretter analysert nærmere ved å bruke Hilbert Spectral Analysis (HSA), for å få en kvalitativ visuell representasjon av dataen. Til eksperimentet vedrørende langvarig eksponering ble det brukt Fourier transform for å tilegne informasjon fra frekvensspekteret.

En signifikant forskjell ble funnet mellom eksponering til de forskjellige fargene. Eksponering til blåfarge ser ut til å gi smale responser i frekvensspekteret med høyere amplitude enn fra rød- og grønnfarge. Videre ser vi at frekvensresponsene fra grønnfargen har høyere frekvens enn det fra blå- og rødfargen. Individuelle forskjeller var store, og det ser ut til at hjernebølge responsen varierer over alle deltakerene. Fra disse resultatene kan vi konkludere med at OpenBCI er velegnet for opptak av kompleks EEG-data, og kan bli brukt til andre applikasjoner uten å nødvendigvis ha behov for medisinsk utstyr.

Contents

Chapter 1

Introduction

Electroencephalogram (EEG) has been used to record electrical activity of the brain for almost a century, and it remains the most effective non-invasive method to acquire brain signals and is superior when it comes to temporal resolution. Traditionally, measuring EEG required equipment that was expensive, and often only expedient in medical applications, but recent technological breakthroughs has made it possible to make EEG equipment a lot cheaper and more convenient in terms of mobility and size. Over the past decade, there has been a dramatic increase in utilizing BCIs for tasks related to EEG measurement. They have emerged as powerful platforms for brain-signal analysis, and is now accessible to a broader audience, as the price has dropped remarkably the last couple of years. Access to information from the human brain is now simple compared to prior equipment.

The main source of information that is interpreted by humans is from visual information, and most of this information is perceived by distinguishing between a range of colors. Visual stimulus produces more efficient BCI systems due to a higher information transfer rate. According to a recent study [1] from MIT, visual images can be identified after just being seen for 13 milliseconds. The visual system is precisely adapted to extracting conceptual information that is received by visual input, which is done with help of the ability to rapidly recognize different colors. Colors is such a vital part of the visual system, and therefore we have chosen color perception as our main area of investigation in this thesis.

In this paper, we have performed experiments and presented the results regarding identification of brain-wave patterns recorded from the scalp, produced by visual exposure of

the primary colors, red, green and blue (RGB) by using the low-cost open-source EEG platform called OpenBCI. A previous study [2], have classified EEG signals as red, green and blue classes from experiments with random visual exposure of the distinct RGB components, and got satisfactory results. Our experiments will be of a similar manner, only with more diverse experiments, such as distinguishing between pulsation of light and a steady-state light source and randomizing the interval timing. Our objective is to see if there are any clear patterns of brain activity that arises from the primary visual cortex, or more generally from the occipital lobe, at the back of the human scalp, when the subject is exposed to visual stimuli.

Problem description

In this thesis we are investigating if visual exposure of primary colors i.e. red, green and blue, will produce any distinct brain-wave patterns or unique EEG signatures. We are also examining if there is any clear frequency difference between visual exposure of each of the distinct RGB colors, as well as any brain pattern differences between subjects. This study is of interest to gain more insight into how the brain reacts to different visual stimuli, and how different subjects responds to the visual stimuli, and at what level visual exposure to light acts as an alert for the conscious mind. The reason for this thesis is also to see if OpenBCI is well-suited for recording complex EEG data, despite the fact that the equipment is not of medical grade.

1.1 Research questions

The following research questions will be investigated throughout this thesis:

RQ1: *Does the visual exposure to each of the distinct light components of the primary colors of RGB produce different brain-wave patterns for each of colors?*

RQ2: *Does the visual exposure to each of the distinct light components of the primary colors of RGB produce different brain-wave patterns for each of individuals?*

Literature Survey

In this literature survey, a annotated bibliography will be presented along with a short summary and conclusion of state-of-the-art research that is of high relevance to our research. For each of the entries, we will provide some information about the research, and evaluate it with respect to the relevance to this thesis.

[3] Worren, F., et al. (2016). A Unified Real-Time Feature Extraction and Classification Process for a BCI Based on Empirical Mode Decomposition and Support Vector Machine, NTNU.

The thesis has served as the main source of research regarding the methods that was utilized in this thesis. The authors of this thesis have studied and implemented a data-driven process combining EEG feature extraction based on Empirical Mode Decomposition (EMD) and classification using a support vector machine (SVM). For the experimental setup, they have used a medical grade 256-electrode EEG geodesic sensor net for measuring, compared to our thesis where we have utilized a cheap open-source EEG for the same purpose. They were able to detect and classify left and right hand movements through the use of normalized Hilbert transformation, and acquired a impressive classification accuracy of up to 95% from multiple subjects. In this thesis we are also utilizing HHT, along with EMD for extraction of Intrinsic Mode Functions (IMFs) and HS for visualization purposes.

[2] S. Rasheed and D. Marini, "Classification of EEG signals produced by RGB colour stimuli," Journal of Biomedical Engineering and Medical Imaging, vol. 2, no. 5, p. 56, 2015

In this paper, an investigation was presented regarding the classification of EEG signals produced by random visual exposure of primary colors RGB. Seven healthy subjects participated in the experiment. Each of the colors was randomly presented for three seconds. They were successful in classifying the colors by using Support Vector Machine (SVM) as classifier and Event-Related Spectral Perturbations (ERSP) as features. As this paper is regarding similar studies as to what we have been conducting, it serves as a good basis regarding the experimental setup and what results we expect to achieve with our thesis.

[4] M. Münch, G. Plomp, E. Thunell, A. Kawasaki, J. Scartezzini, and M. Herzog, "Different colors of light lead to different adaptation and activation as determined by high-density EEG," NeuroImage, vol. 101, pp. 547 – 554, 2014.

This research is regarding the investigation of how the light adaptation of different colors affects brain signals and responses. Sixteen healthy people participated in the study. The study consisted of test with exposure of four colors of light in a randomized-within-subject design. The EEG signals were analyzed by using ERP and Global Field Power (GFP), where GFP is the standard deviation of ERPs at a given time. The study shows that the strongest light adaptation effects was the response to red light, followed by blue then green. We expect to see similar results in our study when distinguishing between the three RGB colors in the experiments we are conducting.

1.2 Limitations

One limitation regarding EEG recording is the low resolution of the spatial and temporal information. The fact that the experiments are conducted with 8 electrodes, will provide less accuracy, and thus risk losing important details regarding brain-wave patterns.

Another limitation lies in the fact that during the experiments, the human subject may make voluntary or involuntary movements. These movements may elicit myoelectrical signals, which will create unwanted brain artifacts and/or disturb the raw EEG data. Movements like this may include the fact that the subject has to blink from time to time, or that the subject is making small muscular movements, such as moving body parts. Another disturbance is the heart rate pulse, which will disturb the EEG signal if the electrode is placed in specific locations on the scalp.

Moreover, a limitation concerning data transfer is that the EEG data is transferred between the OpenBCI board and the computer via Bluetooth, and may be slightly unstable in some environments. Moreover, in terms of physical limitations, we were not able to do our experiments in a neutral environment. The fact that the experiments were done in a room with ambient sound and power grid noise (due to capacitance between power grid and ground), will decrease SNR, and thus may affect the results.

1.3 Approach

The occipital lobe is the rearmost lobe of the brain, situated at the back of the human scalp. One of the main objective of the occipital lobe is to translate visual information. Our approach is therefore to focus on recording EEG data close to the primary visual cortex, which lies in the occipital region. A more detailed explanation about the primary visual cortex is provided in Section 2.3.

For analyzation purposes, Empirical Mode Decomposition (EMD) is utilized to extract meaningful spatial and temporal information. This method provide good qualitative information, that is easily interpretable and are superior when it comes to analyzing EEG data. In a recent study, [5], a comparison between different signal analysis methods has been introduced, which included EMD. The result of this comparison show that EMD outperforms the other methods in the study, and especially when the SNR is high. In light of this, EMD will be our main approach in terms of signal analysis. Details regarding these methods are presented in Section 2.9.

As for the experiments, they are conducted with neutral conditions in a completely dark room. The experiments are replicated with 10 different subjects, to underpin its reproducibility. The complexity of the EEG signal is also something that has to be taken into consideration when choosing the approach. Because of this, averaging techniques has been applied to enhance these important potentials and neglect baseline noise.

The approaches mentioned here will ensure that the results are more precise and accurate, and overall provide more validity to the experiments.

1.4 Structure of the Report

This thesis is organized into 5 Chapters. First, an overview of the main background theory is presented in Chapter 2, along with theory related to the various methods. Next, in Chapter 3, details regarding the experimental paradigm is mapped out, as well as providing a detailed description regarding the data analysis methods that was utilized in the thesis. In Chapter 4, the results of our research is presented and then finally Chapter 5, which contains a conclusion of our results, a discussion about the implications of our

findings and last a section with suggestions for future research. Additional appendices are attached with qualitative plots and diagrams for each subject to support the results.

Chapter 2

Background literature

The objective of the following chapter is to provide the reader with background theory and relevant literature that treat similar problems as to what this thesis is studying. The chapter starts by introducing EEG, some anatomy of the brain, and then continues on with explaining about BCI. At last the theory related to the various approaches are presented.

2.1 Electroencephalogram

The average human brain has about 100 billion neurons. Each of these neurons can produce time-dependent electric fields that are measurable via electrodes placed on the human scalp, as illustrated in Figure 2.1. Each electrode measure a sum of potentials from between approximately 100 million and 1 billions neurons, according to [6]. The signals that are picked up by these electrodes are called electroencephalogram, or EEG for short. The history of EEG can be traced back to the German professor of psychiatry, Hans Berger. His dedication to the subject was driven by one belief, that with EEG he would be able to discern some well defined and measurable physical properties which represented true expressions of mental processes. In 1929, he published his first paper on the human electroencephalogram [8]. The publication had little impact on the scientific world at the time, but is recognized as the paper that initiated the new era of neurophysiology. He used an electroencephalograph, which is an instrument with the purpose of measuring and recording rhythmic changes in the electric impulses of the brain, more commonly known as brain-wave patterns. This was done by measuring electrical activity of the human brain by placing electrodes on the surface of the scalp and then amplifying the signal. Today

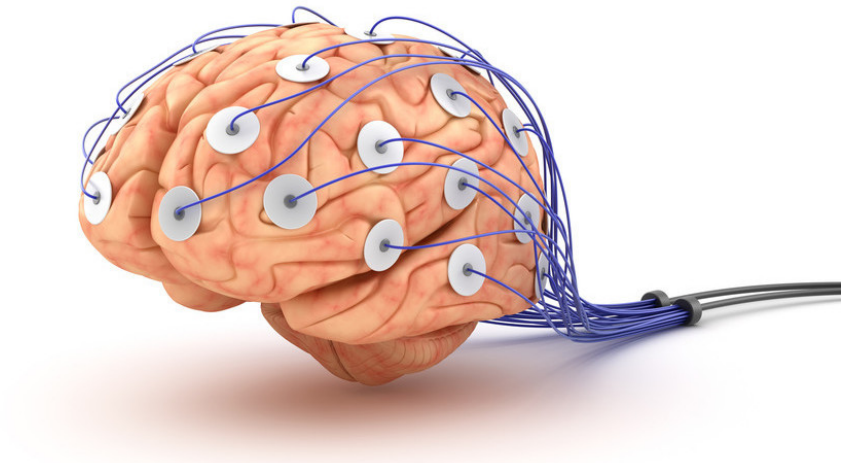

Figure 2.1: Illustration of EEG recording [7]

EEG is a widely used method in the field of neurophysiology, with applications such as diagnose of epilepsy [9]. In the field of neurophysiology, EEG is a commonly used method to study the functions of the brain. Moreover, the number of electrodes in BCI applications range from as few as 8 for simple applications, to Geodesic Sensor Nets (GSN) with as many as 256 electrodes for more complex and accurate applications.

2.2 Anatomy of the brain

The largest part of the human brain is the cerebrum, or the cerebral cortex, and is associated with higher brain functions such as action and thought. The cerebrum is divided into four so called "lobes". The frontal lobe is associated with personality, emotions, concentration, planning, reasoning, voluntary movement and problem solving. The parietal lobe is associated with orientation, proprioception, recognition and perception of stimuli. The occipital lobe takes care of the visual processing and the temporal lobe is associated with perception and recognition of auditory stimuli, speech and memory. The visual system will be the main focus area for this thesis, and the occipital lobe, marked in red in Figure 2.2, will therefore provide us with the best source of information.

2.3 Visual Cortex

The visual cortex of the brain is a part of the cerebral cortex that plays an important role in processing visual information. It is located in the occipital lobe on the back of the

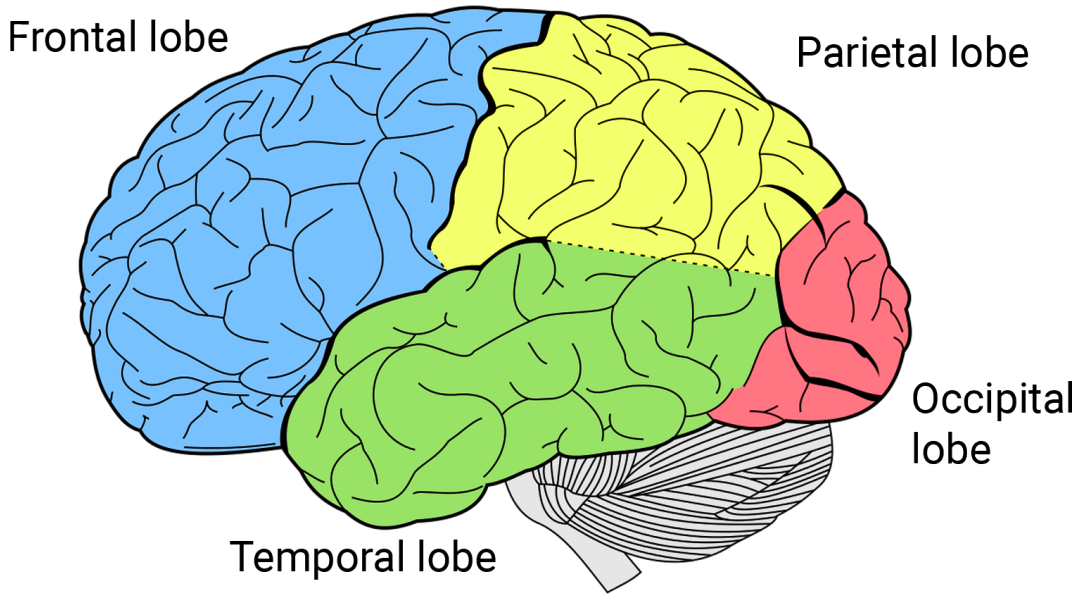

Figure 2.2: Particular sections of the cerebral cortex [10]

skull. The objective of this thesis' experiments are regarding perception of RGB colors, and the main focus area is then where visual processing of colors takes place. The most important area in the brain regarding visual processing lies close to the calcarine sulcus (the fissure that divides the visual cortex in twain), and is a region named the primary visual cortex (V1), also referred to as the striate cortex. In this region, the neurons are responding to color, direction of movement, contour and depth. This is also where the simple three-color segregation begins to break down. This region is illustrated as V1 (bright yellow area) in Figure 2.3. The primary visual cortex is a structure that is essential to the conscious processing of visual stimuli.

2.4 Frequency bands of the brain

The term "neural oscillations" refers to the periodical electrical activity that is spontaneously generated as a response to stimuli in the central nervous system (CNS). EEG reveals these brain rhythms in specific frequency bands. The discovery of these frequency bands is generally credited to Hans Berger, and among the first brain waves he discovered, was the *Alpha wave*, which is also called the *Berger's rhythm*, in memory of the founder. According to [12], these frequency bands are well known and have been observed to its

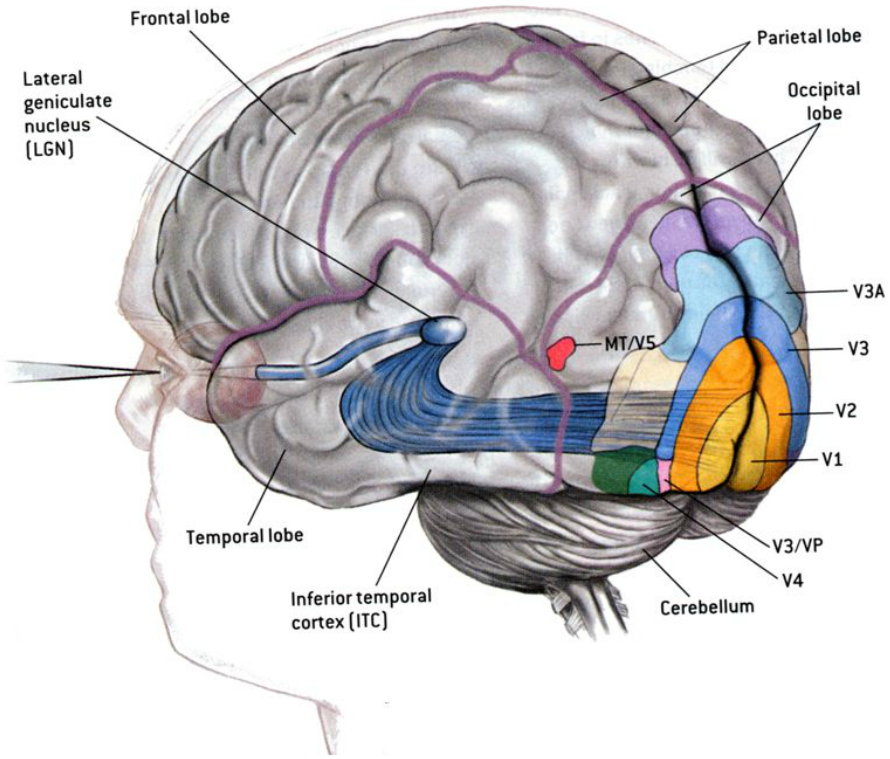

Figure 2.3: Particular sections of the visual cortex [11]

distribution over the human scalp and its biological significance. These frequency bands are referred to as delta (δ), theta (θ), alpha (α), beta (β), and gamma (γ) from low to high frequency, respectively. The different frequency bands are also specified with its corresponding frequencies in Table 2.1.

Brain rhythm	Symbol	Frequency
Delta wave	δ	0.5-4 Hz
Theta wave	θ	4-8 Hz
Alpha wave	α	8-12 Hz
Beta wave	β	12-30 Hz
Gamma wave	γ	>30 Hz

Table 2.1: Frequency bands of the brain

State-of-the-art characteristics regarding each of the specific brain frequency bands and their corresponding mental states are presented by [13], and is given as a brief summary below.

Delta waves: The Delta waves refers to the mental state of being asleep. During this state, the brain produces very slow Delta waves with high amplitude. These frequencies may

be confused with artifact signals, which are caused by contraction of the large muscles of the body.

Theta waves: The Theta waves refers to being in a drowsy state, and is one of the more elusive and extraordinary mental states. A large amount of these frequencies can be seen in younger and older children, and in adults that are about to fall asleep or is in a meditative or sleep state. According to [14], the Theta waves are also associated with meditative concentration.

Alpha waves: The Alpha waves predominantly originate from the occipital lobe during relaxation, and refers to being in a pleasurable state of consciousness, which is important in stress reduction and high levels of creativity. As stated in [15], the amplitude of the alpha wave increases when the eyes are closed and then attenuate when the eyes are open. These brain rhythms primarily reflect visual processing in the occipital region, and may also have some relation to memory function of the brain, according to [16].

Beta waves: The Beta waves are mostly present in the frontal and central regions of the brain, and is closely related to being wide-awake and on alert. This means that your mind is being sharp and focused, and making neural connections more easily and quick. Also, neurons fire abundantly, and in rapid succession which helps to achieve peak performance. This state is ideal for work that requires full attention. These brain rhythms are also associated with motor activities, and are desynchronized during motor imagery and real movement, according to [17].

Gamma waves: The Gamma waves are the brainwaves that have the highest frequencies, and is closely related to being in a excited state. These waves are associated with peak concentration and is the optimal frequency regarding cognitive functions of the brain. The presence of these waves of a healthy adult is related to certain perceptions, attention and motor functions, as stated in [18]. There are also several studies [19], [20], and [21] that have provided evidence for presence of gamma activity in perception of both auditory and visual stimuli.

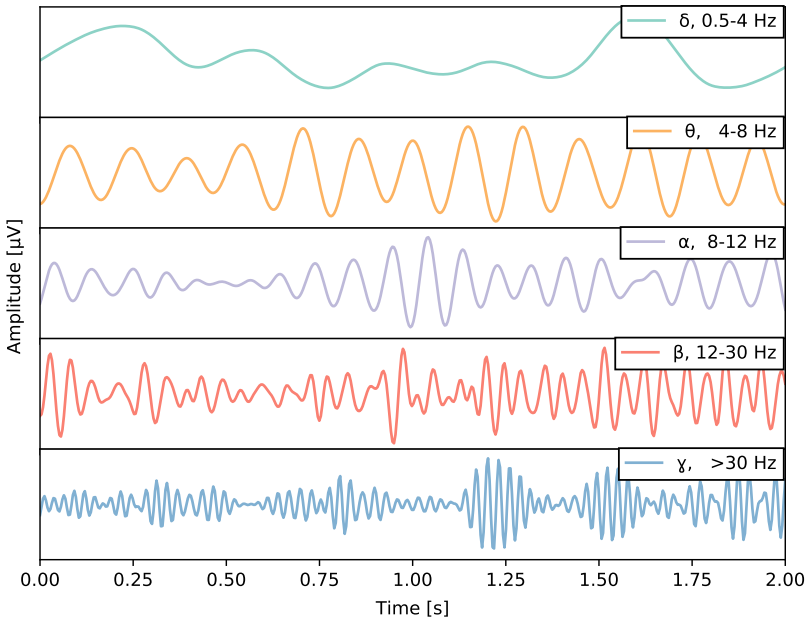

Figure 2.4: Illustration of the brain rhythm frequencies

An illustration of these frequencies of brain rhythms are shown in Figure 2.4. As the purpose of this thesis is regarding visual stimulus, the frequencies that is related to the occipital region is of interest. The frequencies that occurs in the occipital region is mostly high-frequency beta and gamma activities, which are the frequencies we expect to see most activity. A study [22], found that there was increased energy between 20-40Hz as multiple peaks that was recorded from the visual cortex of a Rhesus monkey when responding to a visual stimulus. As the brain functions of monkeys and humans are closely related, we expect to see results of a similar manner in our experiment.

2.5 EEG Terminology

Epoch

Epoching is a term used frequently in the field of EEG. Epoching is essentially the procedure of extracting a window of time-series data relative to a specific event time-stamp. These time windows are called "epochs", and are usually time-locked with respect to an event. These epochs can be of different size, depending on the type of events that are of interest and how long the segments of event are expected to last. In this thesis, epochs are used to store time-series data as a response of visual stimuli for further analyzation.

Event-Related Potential

The direct measured brain response of a specific cognitive, sensory or motor event is called an Event-Related Potential (ERP), or more generally called the electro-physiological response to a stimulus. The epoch windows are usually larger than the width of the ERPs, to ensure that ERPs are covered within the window.

Event-Related Spectral Perturbation

By averaging the power spectrum of short sliding time windows in multiple epochs of similar experimental events, the resulting Event-Related Spectral Perturbation (ERSP) will be the unique signature to the action or stimuli that the ERP was a response to.

2.6 Brain-Computer Interface

Brain-Computer Interface is an alternative to the natural communication and control of the body by providing a artificial direct communication pathway between a wired brain and an external device. BCI is used to bypass the neuromuscular output channels, also known as the efferent pathways of the body. Efferent is the outward communication from the central to the peripheral nervous system and further to an effector, or more commonly known as a muscle. The BCI uses direct measurements of the brain activity instead of being dependent of peripheral nerves and muscles. Put simply, a BCI is a computer-based system, which acquires signals from the brain, analyzes them, and then finally translate them into commands which is passed on to an output device to finally carry out a desired action, as illustrated in Figure 2.5. Although there are many definitions of the term, the most commonly definition according to [23], is summarized by these four distinct components:

1. The system must record activity directly from the brain, either invasively or non-invasively.
2. It must provide feedback to the user.
3. Feedback must be provided in real-time.
4. The system must rely on intentional control.

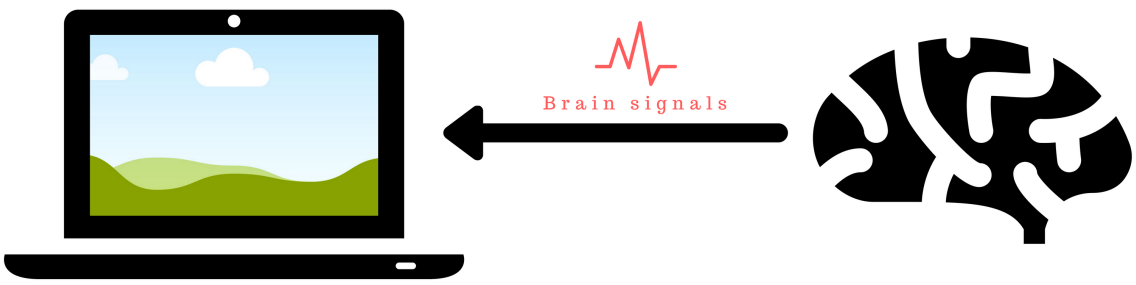

Figure 2.5: Illustration of Brain-Computer Interface

BCI is a relatively new field of science with almost limitless range of applications. Although most of BCI units have been expensive in the past, there has been numerous technological advances in the field in the last couple of years. Today, humans can utilize the technology and use brain-signals to interact with and influence the environment. As mentioned in [24], the dramatic growth of brain-computer interfaces is driven by factors such as:

- Cheaper, smaller, and faster electronics and related instrumentation.
- Increased understanding of normal and abnormal brain function.
- Improved interfaces and environments.
- Additional testing and experimentation with target users in field settings.
- Improved methods for decoding brain signals in real time.
- Improved sensors, such as active and dry electrodes and improved invasive electrodes.

There are numerous different BCI devices on the market, but our focus will be exclusively on the open-source EEG platform OpenBCI.

2.7 OpenBCI

OpenBCI is a low-cost, programmable, open-source EEG platform, which is built around the Texas Instrument's ADS1299 IC. The chip is an 24-bit analog-to-digital converter (ADC) designed specifically for measuring tiny EEG signals and consist of 8 separate channels that measures different parts of the brain in a non-invasive manner. The communication between the board and the computer is via Bluetooth, and is thus more safe, as hazardous situations due to power supply is avoided. The main concern about using low-cost equipment instead of high-cost medical equipment is that it may not have the same accuracy and performance. A study [25] has compared OpenBCI and medical equipment and concluded that OpenBCI's effective performance and features are quite similar to that of the medical equipment, making OpenBCI a good alternative, as long as it is not to be employed in sensitive context such as medical applications. The OpenBCI board is depicted in Figure 2.6.

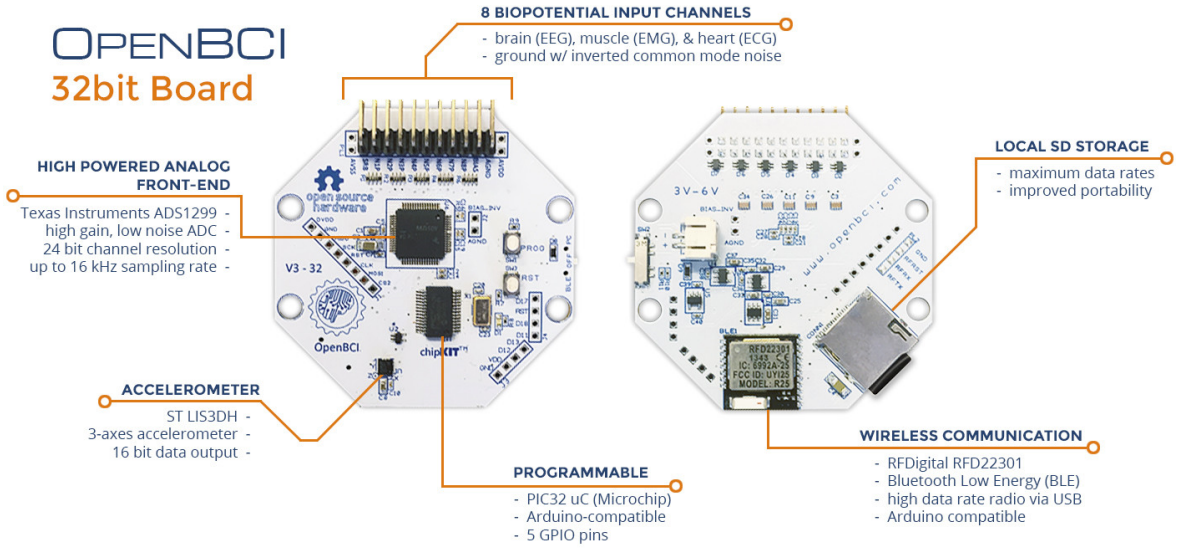

Figure 2.6: OpenBCI board overview [26]

Headwear

The OpenBCI is delivered along with a headwear, which is utilized as the frame for the EEG measurement system in this thesis. The headset is an open-source, 3D-printed headset intended to work with the OpenBCI system. It is capable of recording EEG, as well

as muscle activity (EMG) and heart activity (ECG). It consist of a frame where the electrodes and OpenBCI system is mounted on, as seen in the concept illustration in Figure 2.7. Since this system is open-source, OpenBCI provides the sufficient `.STL` files to 3D print the headwear by yourself. To assemble the 3D-printed parts we followed the complete manual[1].

Figure 2.7: Ultracortex Mark IV [27]

Electrode placement standard

There are numerous ways of placing the electrodes, but there are two standards which is widely used on an international level, namely the *10/10 system* and the *10/20 system* [28]. The first and the second number correspond to the relative distance between the cranial landmarks over the head surface of the total front/back and right/left distance of the skull respectively. Each location has identification letters to identify the lobe and a number to a corresponding hemisphere location. The identifications letters to the corresponding lobes is described in Table 2.2 and the locations are illustrated in Figure 2.8. The electrode channels marked in red are the ones that are available in the headwear supplied by OpenBCI.

[1] http://docs.openbci.com/Headware/01-Ultracortex-Mark-IV. Accessed: 3/7-17

Lobe	Letter
Frontal	F
Temporal	T
Parietal	P
Occipital	O
Center[2]	C

Table 2.2: Identification letters corresponding to different brain lobes

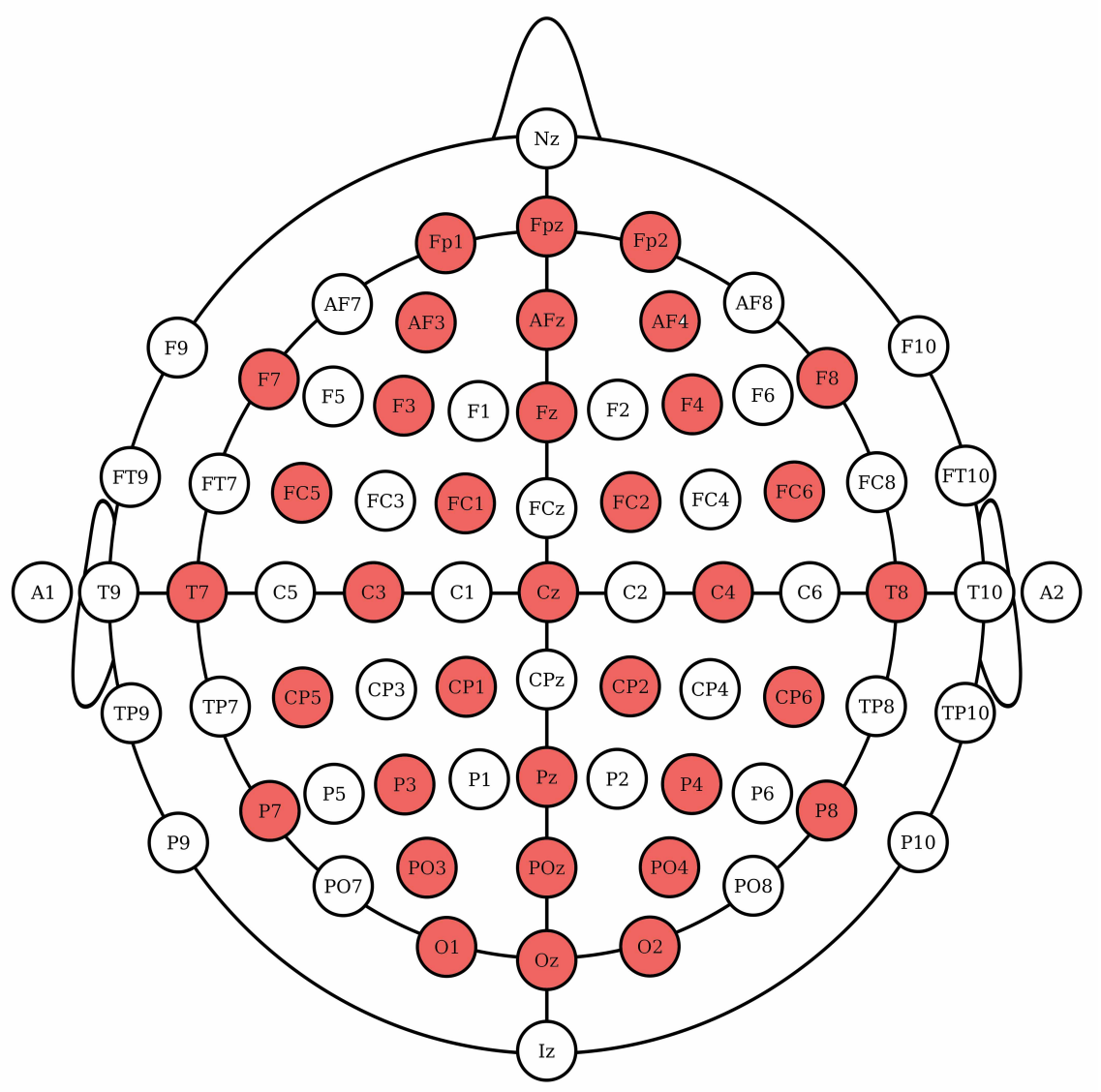

Figure 2.8: Overview of the *10/10 system* with the available electrodes for the OpenBCI headset [29]

[2]Center is not actually a lobe, but a category that encapsulates all the center nodes

2.8 Hilbert Transform

Hilbert Transform (HT) of a signal $x(t)$ is defined as the transform in which phase angle of all components of the signal is shifted by $\pm 90°$. As presented in [30], the Hilbert Transform for a signal *x(t)* is given by

$$y(t) = \mathscr{H}[x(t)] = \frac{1}{\pi} P \int_{-\infty}^{\infty} \frac{x(\tau)}{t-\tau} d\tau \tag{2.1}$$

in which P indicates the Cauchy principal value. The HT, $y(t)$ and the original signal $x(t)$ are orthogonal. They have properties such as having the same amplitude spectrum, autocorrelation function and the same energy spectral density.

Instantaneous frequency and amplitude

Instantaneous frequency is an important concept in signal processing regarding representation and analysis of time-varying functions. As proposed in [31], the instantaneous frequency can be obtained in the following procedure. By utilizing HT, the imaginary part $y(t)$ is obtained from the analytic signal $z(t)$, which is given by

$$z(t) = x(t) + iy(t) = a(t)e^{i\theta(t)} \tag{2.2}$$

in which

$$a(t) = \left\{x^2(t) + y^2(t)\right\}^{1/2} \text{ and } \theta(t) = tan^{-1}\frac{y(t)}{x(t)} \tag{2.3}$$

from the canonical pair, $\left[a(t), \theta(t)\right]$, associated with $x(t)$. The instantaneous amplitude is given by $a(t)$, while the instantaneous frequency is then defined as the time derivative of the phase, i.e., the rate of change of the phase of the analytic pair, given by

$$\omega(t) = \frac{d\theta(t)}{dt} \tag{2.4}$$

2.9 Empirical Mode Decomposition

Empirical Mode Decomposition (EMD) was originally introduced to study water surface wave evolution in the late 1990s [30]. Since then, it is widely used in various signal analysis fields. EMD is a fully data-driven algorithm which is used to decompose a signal

into its own intrinsic oscillations called Intrinsic Mode Functions (IMF), which is done in a process called *sifting*. These IMFs are amplitude/frequency (AM/FM) modulation components of the signal. In the EMD approach, the data $x(t)$ is decomposed in terms of IMFs according to

$$x(t) = \sum_{i=1}^{n} c_i + r_n \tag{2.5}$$

where c_i are the IMFs and r_n is the monotonic residue, after n number of IMFs are extracted. The method that is useful for analyzing natural signals, which are most often non-linear and non-stationary. Because EMD does not leave time domain, it is adaptive and highly efficient. EMD based algorithms has been used in high extent for high-quality seismic records, as seen in [32], where EMD utilized as an approach to enhance seismic reflections and to make seismic events more coherent. A more thorough tutorial on EMD is presented in [33], but a simple explanation of IMF and the sifting process is explained in the following subsections.

Intrinsic Mode Functions

The IMFs arise as basic modes from the application of EMD to functions or signals. They are characterized by being narrowband modes, having a large time-bandwidth product and being nearly monocomponent, i.e. signals with only one local extremum per zero crossing. These allows for well-defined Hilbert Transforms, which ensures extraction of physically meaningful instantaneous frequencies. Meaningful instantaneous frequencies is defined as functions that have the same number of zero crossings and extrema and that it is symmetric with respect to the *local zero mean*, as defined by Professor Norden Huang in [30]. The definition of an IMF can be summarized by the following two conditions:

1. The number of extrema and the number of zero crossings must either equal of differ at most by one throughout the whole data set.

2. The mean value of the envelope defined by local maxima and the envelope defined by the local minima is zero for any point.

An example for visualization purposes is illustrated in Figure 2.9, where a EEG signal $x(t)$ has been decomposed into 7 distinct IMFs $c1(t), \cdots, c5(t)$ where the remaining residue have been extracted as IMF 7.

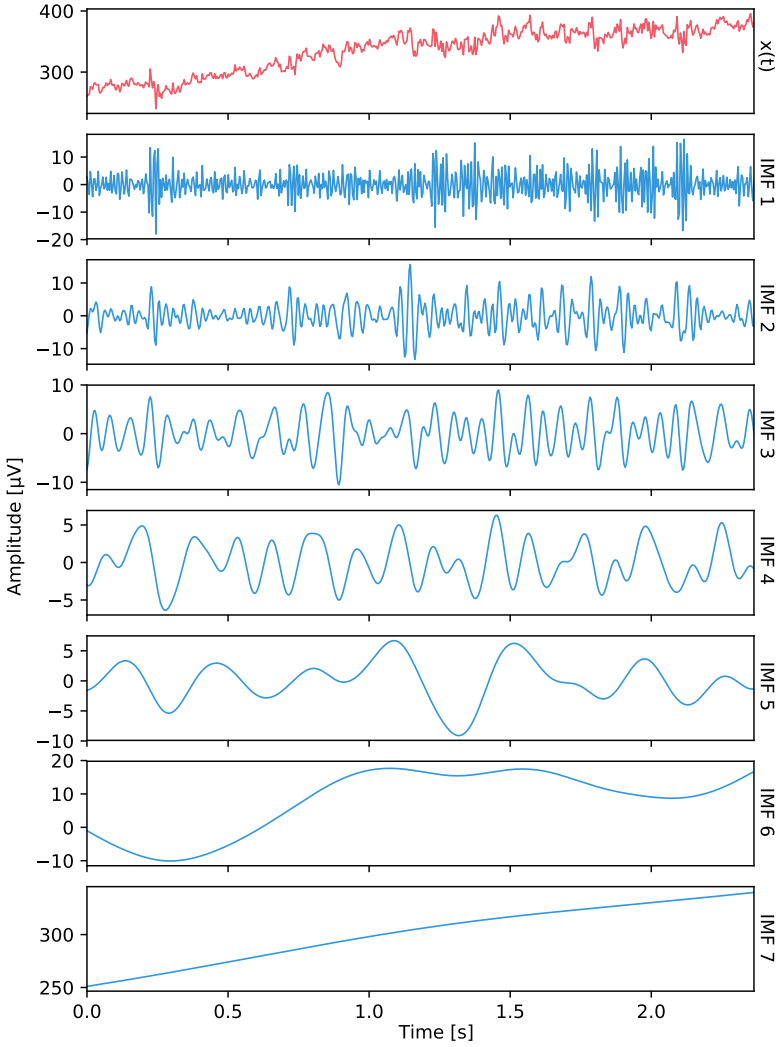

Figure 2.9: An example signal $x(t)$ decomposed by the the Ensemble Empirical Mode Decomposition of an EEG signal, resulting in 7 IMFs.

Sifting

The procedure of extracting an IMF is called sifting. Sifting is a general term in signal processing related to separating out components of a signal one at a time. It is frequently used in context of wavelet decomposition since this process is very similar in this respect. The sifting starts by interpolating local minima and local maxima points with a cubic spline, to determine the upper and the lower envelope, respectively. The mean envelope is then subtracted from the initial signal, as shown in the illustrated example in Figure 2.10. A new iteration will start and the interpolation scheme is reiterated on the remaining signal. The process terminates when the mean envelope is approximately zero along the signal, and the resulting signal is then designated as an IMF. The procedure of using EMD together with the Hilbert Transform is referred to as the Hilbert-Huang Transform (HHT)

and is described more in depth in the Section 2.10.

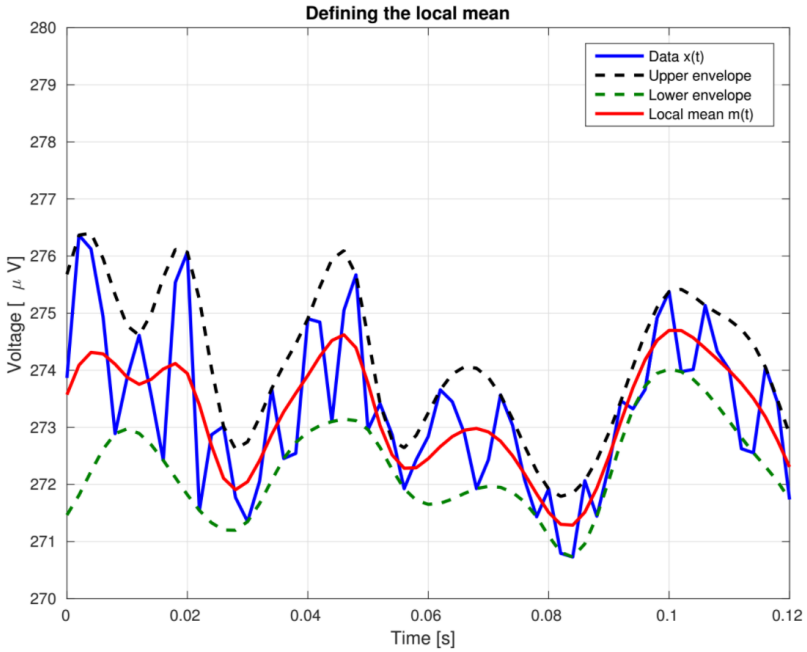

Figure 2.10: An example illustrating the cubic spline interpolation between the minima (lower envelope) and maxima (upper envelope) to define the local mean. Illustration in courtesy of [3]

Limitations

According to [34], one of the main drawbacks of EMD is a phenomenon called mode mixing, which occurs during the EMD process. The definition of mode mixing can be summarized by two reasons:

1. The IMF contains signals of widely disparate scales

2. Signals of a similar scale reside in different IMF components

The recently proposed Ensemble Empirical Mode Decomposition (EEMD) algorithm [35] uses a large number of noisy signals as masking signals. It is shown that EEMD can resolve the mode mixing problem in some real-life signals.

Ensemble Empirical Mode Decomposition

The idea of EEMD is to introduce white noise to the single data set, $x(t)$. The added white noise is treated as random noise that would be encountered when measuring EEG

data. The resulting "artificial" observation will then be

$$x_i(t) = x(t) + w_i(t) \tag{2.6}$$

Adding white noise to the signal may result in smaller SNR, but the added white noise will provide relatively uniform reference scale distribution to facilitate EMD, thus the low SNR does not affect EMD, but actually enhances it to avoid the mode mixing problem. As proposed in [35], EEMD is executed according to the following sequence:

1. Add a white noise series to the targeted data
2. Decompose the data with added white noise into IMFs
3. Repeat step 1 and 2 over a defined number of ensembles
4. Obtain the ensemble means of corresponding IMFs of the decomposition as the final result

With a given amount of ensembles, the added white noise will cancel out and result in an average of the ensemble IMFs. However, this procedure does have some drawbacks. The ensemble IMFs will not always contain strict IMF properties. However, as mentioned in [35], it will not interfere notably with the Hilbert Transform. An overview of the functionality of EEMD is illustrated in Figure 2.11.

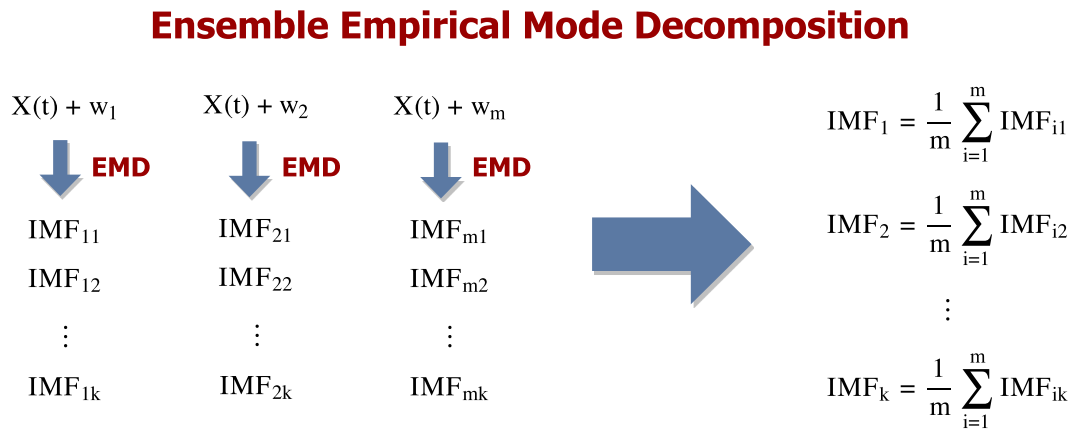

Figure 2.11: Overview of the EEMD functionality.

2.10 The Hilbert-Huang Transform

The Hilbert-Huang Transform (HHT) is a relatively new data analysis method, and is first published in 1998 by Professor Norden E. Huang et.al. in [30]. HHT is an adaptive feature extraction algorithm, which uses an empirical approach (EMD), rather than theory based, as algorithm such as the Fourier- and Wavelet Transform. Because of the fact that the decomposition is based on the local characteristic time scale of data, the algorithm is capable of handling non-linear and non-stationary time series data, and is thus more convenient regarding the study of complex signals, such as EEG signals. HHT is widely used in voice signal processing, like in [36], where an HHT algorithm is utilized for speech enhancement, and in [37], where HHT is used to characterize loudspeaker nonlinearities. An overview of the functionality of HHT and how EMD is embedded as part of HHT, is presented in Figure 2.12. The purpose of HHT is to utilize EMD to decompose a

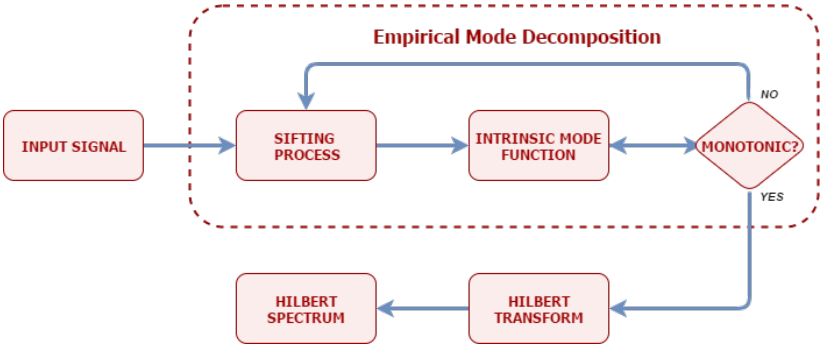

Figure 2.12: Overview of Hilbert-Huang Transform functionality

signal into IMFs along a trend, and then differentiating the phase with respect to time which returns an instantaneous frequency. The instantaneous frequency is then applied to the HT, so that the final result of the algorithm is a frequency-time distribution of signal amplitude. The resulting distribution is then visualized with Hilbert Spectrum (HS), as elaborated in the next subsection.

Hilbert spectrum

Hilbert spectrum (HS), named after David Hilbert, is a statistical tool that gives a qualitative interpretation of a mixture of moving signals. Before utilizing HS, the dataset to be in the correct format, and HT has to be performed on each IMF. According to [30], when

HT has been applied to each IMF, the data can be expressed in the following form

$$X(t) = \sum_{j=1}^{n} a_j(t) \exp\left(i \int \omega_j(t) dt\right) \tag{2.7}$$

Equation (2.7) enables visual representation of the amplitude and the instantaneous frequency as functions of time in a three-dimensional plot, in which the amplitude can be contoured on the frequency-time plane. This frequency-time distribution is denoted as $H(\omega, t)$. The HS can also be substituted by using amplitude squared to get energy density, and then a Hilbert energy spectrum can be presented. There are multiple way to visualize the Hilbert spectra, both with color coded maps and contour maps with and without smoothing. An example of HS visualization is depicted in Figure 4.2.

2.11 Fourier Transform

The Fourier transform is a generalization of the complex Fourier series in the limit $L \to \infty$. The way it works is that it decomposes a function of time into the frequencies that make up the signal. The Fourier transform of a function f, is traditionally denoted as $\hat{f}$ and is defined as

$$\hat{f}(\xi) = \int_{-\infty}^{\infty} f(x) e^{-2\pi i x \xi} dx \tag{2.8}$$

for any real number ξ.

Chapter 3

Methods

The objective of the following chapter is to map out the methods that we utilized in this thesis, and to provide a thoroughly description of the experimental paradigm and how the data was acquired, processed and analyzed.

3.1 Experimental paradigm

Participants

Nine healthy male participants and one healthy female participant were recruited. All of the participants are of similar age (26 years, SD = 1 year), and normal or corrected-to-normal vision, and none of them were colorblind. One of the participants had elliptical seizures at a young age, but the rest of the subjects did not report any current or past neurological or psychiatric illness.

The participants had given their informed consent and was able to withdraw from the testing at any time without consequences. The experiment caused no physical harm to the participants. Participants along with some description for each subject is provided and enlisted in Table 3.1.

#	Age	Sex	CB[1]	RH[2]	OD[3]
1	27	M	No	Yes	R
2	25	M	No	Yes	R
3	25	M	No	Yes	R
4	26	M	No	Yes	R
5	27	M	No	Yes	L
6	26	M	No	No	L
7	25	M	No	Yes	R
8	24	M	No	No	R
9	26	F	No	Yes	R
10	27	M	No	Yes	R

Table 3.1: List of participants

Paradigm

The experiments that are conducted in this thesis are all regarding visual stimuli of three distinct primary colors, red, green and blue (RGB) recorded in a completely dark room. The paradigm consist of six distinct experiments, two for each of the three colors projected at the subject. The experiments were divided into the following sub-categories regarding how they are projected at the participant:

1. Short pulse light stimuli of each of the distinct RGB components.

2. Steady-state light stimuli of each of the distinct RGB components.

Regarding the short pulse experiments, the light pulse duration is static and was set to 1 second, and were presented in a pseudo-randomized order with the interval given as a random uniform number between 10.0 and 18.0 seconds. The randomization was done to ensure that brain activity due to prediction from the subject would be minimized in the resulting EEG data. Regarding the steady-state experiments, the experiment starts with having the light source switched off for 30 seconds, then the light source is switched on and maintained for 60 seconds, before ending with another 30 seconds with the light

[1]Colorblind: displays if the subject is colorblind or not.
[2]Right-handed: displays if the subject is right-handed or not.
[3]Ocular dominance: displays which eye is the dominant eye of the subject (the tendency to prefer visual input from one eye to the other), R for right and L for left.

source switched off. These experiments were conducted to see if they would invoke any distinct ERPs or brain-wave patterns, due to the light stimuli. We concentrated on signals recorded close to the striate cortex and is expected to display localized neuronal activity of the primary visual cortex in both experiments.

Setup

The experiment is conducted in a completely dark room, with the RGB light strips mounted on a wooden bracket, as depicted in Figure 3.2. The connections that was made for the Arduino is depicted in Figure 3.1. Moreover, a matte acrylic glass plate was mounted in front of the RGB light strips to diffuse the light into a more pleasant glow. This was done to prevent sharp stinging points of light, and to distribute the light uniformly across the surface. During the experiment, the subject is situated on a chair approximately 50

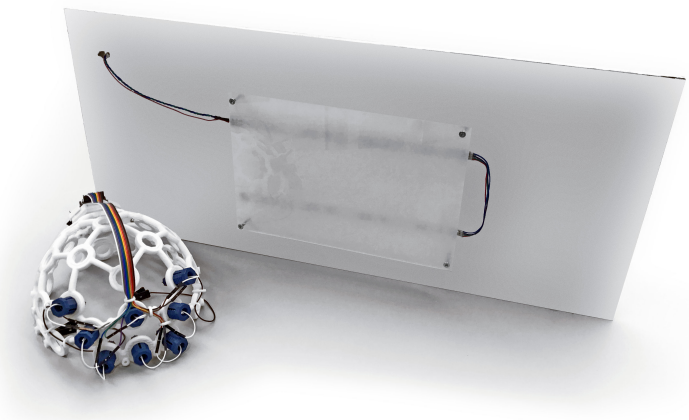

Figure 3.1: Wooden bracket along with the EEG headwear.

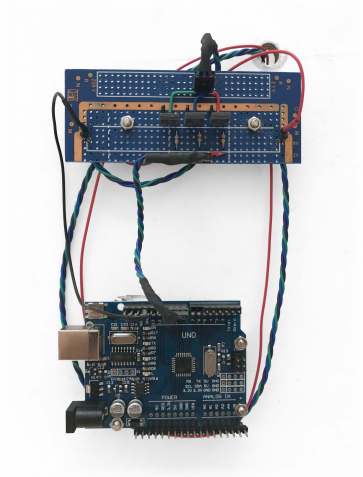

Figure 3.2: Connections for Arduino and RGB strips.

centimeters from the plate, with the participant facing directly towards the light source. The luminosity of each color was kept constant. Experiments for red, blue and green light sources are depicted with a subject in Figure 3.3, 3.4 and 3.5, respectively.

Procedure

The participants were asked to meet up in a specified room separately at a given time. They were then presented with a few explanatory sentences regarding the tasks assigned

Figure 3.3: Red light source

Figure 3.4: Green light source

Figure 3.5: Blue light source

to the participant. Participants were asked to keep their eyes open during recording session, and to blink only during the dark inter-stimulus intervals. They were also told to sit completely still and gaze towards the two light sources, situated in front of the participant. The headwear was then carefully mounted on the subjects head, and all the electrodes was tightened so that it gently touched the scalp of the subject, as well as clamping the reference and bias pins onto each of the subjects ears flips. A participant with the headwear mounted on is depicted in Figure 3.6. EEG signals from each electrode channel were

Figure 3.6: Girlfriend of one of the authors happily participating in the experiments.

then tested separately prior to the experiment. If there were any inconsistencies in a given channel, it was checked and fixated such that the signals received were stable. After making sure that the task assigned to the participant was fully understood, the testing session began. The six different experiments required all participants to sit completely still and focus on a given point between the two light sources. The test session were monitored by watching a live plot, in case of any signal issues during a test session. The experiment starts by choosing the experiment type and color in the Python program. Then the Python

program establishes a connection to the OpenBCI headset and the Arduino controlling the light source. The experiment will then last for a given duration, with light source intervals given by the Python program. The RGB light source will light up according to the interval and color commands sent to the Arduino. While experiment is ongoing, the OpenBCI will collect data from EEG and send it via Bluetooth to the Python program, which will provide a live plot. After the recording is done, the recorded data is exported as a data array as a `.csv` file, which is compatible with the other Python software modules used for data analysis purposes. A more thorough description of how the software is implemented, and how it works in detail is given in 3.3. An overview of the experiment sequence and interface is presented in Figure 3.7.

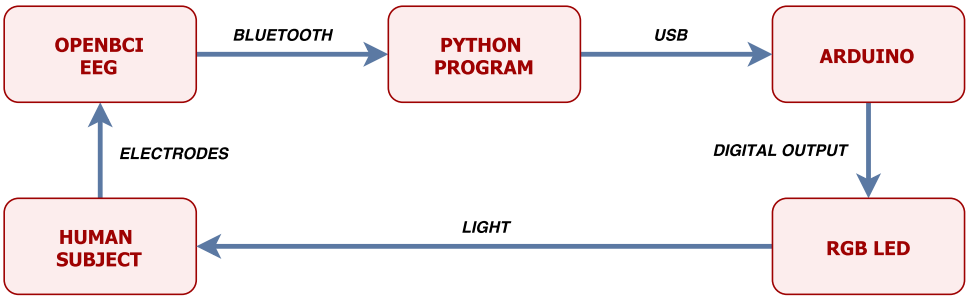

Figure 3.7: The sequential steps and interface of the experiment

Experimental Limitations

The location that was utilized for the recording sessions did not have any protection against electromagnetic disturbances nor any acoustic damping, and is thus not a perfect location for acquiring sensitive EEG data. Another important aspect is that the subjects reacted differently to the brightness of the light source, and some had small involuntary movements due to this. Since the EEG data measured is of a very small scale (microvolt), it may be affecting our results.

Data acquisition

The electrical activity of the brain was recorded using OpenBCI headset with 8 dry electrodes. Furthermore, the EEG signals are sampled at a rate of 250 Hz. Technical details about OpenBCI is explained more thoroughly in Section 2.7. The packets that are re-

ceived from the board is divided into byte frames, as given in Table 3.2. To interpret the data collected in a useful and quantitative way, a scale factor is applied to the data channels so that the signals are converted to microvolts. The formula is derived from the data format section on the OpenBCI website[4] and is

$$\lambda = 10^6 \cdot \frac{V_{ref}}{k(2^{23}-1)}[\frac{counts}{\mu V}] \tag{3.1}$$

where V_{ref} is the reference voltage and k is a user-configurable gain, which is set to 24 by default and λ is the scale factor to convert signal to microvolt. Due to limitations of the RFDuino wireless link, the sample rate is limited to 250 Hz. Higher sampling rate is possible for offline use with modifications to the device firmware and adding in a SD card in the SD card reader on the device.

Information	**Bytes**
Packet Number	1
Sample Number	2
Channel 1	3-5
Channel 2	6-8
Channel 3	9-11
Channel 4	12-14
Channel 5	15-17
Channel 6	18-20
Channel 7	21-23
Channel 8	24-26
Auxiliary Data	27-32

Table 3.2: Format of data packet

[4] http://docs.openbci.com/Hardware/03-Cyton_Data_Format. Accessed: 3/7-17.

3.2 Hardware implementation

This section provides a detailed overview of all the different hardware components of the system, ranging from equipment used for measuring to equipment for controlling the sequence of light exposure.

OpenBCI electronics

The OpenBCI electronics consists of two PCBs, the OpenBCI device and the the RFduino host dongle, depicted in Figure 3.8 and 3.9 respectively. The RFduino dongle is a single PCB with an USB connector on the end, GPIO pins used for updating firmware on the OpenBCI device and a RFduino IC for wireless communication. The OpenBCI device is the core component of the system, consisting of an analog-digital converter designed specifically for EEG-signals, an Arduino compatible microcontroller, 3-axis accelerometer and an RFduino to connect to the host dongle. By default this system supports up to 8 electrodes, but it is possible to supplement with an additional daisy-chain board that extends the support for up to 16 electrodes.

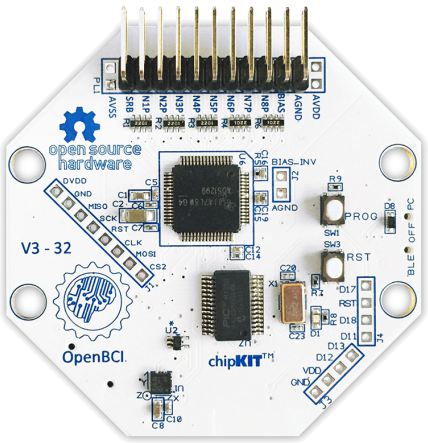

Figure 3.8: OpenBCI Device [38]

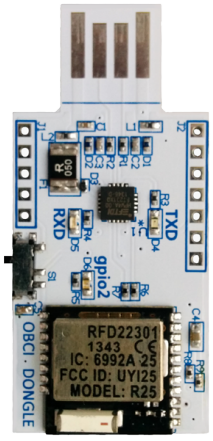

Figure 3.9: RFduino Host [39]

Electrode placement

For the purpose of recording brain responses from visual stimuli, the occipital lobe is where visual signals from the thalamus is received and processed. More specifically the

electrodes were chosen to be placed as a close cluster around the primary visual cortex/the striate cortex (V1), which is the most important area in terms of visual processing, as described more thoroughly in Section 2.3. Hence, the electrode placement specified using the 10/10 system, are as following

Left hemisphere: $P3 - PO3 - O1$

Right hemisphere: $P4 - PO4 - O2$

Midline: $POz - Oz$

The OpenBCI headset can support up to 16 electrodes utilizing a daisy board, but as the 8 electrodes already occupies the headwear's closest nodes of interest, any further nodes would have been placed well outside the area of the occipital lobe. The electrodes employed are illustrated with the color red in Figure 3.10, while the possible placements of electrode nodes are illustrated in Figure 2.8. There are also some additional connections that needs to be made, such as reference and bias. A reference pin (SRB-pin on the OpenBCI board), or ground pin if you like, is the reference signal in which all electrodes are compared to, so that changing potentials across the brain can be measured. Another necessary pin is the BIAS-pin. This pin detects and negates common-mode voltage interference from power-line or other sources. This is an built in function on the ADS1299 ADC on the OpenBCI device. Hence, both of these pins are required to be connected to each of the earlobes, denoted as *A1* and *A2* in Figure 3.10.

Arduino

Arduino consists of both a microcontroller and a piece of software, or IDE (Integrated Development Environment) that runs on your computer, used to write and upload computer code to the physical board. Since it has a built-in microcontroller, it is suitable for controlling the RGB light source for our experiment. Arduino UNO does also have a serial connection, that we will utilize for the interface to the Python script running on a PC. Another important reason for using Arduino to control the RGB light sequence is for more exact timing of events, as the light event times can be synchronized with commanding the Arduino.

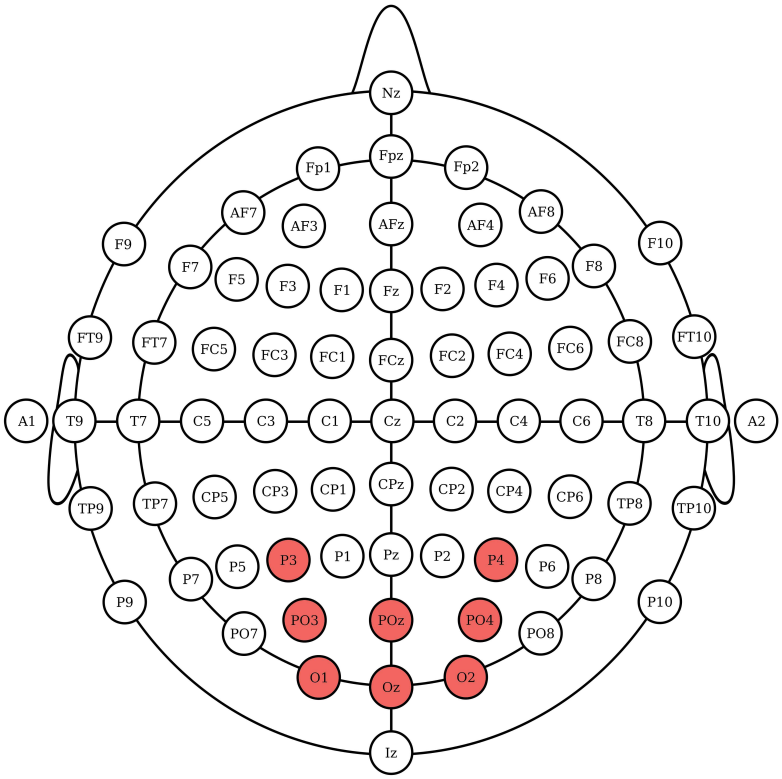

Figure 3.10: Overview of the *10/10 system* with the utilized electrodes marked in red [29]

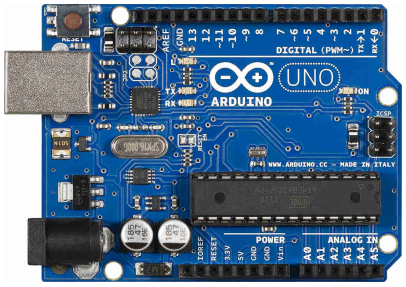

Figure 3.11: Arduino UNO [40]

RGB LED strip

The light source that is used for the experiments are two 12V RGB light strips that are mounted on a wooden bracket, which is situated in front of the subject. It was placed a matte acrylic glass plate in front to diffuse the passing light, as the light is generated as small very bright points along the LED strip.

Figure 3.12: RGB LED strip [41]

3.3 Software implementation

This section provides a detailed overview of all the Python software that was tailor-made for this thesis, both for recording purposes and data analysis. Dependencies required for the Python program is presented, as well as a description of the program procedures and information about the different modules.

Dependencies

The software implemented in this thesis is programmed in Python, due to its extensive libraries regarding signal analysis. The project implementation dependencies consist of the following Python packages:

PySerial: PySerial encapsulates the access for the serial ports needed for communication between both the Arduino and the OpenBCI board.

SciPy: SciPy (pronounced "Sigh Pie") is a Python-based ecosystem of open-source software for mathematics, science and engineering. Provides necessary core packages.

Numpy: Numpy is a core package in SciPy and is fundamental for scientific computing with Python. We utilize it because it provides us with N-dimensional array that is more powerful, and has more opportunities than the default Python arrays.

Matplotlib: Matplotlib is a python 2D and 3D plotting library which produces publication quality figures, and with the Pyplot interface, plots can be provided with a Matlab-like interface.

PyQtGraph: PyQtGraph is a plotting library that is better for live plotting. For this thesis it is utilized for live plotting of EEG data during experiment.

Hierarchy

The software that was made for this thesis is extensive. Because of this, the software is divided into separate modules, so that the software is structured in a good manner. The hierarchy of Python scripts with corresponding descriptions are presented in the following tables. Table 3.3 shows an overview of the main scripts that is accessed by a user. As for all the scripts that are related to recording, are listed in Table 3.4.

Script name	Description
`Analyze.py`	Main analyze script
`Record.py`	Main script for EEG data recording
`Plot.py`	Main script for plotting raw EEG data
`EEMD_decomp.py`	Script that runs EEMD on raw EEG data in a given folder

Table 3.3: List of the main Python scripts

Script name	Description
`arduino.py`	Arduino related logic
`dmc.py`	Supportive functions
`livefiltering.py`	Livefilter of EEG signal
`liveplot.py`	Liveplot of EEG data while recording
`logic.py`	General logic for EEG recording
`obci.py`	OpenBCI interface logic
`ringbuffer.py`	Basic ringbuffer for liveplot cache
`timer.py`	Timing and threading logic for EEG data recording

Table 3.4: List of Python scripts related to recording

And all of the scripts that are related to data analysis are listed in Table 3.5. Because of

Script name	Description
`analyze.py`	Logic for EEG data structure
`analyze_funcs.py`	EEG signal analysis functions
`emd.py`	EMD algorithm[5]
`plot_funcs.py`	Script containing function regarding plotting
`supportive_functions.py`	Script containing a range suuportive functions

Table 3.5: List of Python scripts related to data analysis

the fact that this thesis has multiple authors, version control was utilized through the use of GitHub, to ensure that changes in code are managed in a favorable manner.

[5] Courtesy of Geir Kulia, Signal Analysis Lab AS, 2017

Data acquisition procedure

A data acquisition script has been made to save recorded data and present live data during recording sessions of the different experiments that have been conducted. The script presents the user with three experiment choices, pulse, steady-state and random. Depending on which experiment is chosen, a choice between each of the three RGB colors is presented. When experiment and color is chosen, the experiment sequence start. Serial connection is then initialized and established between both the Arduino and the OpenBCI. A serial command is sent to the OpenBCI to reset buffer and start streaming data. Experiment starts running, and data is streamed from OpenBCI to the PC running the script via Bluetooth. The live plot is continually updated for each iteration sample retrieval. All commands are sent to the Arduino with intervals produced by interval values given in the `config.py` script. Color commands are sent over serial as 'R', 'G' and 'B' literals, for red, green and blue respectively. The commands are received by Arduino and instantly emitting the color corresponding to the command. The timing error between the recorded data and enabled lights was measured using a 240 fps high speed camera, and the resulting timing error was always less than one frame, this results in a timing error for the recorded data generally within one sample of each other at a 250 Hz sampling rate. As this thesis only focuses on frequencies below 50 Hz this will have a negligible effect on the recorded data. The event timestamps are saved in an array for data analysis purposes post-experiment. An overview of the program sequence is illustrated with a flow chart in Figure 3.13.

Data analysis procedure

The amount of data from the experiments are substantial. In fact, there are 160 minutes worth of data per electrode, divided over a total of 60 experiments. Because of this, the data analysis had to be split up in separate stages. Firstly, a script decomposing the raw EEG data into its IMF components with EEMD was run overnight, due to the amount of ensembles that had to be computed. When the script has completed, it saves the IMFs into a compressed Numpy array on locally the disk for further analysis.

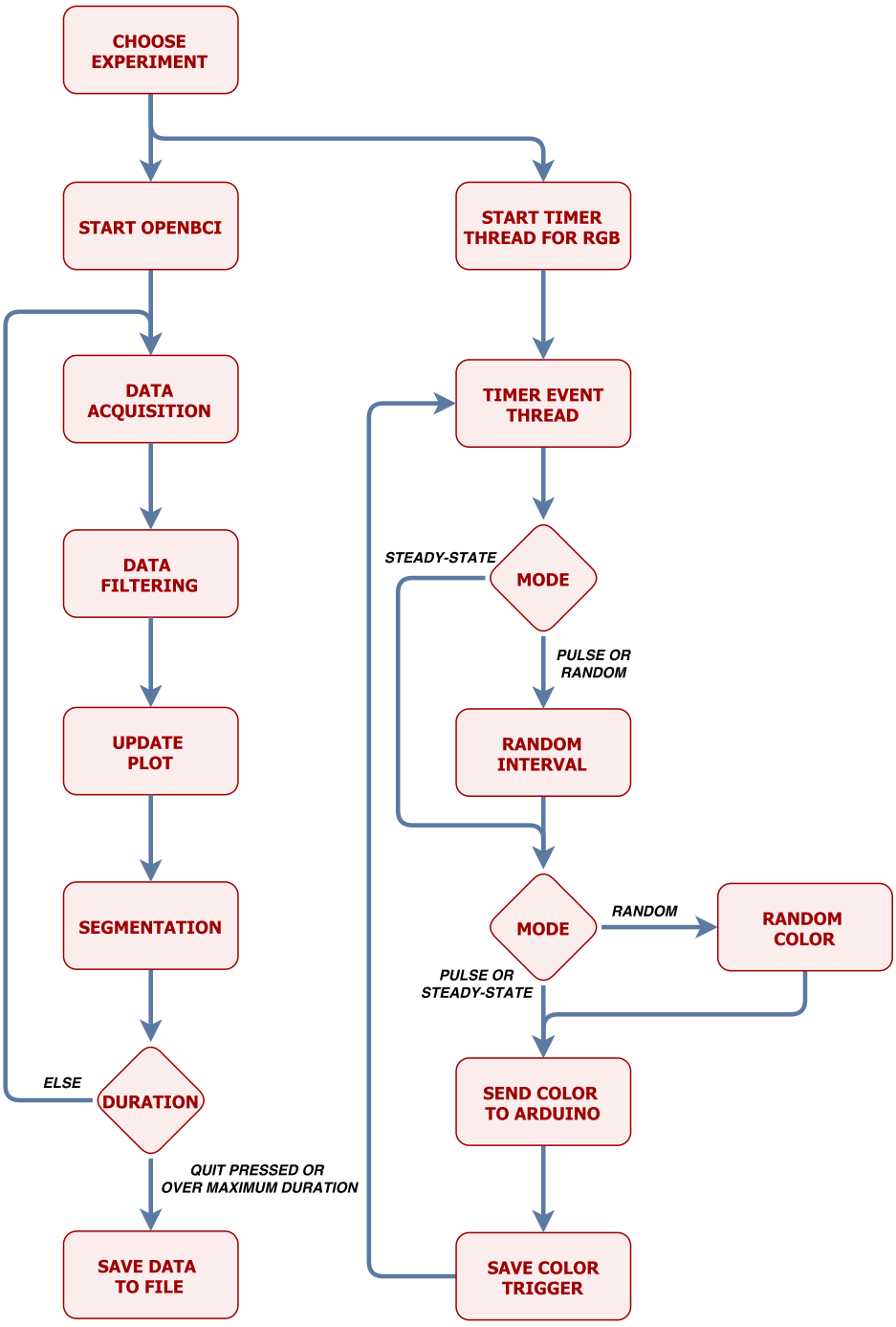

Figure 3.13: Flowchart illustrating the data acquisition program

Short pulse experiment

Regarding short light pulse experiment, to analyze the EEG data, it needed to be in a proper state. This means that the line-noise needs to be filtered out, and any EEG artifacts that occurred while recording needs to be excluded from the data set, as well as focusing on a given time window epoch surrounding the event. This exclusion is done by bandpass-filter the raw EEG data between 1-40 Hz, followed by visual inspection of the

resulting time-plot to ensure that it went well. Recording-artifacts from bad skin-electrode connection will manifest as excessive spikes or oscillations in the data with often greater than $100\mu V$. The areas in the time-plot which contain these artifacts are then manually added to a list of errors. Combining the event and error data, an event list is generated with only the healthy time-series. By using this event list, the time series for each channel is epoched according to the time-windows illustrated by Figure 3.16 and Figure 3.17 for pulse and steady-state experiments, respectively. For each set of epochs for every IMF, in every channel, the instantaneous amplitude and frequency is calculated using the Hilbert Transform. For each of these sets of instantaneous frequency/amplitude, the epochs are stacked on top of each other and medianed sample-wise to end up with a single median instantaneous frequency/amplitude for each separate IMF. Median was chosen over averaging, so that outliers did not effect the results too much. By doing this, the baseline of brain-activity is reduced resulting in a more clear and accurate ERP. Moreover, a flowchart illustrating the data analysis regarding pulse light experiment is shown in Figure 3.14.

Steady-state experiment

As for the steady-state experiment, the requirement for the data structure is less complicated. Using the same method for visually inspecting the raw EEG data, two epochs that does not contain any recording-artifacts were selected, in which one of the epochs contain information from active period during stimuli, and the other epoch containing inactive period (non-stimuli period). The IMFs of interest in the given epochs were then recombined, and Fourier Transform were executed on the resulting data. Moreover, a flowchart illustrating the data analysis regarding steady-state light experiment is shown in Figure 3.15

3.4 Data analysis

This section will provide a description of the procedural approach from the obtaining of the raw EEG recording to the data analysis methods that are utilized on the recorded data, as well as some diagrams to present the algorithms in a qualitative manner.

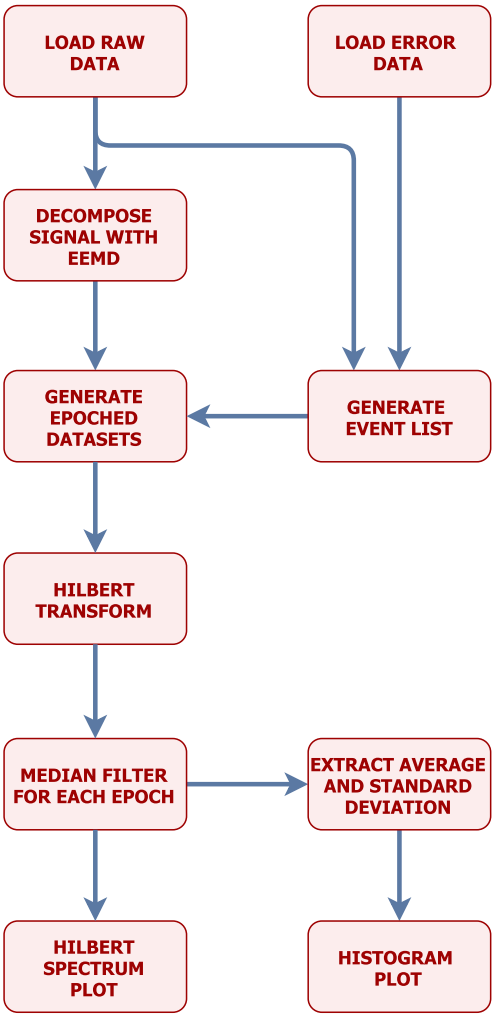

Figure 3.14: Flowchart illustrating the data analysis program for short pulse

Data analysis format

To be able to access the time-series data from all subjects over each of the two experiments, the data was saved into a single Numpy array of 5 dimensions. The dimensions are implemented in the Python script as "number of subjects, number of colors, number of channels, number of IMFs, number of samples".

Short pulse experiment

Regarding the short pulse experiments, the EEG data needs to be epoched in a suitable time-window. This is done to ensure that information regarding the stimuli is consistent, and from the same time-window for each of the events. We have chosen the parameters such that each epoch has a length of 2500ms, in which it is divided into 500ms pre-stimuli, 1000ms event-length and 1000ms post-stimuli, as illustrated in Figure 3.16. The specific

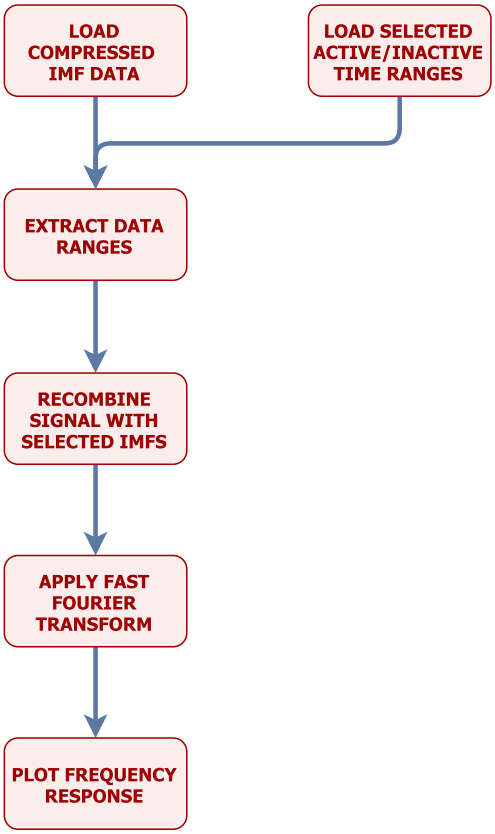

Figure 3.15: Flowchart illustrating the data analysis program for steady-state

epoch parameters are chosen to neglect irrelevant areas way outside of events, and to retain information about possible after effects that may occur post-stimuli. To accentuate the changes related to the light stimulus while diminishing the nominal brain-activity, the epochs are stacked on top of each other and medianed sample-wise.

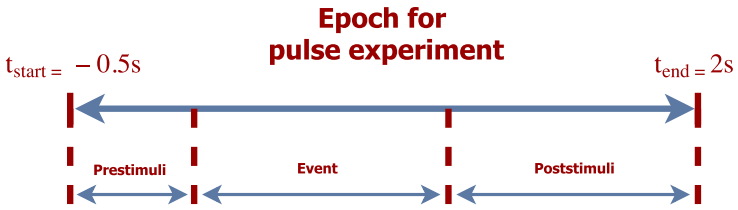

Figure 3.16: Illustration of the epochs that are chosen for the pulse experiment.

Steady-state experiment

For the steady-state experiment, a sufficiently long time-window for the lights where both active and inactive, while also include as little recording-artifacts as possible. As we wanted to have a same sized epoch for all extracted datasets that fit with the constraints in

mind, an epoch length of 16 seconds were chosen, as shown in Figure 3.17

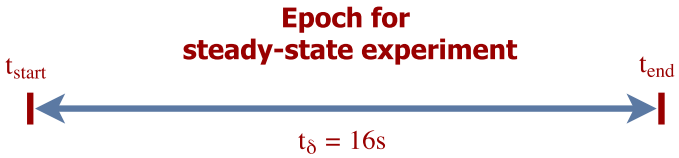

Figure 3.17: Illustration of the epochs that are chosen for steady-state experiment.

Linear filtering

Filtration plays a vital role in EEG data acquisition, as brain-wave signals recorded with EEG operates in the 1-100 μV range and is thus very sensitive to nearby changing electromagnetic fields, such as power-line noise. Extracting useful data can therefore be problematic, as the induced power-line interference can exceed $1mV$, the Signal-To-Noise ratio (SNR) can end up being too low. The EEMD algorithm employed in this thesis is severely affected by this, and the performance of the decomposition will yield unusable IMFs. An illustration of how a signal with and without linear filters applied are shown in Figure 3.18, where a band-pass and a band-stop filter has been applied. This will remove the power-line noise and any common-mode voltages between the electrodes and the reference.

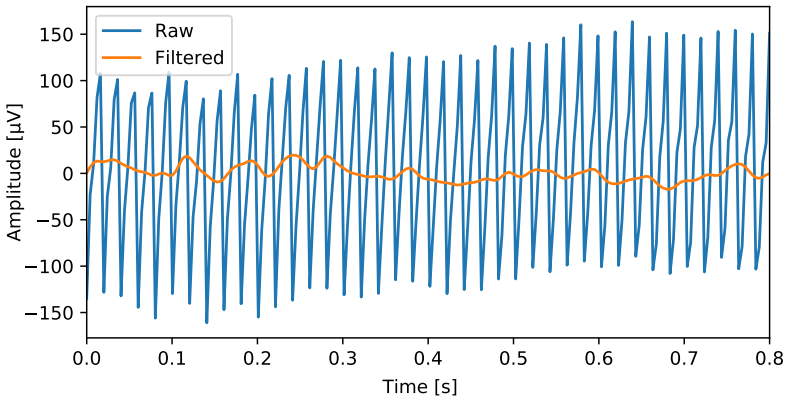

Figure 3.18: Sample data to compare filtered to non-filtered data

Empirical Mode Decomposition

The EMD algorithm that is being utilized for extracting IMFs, is a modified version of the EMD algorithm proposed by Signal Analysis Lab in [42]. The algorithm is illustrated in

Figure 3.19. The algorithm uses the input signal $v(t)$ and returns the fewest IMFs possible to describe it as $v_1(t), \cdots, v_{N_{IMF}}(t)$ and a monotonic function $v_r(t)$. The upper and lower envelopes are calculated using cubic spline interpolation.

Ensemble Empirical Mode Decomposition

EMD is not effective in all situations, and in situations where mode-mixing is an issue, EEMD may be applied. EEMD takes advantage of the statistical attributes of white noise and with enough ensembles will return separate scales for amplitude and frequency while cancelling itself out. In our thesis it performed well with clearly extracting IMFs consistently without mode-mixing and closely relating to the brain-wave ranges shown in Table 2.1. A limitation to EEMD is that if there is an uneven distribution of noise across different electrode channels, it may weaken its ability to return consistent results, and as the SNR over the 8 channels in the same recording could vary greatly, this was corrected with applying linear filters to mitigate the power-line noise and its high-frequency harmonics. Finally the parameters for white noise and number of ensembles for the EEMD algorithm must be carefully chosen to yield good mode-mixing rejection while not corrupting the underlying signals with the white noise. The choice of standard deviation of the noise and the number of ensemble members that is applied to EEMD is chosen according to [35], where the following equation is purposed.

$$\epsilon_n = \frac{\epsilon}{\sqrt{N}}, \tag{3.2}$$

where N is the number of ensemble members, ϵ is the amplitude of the added noise, and ϵ_n is the final standard deviation of error, which is defined as the difference between the input signal and the corresponding IMFs. With $N = 800$ and $\epsilon = 20$, the resulting IMFs had no mode-mixing issues. The white noise with a standard deviation of $\epsilon_n = \frac{1}{\sqrt{2}}$ was applied, and had a negligible affect on our results.

Hilbert-Huang Transform

HHT is utilized as the main method for data analysis in this thesis due to its capabilities in time-frequency-energy representations, and offers a potentially viable method for non-linear and non-stationary data analysis. According to a thorough review on HHT [43], in

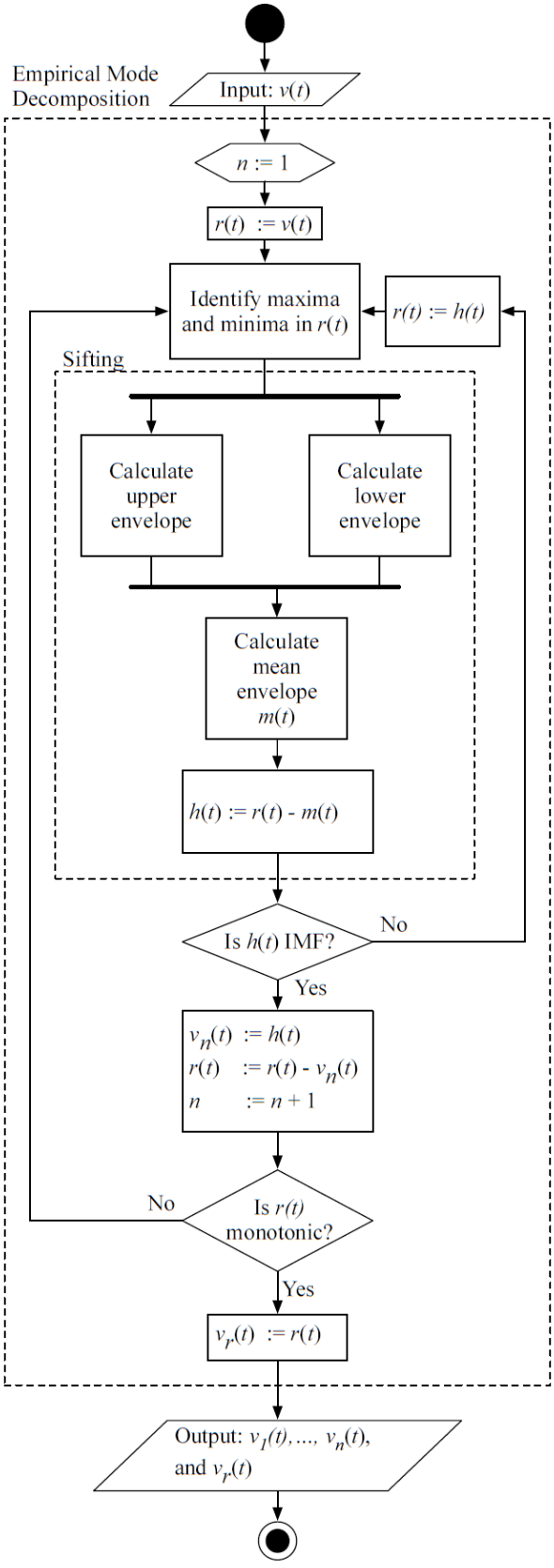

Figure 3.19: UML diagram of the the EMD algorithm, courtesy of Geir Kulia [42]

all the cases studied, HHT gives results much sharper than most of the traditional analysis methods, and in most cases, it reveals true physical meanings. To obtain the instantaneous frequency, the HT needs to be computed. The SciPy library includes a function for computing HT, in which is executed for an analytic signal $z(t)$

$$z(t) = F^{-1}\left[F(x)2U\right] = x(t) + i\,y(t), \tag{3.3}$$

where F is the Fourier Transform, U is the unit step function, and $y(t)$ is the HT. The resulting HT can then be differentiated with respect to time to obtain the instantaneous frequency

$$\omega(t) = \frac{d\phi(t)}{dt}, \tag{3.4}$$

where ω is the instantaneous frequency and ϕ is the instantaneous phase angle. The phase angle is also unwrapped in the algorithm to prevent discontinuities in the phase angle which will result in dirac delta impulses. The instantaneous amplitude $a(t)$ can be obtained as

$$a(t) = \sqrt{(x(t))^2 + (i\,y(t))^2} \tag{3.5}$$

Chapter 4

Results

The objective of the following chapter is to present the results from the experiments that was conducted. The chapter starts by presenting general results of the experiments, followed by an overview of the subjects. Results are then presented with respect to different experiment types, followed by a presentation with respect to individual differences and differences between each of the colors. A selected few of the different plots and diagrams are presented along with the results, with the rest listed in the appendices.

4.1 Preliminary analysis

The results are presented with EEG data, recorded from 10 different participants. Each participant performed 2 types of experiments, namely short pulse experiment and steady-state experiment, in which both are performed for each of the primary colors RGB. Data from all of the participants were used, however, some epochs are excluded from the dataset due to recording artifacts. The EEMD algorithm was applied on the recorded EEG data, in which the 7 most relevant IMFs were extracted. The acquired IMFs with its corresponding mean frequencies and its 2σ variations are presented in Table 4.1. The same IMF values are also presented and compared along in Figure 4.1. Moreover, the extracted IMFs frequency ranges is comparable to the different

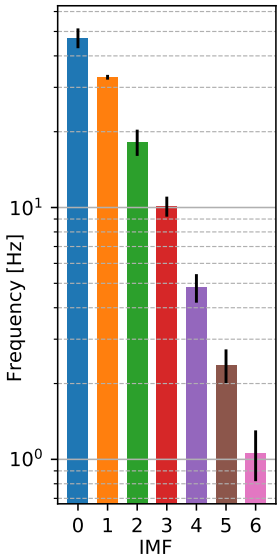

Figure 4.1: Mean frequency per IMF visualized with 2σ SD

brain-wave classifications, in particular IMF 1-5, to that of the 5 state-of-the-art brain rhythms enlisted in Table 2.1. The specific brain patterns from different subjects var-

IMF	Frequency	SD[1]
0	47.2 Hz	4.260
1	32.9 Hz	0.726
2	18.2 Hz	2.170
3	10.1 Hz	0.935
4	4.81 Hz	0.624
5	2.37 Hz	0.363
6	1.06 Hz	0.242

Table 4.1: List of IMFs found with corresponding mean frequencies

ied a lot. Some subjects had a flat response across all or some of the electrodes, and some subjects had a more intensified response from a few electrodes. There were also some differences in terms of which colors that elicited the more intense response. A list of the subjects along with information regarding corresponding individual response are therefore presented in Table 4.2.

#	Area[2]	Color[3]	P[4]	SS[5]
1	O2/Oz	R	A.1	B.1
2	O1/Oz	B	A.2	B.2
3	O2	R	A.3	B.3
4	Flat	R	A.4	B.4
5	O1	B	A.5	B.5
6	Flat	B	A.6	B.6
7	Oz	R	A.7	B.7
8	Oz	B	A.8	B.8
9	Flat	B	A.9	B.9
10	Oz	B	A.10	B.10

Table 4.2: Results for different participants

[1] Displays the standard deviation with 2σ

[2] Describes the electrode locations of the occipital lobe that displays the highest level of response. If the response is very spread out, typically >3 electrodes, "Flat" is displayed.

[3] Displays the color that gave the most significant energy response

[4] Figure reference to the Hilbert spectrum plots regarding short pulse experiments

[5] Figure reference to the frequency response plots regarding steady-state experiments

4.2 Hilbert spectral analysis

With the instantaneous frequency and amplitude that is obtained by applying the Hilbert transform on the IMFs, the average results from each experiment and color are computed. That is, the average time-frequency solutions, averaged over all the accepted epochs separately for each of the participants. Using the recorded EEG data from each subject and each color, the average power for IMF 1-6 was computed from approximately 14 separate stimuli events, recorded over all electrodes for the short pulse experiment and visualized as an Hilbert spectrum. Results from green light exposure on electrode *O1* for *Subject 2* is presented in the Hilbert spectrum in Figure 4.2.

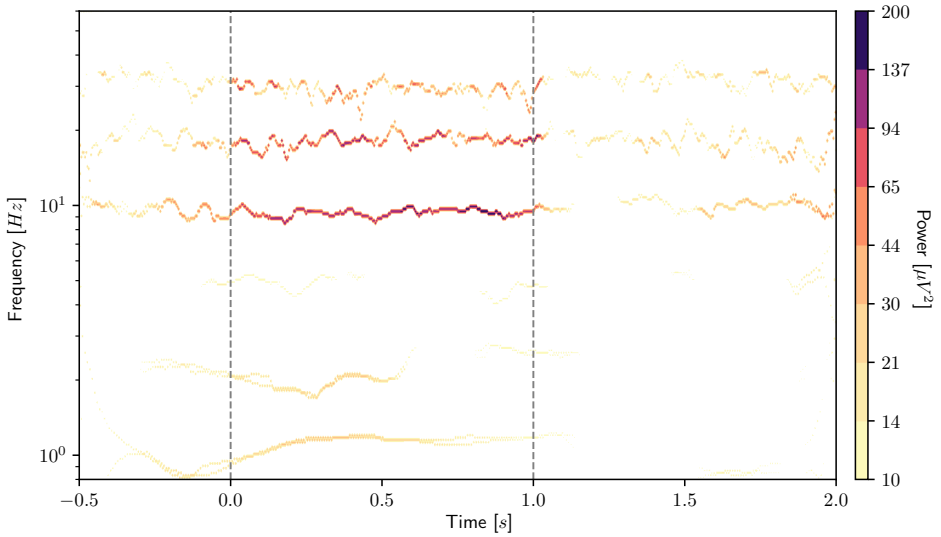

Figure 4.2: Hilbert spectrum visualization of IMF 1-5 from ***Subject 2*** with exposure to green color and from electrode *O1*.

In most of the subjects, a significant rise in energy was found for both IMF 1, IMF 2 and IMF 3, which has a mean frequency of approximately *30Hz*, *16Hz* and *10Hz*, respectively. This rise in energy occurs from different parts of the occipital lobe, depending on which subject it is. The electrode that recorded the clearest response differed greatly between subjects, ranging from left to the right hemisphere of the occipital lobe. Moreover, a few of the subjects had a more significant rise in energy compared to what was found in others, while some had a insignificant change. The energy difference between active (data during event) and inactive (data in between events) for *Subject 1* is presented as histogram plots for both IMF 1 and IMF 2 in Figure 4.3 and Figure 4.4, respectively. The plots are presented with a distribution of all the different electrode channels and with a

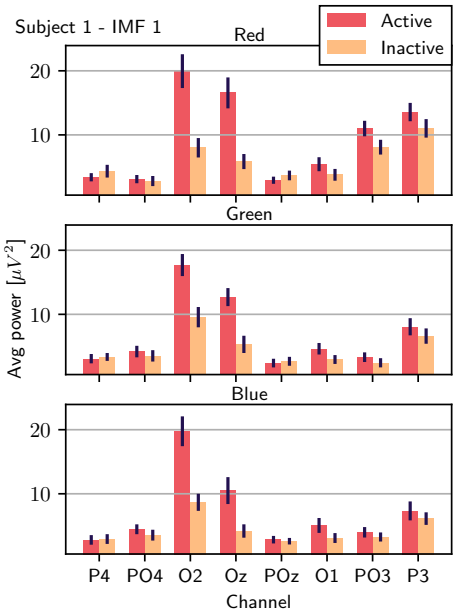

Figure 4.3: Event-related power in IMF 1 for ***Subject 1***

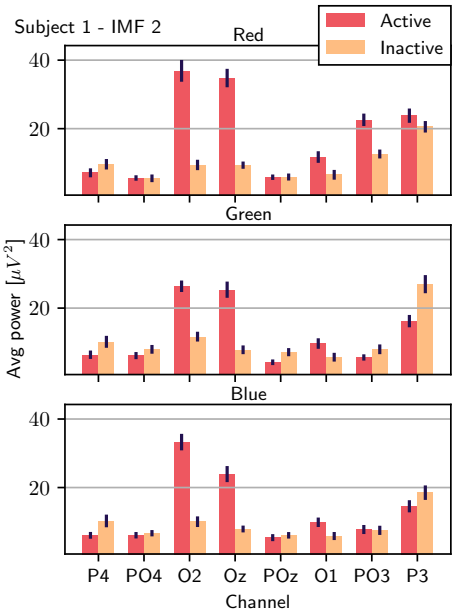

Figure 4.4: Event-related power in IMF 2 for ***Subject 1***

separate plot for each of the RGB colors. The desired level of the confidence interval is set to *95%*, also represented as approximately 2σ (two times standard deviation), which is shown as a black line on top of each histogram. With the chosen confidence interval, it is clearly that the difference between power in active and inactive is significant in channels *O2* and *Oz* for this subject. A complete presentation with the distribution of all of the subjects are listed in Appendix C.

4.3 Color characteristics

Regarding differences between exposure to the different RGB colors, we did not find any clear statistical significant differences when examining the temporal information from the short pulse experiments. There is a slight tendency that the average normalized power between active and inactive state for blue and green light is higher than red light as a total over all subjects, as seen in Figure 4.5. It can also be seen that the response from red light has a slight phase offset compared to the response from blue and green light, this can be observed per individual in Appendix D. All of the colors elicits a similar response over *IMF 1* and *IMF 2*, and a clear increase in power can be seen in the event area between the grey dotted lines. However, by analyzing spectral information from the steady-state experiments, we obtained surprisingly good results from the frequency response by utiliz-

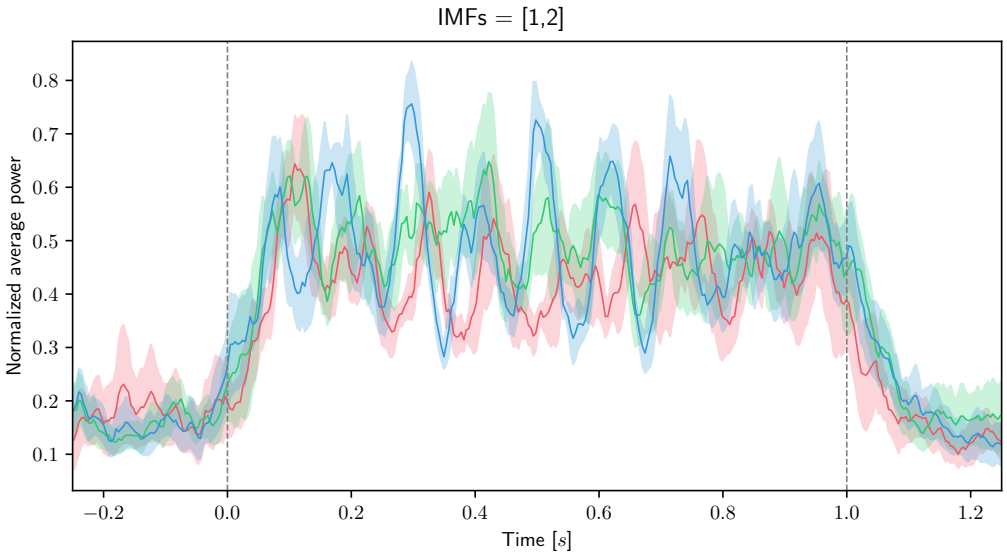

Figure 4.5: Normalized power from components IMF 1 and 2, averaged from the electrode with the best response for each subject per experiment color.

ing the Fourier Transform. Spectral information from one of the subjects are presented in Figure 4.7. Here it can be seen that blue light has a tendency to elicit a more narrow frequency response with larger amplitude than that of red and green. Moreover, it can also be observed that green color elicit a slightly higher frequency than that of red and blue color.

To visualize the average difference between the different frequencies for each color, for each of the IMFs, a histogram distribution plot has been made and illustrated in Figure 4.6. The goal of this was to see if there was a universal repose that accounted for all of the subjects in this thesis. The visualization shows the average over all subjects' frequency response listed as IMF correspondents along with the 2σ standard deviation, which then clearly highlights the frequency shift that can be seen in green light, compared to that of red and blue light.

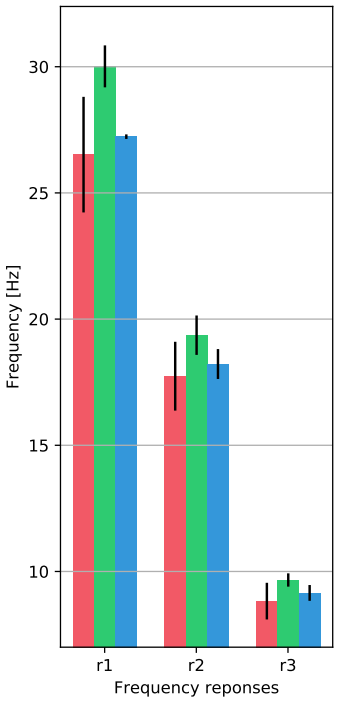

Figure 4.6: Color comparison for each IMF with each bar in the corresponding RGB color

4.4 Subject characteristics

The individual brain responses for each of the subjects are visualized by Hilbert spectrum and listed in Appendix A. A clear trend can be recognized by taking a closer look at each

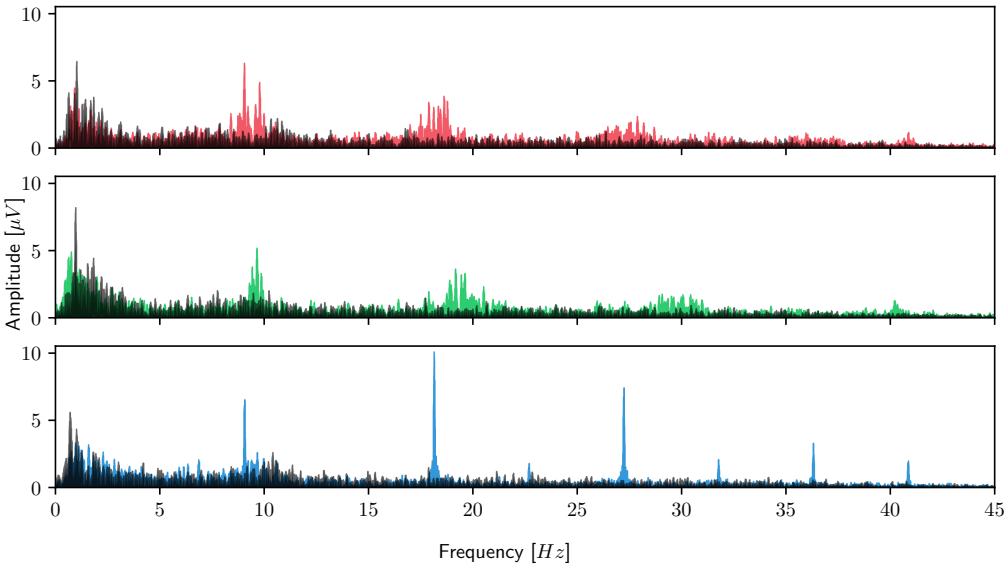

Figure 4.7: Spectral information on channel ***Oz*** for ***Subject 7***.
Subplots are for color red, green and blue, respectively.

individual. A rise in energy is clearly seen in some individuals in IMF 1, which lies in the gamma wave range with a frequency of about *30Hz*. The electrode channel that received the most significant response varied greatly between the different subjects, and for some subjects shows a very localized response where only a single channel is of statistical significance.

Chapter 5

Conclusion

The objective of the following chapter is to give a summary of what has been done and present conclusions drawn from the experiments with regards to the research questions presented in the introduction, as well as discussing the strengths and limitations of the findings and presenting some recommendations for further work.

5.1 Summary

The entire implementation in this thesis contains separate modules for recording and analyzation of EEG data. The steps include filtering of power-line noise, signal mode extraction with EEMD, time-frequency analysis with Hilbert Spectrum Analysis (HSA) and frequency response analysis with the Fourier Transform (FT).

Some vital advantages of EEMD has been outlined, in which the most important one is the fact that it suppresses mode-mixing, compared to EMD, which may introduce mode-mixing between the different IMFs. No prior knowledge of the spectral nor temporal information are required, meaning that almost any signal can be decomposed by EEMD, which will ensure that the resulting IMFs contain the most valuable information.

Furthermore, the frequency spectra of the IMFs that were obtained through EEMD seem to correlate closely with the state-of-the-art recognized brain rhythms, which underpins that our results are in line with that of other researchers.

Moreover, the short pulse experiments, as well as the steady-state experiments, proved to yield satisfactory results. Regarding differences in brain response to the different col-

ors, the steady-state experiment provided good spectral information from the frequency response through the use of Fourier transform, in which was manifested as distinct transients in energy at a range of different frequencies. The short pulse experiments, on the other hand, gave us good qualitative temporal information. Distinguishing between different subjects through the use of Hilbert spectrum and statistical analysis granted us with information regarding how individually brain responds to visual stimuli.

Regarding **RQ1**, looking at the steady-state results, there was a significant difference between exposure to the different colors. Exposure to the blue color seemed to generate considerable narrower frequency band with a larger amplitude than that of the red and green color. While the frequency responses for green light was always shifted towards higher frequency compared to that of the red and blue light. Moreover, when it comes to **RQ2**, the individual differences were quite significant, and it seems that the brain responses varied across subjects, as argued further in 4.4.

The results from our thesis proves that OpenBCI, even though it is not of medical grade, provides surprisingly satisfying results with good spatial and temporal resolution. From this, we can conclude that OpenBCI is well-suited for recording complex EEG data, and can be utilized for other EEG related applications without the need of more expensive equipment for recording of the EEG data.

5.2 Discussion

Recording implications

Linear filters will deform the original signal due to phase shifting, which is something that we tried to avoid. However, due to excessive environmental noise during recording, the SNR of the resulting EEG data was very low. This severely hindered EEMDs ability to properly extract the underlying IMFs. The exact reason for the disturbance is not known, but future EEG experiments with the OpenBCI headset should be held in a more neutral noise-free environment to mitigate this issue. This will increase the SNR, which in terms will remove the need for linear filtering.

Another limitation lies in the fact that the electrodes used with the OpenBCI board are

dry-electrodes. This may create differences in impedance between subjects, but also between electrodes on the same subject, which in terms will complicate the data analysis. This may be solved by utilizing a EEG headset with wet-electrodes instead. This will probably increase the cost and decrease practicality of the headset, but a more stable and accurate measurement will be acquired.

Regarding the recording procedure, there were a couple of implications and considerations that could have been taken more into account. One of the most important one being the fact that the number of events for each experiment could have been set to a higher number. Even though the length of the experiment is decent, a longer interval between the events was prioritized to make sure lasting effects would not be included in the subsequent event. As nominal brain activity seem to generally be reestablished after approximately 2 seconds, this interval was clearly chosen too large. Decreasing this interval would have enhanced our results by providing significantly more data, and when averaged, the baseline brain activity would have been further neglected, as well as highlighting the response from short light pulse stimuli. Another important experimental parameter that would strengthen the results is the number of subjects, as the variation between the responses of the 10 subjects in this thesis varied greatly. Having more participants in the experiments would increase accuracy of the results, and highlight the average trend across participants in a more accurate way.

Moreover, in terms of EEG recording, some of the EEG data will be contaminated by artifacts. All EEG signals that does not originate from the brain activity are considered an artifact, which can be divided into external and internal artifacts. External artifacts originate from external sources, such as power-line noise, electromagnetic fields and bad skin contact between electrode and scalp, which were eliminated by visual inspection. On the other hand there are internal artifacts, such as moving muscles, eye blinks, eyeball movement, jaw clenching e.g. which could be related to involuntary actions linked up with the visual stimuli. These could affect the results without being directly obvious while doing the visual inspection, but only appearing under closer analysis, contaminating the results. An example of this can be observed in Figure A.10, where an increase in the 10 Hz IMF lasting approximately 0.2 seconds can be seen. Other than a visual response, this could possibly be an involuntary twitching motion due to the sudden change in brightness. This

could be tested by decreasing the intensity of the light gradually and if the response shape changes from uncomfortably bright to dim.

Analysis of results

According to the state-of-the-art research on the different frequency bands of the brain we did in Section 2.4, we expected to see higher energy in beta and gamma bands during light stimuli. The IMFs that was obtained from EEMD proved to be similar to these bands, whereas the mean frequencies of IMF 1 and IMF 2 were close to the frequencies of gamma and beta bands, respectively. As can be seen in the average event-related power in Appendix C, there is an indication that for most of the subjects there is a significant rise in energy in both IMF 1 and 2, in some of the electrodes during stimuli. This seems to be in line with other research [22], where they found increased energy in beta and gamma bands recorded from the visual cortex of a Rhesus monkey in response to visual stimulus. However, in a few subjects, the energy in the beta and gamma range was quite low, and thus seems like the frequency responses from the brain is individual, or is limited by some unknown factor which has not been corrected for.

When examining the results, we noticed, to our surprise, that there were big differences between individuals in terms of recorded EEG activity. Some individuals, such as e.g. *Subject 3*, had a very flat response across all electrodes, as seen in Figure A.3. As a contrast to this, some subjects, such as *Subject 5* and *Subject 7*, seemed to have a more intensified response locally on a single electrode, *O1* and *Oz*, in Figure A.5 and A.7, respectively.

Looking more closely at the different response for each of the distinct colors, it also seems that the response is quite individual there as well, even though there is a trend across most participants, as stated in Section 4.3. A few of the subjects, such as *Subject 10*, appear to have a limited frequency response, as seen in Figure B.10. We cannot be confident in what causes this, but an hypothesis is the fact that the subject was the one taking the experiments, and was being exposed to the colors in for the 10 hours it took to record, and thus being used to the experience.

The power figures in Appendix D shows the change in energy from the sum from IMF

1 and 2, and then normalized. There seem to be a slight phase delay of the increase in power from red light stimuli, as compared to green and blue. However given the number of events per color this data is based on, we do not have a too high confidence in these results, as explained why in Section 5.2.

It can also be observed a distinct pattern that seems to be repeating for a subset of the subject pool, which can be seen in the Hilbert spectrum plots that is listed in in Appendix B. There is a trend that when the center of energy for each response in red and blue light lines up with each other, the bandwidth of the responses from red light seem to be higher, as can be seen in Figure B.1, B.2, B.5, and B.7. In contrast to this, the other subset have a smaller frequency bandwidth for the red light, and for them it can be seen that all three color responses have unique frequencies, as can be seen in Figure B.8 and B.9. This is only a pattern that we recognized, and we cannot conclude anything from this, other than that the responses seems to be categorized across individuals.

There are other factors we have not taken into account, such as state of mind, tiredness and alertness. All subjects was asked to focus on the lights, but the statistical significance of how much this affects the results is not tested. This however would require a different experimental paradigm and a much larger subject pool to give conclusive results. Another interesting observation that was made was that the subjects that had a dominating 10 Hz alpha wave during the inactive periods seemed to respond less to the light stimuli, as if in a less alerted state. This correspond well to the fact that alpha wave is related to being in a relaxed state of mind, as more thoroughly described in Section 2.4. However, we cannot draw any conclusive statement regarding this topic from our data, as more specific regarding this has to be conducted. Furthermore, initially Wavelet transform was the preferred technique for analyzing EEG data, due to its capabilities regarding good qualitative energy plots. However, due to the fact that the frequencies of interest are in the higher region in this research, Wavelet transform is not adequate. This is because Wavelet plot seemed to be biased towards the energy from the lower frequencies, and neglect the energy from the higher frequencies. This made us consider utilizing other methods for analyzing. As stated in 1.3, the EMD outperforms other techniques, and was therefore the obvious choice as the analyzation technique.

In the preliminary data, we had some appearance of mode mixing between different IMFs.

This was solved by utilizing EEMD to extract IMFs, instead of the standard EMD. We were successful in eliminating mode-mixing from the IMFs by choosing the correct parameter choices for the standard deviation of the applied white noise, as well as the number of ensembles.

As observed in Figure 4.6, there is a trend towards different frequency responses for each of the primary colors, in which the data generated for this plot was extracted by visually inspecting each of the plots in Appendix B. Retrieving the mean frequency of the actual IMFs from an active light period, is shown in Figure 5.1, shows that the results have a similar trend as in Figure 4.6, but with a high variance, which signifies that it is not statistically significant. Looking at Table 4.1, we see that the mean frequency of IMF 0 and 1 both lies in a higher range than shown in the spectrum plots. This means that the components shown in the spectrum plots that lies above 30 Hz are possibly blended with IMF 0 and 1, or that these synchronization events above 30 Hz are spikes that happen as short events in time. The problem with these presumably short changes in synchronization frequency and the current implemented EEMD algorithm is as explained in Section 2.9, which is that the result are not strictly IMFs and causes artifacts when the Hilbert Transform is executed on them. These artifacts are then removed by a short kernel median filter, which will also remove these events.

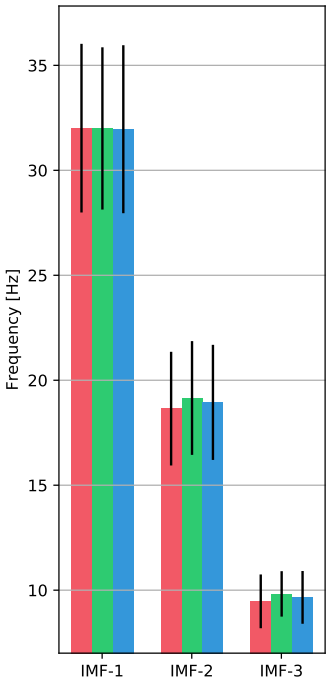

Figure 5.1: Color comparison for each IMF with each bar in the corresponding RGB color

In terms of visualization, steps were made to ensure that the most vital changing patterns in the brain during stimuli, were highlighted. An approach to tackle this was to neglect the slowly varying low frequencies that had high energy, as this low frequency range was not where a response was anticipated. This proved to be a great way to remove the baseline EEG activity, to focus more on the higher frequency brain patterns that changed according to the events.

5.3 Recommendations for Further Work

The experiments that was conducted with hobby grade hardware with a non-invasive measurement system and 8 electrodes. To achieve better resolution and more accurate results, medical grade equipment may be used for the same experiments if more specific precision is needed. Moreover, as mentioned in Section 1.2, the experiments were not conducted in neutral environments. We highly recommend finding a more suitable location for doing EEG experiments, as it could greatly improve the the recorded data and get rid of a lot of the power-line noise that needed to be tackled. If doing further work on a light pulse type experiment, shortening the pulse duration from 1.0 second to less than 0.5 seconds might be beneficial. This is due to the fact that the response during the light pulse had the same characteristics as the steady-state response.

Looking at the phase shift of the synchronization evoked by red, blue, and green light might be a possible vector for a signature for each of the colors. As seen in the figures in Appendix D, there seem to be slight differences for each of the colors in response to the corresponding light, where it could be underlying responses that could be individually classified.

Increasing the number of events per experiment is also recommended, with the observation of nominal brain activity is reestablished after approximately 2 seconds, granting the possibility of having events of visual stimuli much closer than what is achieved in this thesis. Moreover, as stated in Section 4.3, we obtained good results from the frequency responses, as seen in Appendix B. In light of this, we highly recommend utilizing the difference in frequency response between the colors as a classification signature.

As argued in Section 5.2, because of the way HHT is implemented in this thesis, a median filter is required to remove the artifacts that are generated. This will also remove important changes in the data. As the basic EMD functionality was implemented as a NDA, it cannot be shared. Future work should then be focused on developing a EEMD algorithm that is open to use, and which can be iteratively improved on. As proposed in [35], post-processing the resulting signals obtained by EEMD can be run through EMD to extract the strict IMFs. This would benefit the Hilbert Transform and result in less to none artifacts in the instantaneous amplitude and frequency data. It can also be mentioned

that EEMD takes a lot of time to compute. This issue can be mitigated by using other approaches to handle mode-mixing, such as using EMD along with a masking signal, as proposed in [44].

Appendix A

Hilbert Spectrum

The following appendix contains Hilbert spectrum visualization for each of the subjects. Energy is visualized as a colorbar ranging from bright yellow (weak), to dark purple (strong). Interval for x-axis is set to 500ms before stimulus to 1 second post-stimuli. Dashed grey lines represents the stimulus onset (first line) and the stimulus offset (second line). The 7 first IMFs are plotted across each of the electrode channels and for each of the RGB colors. The scales are individually chosen to highlight the main response to the stimulus for each subject.

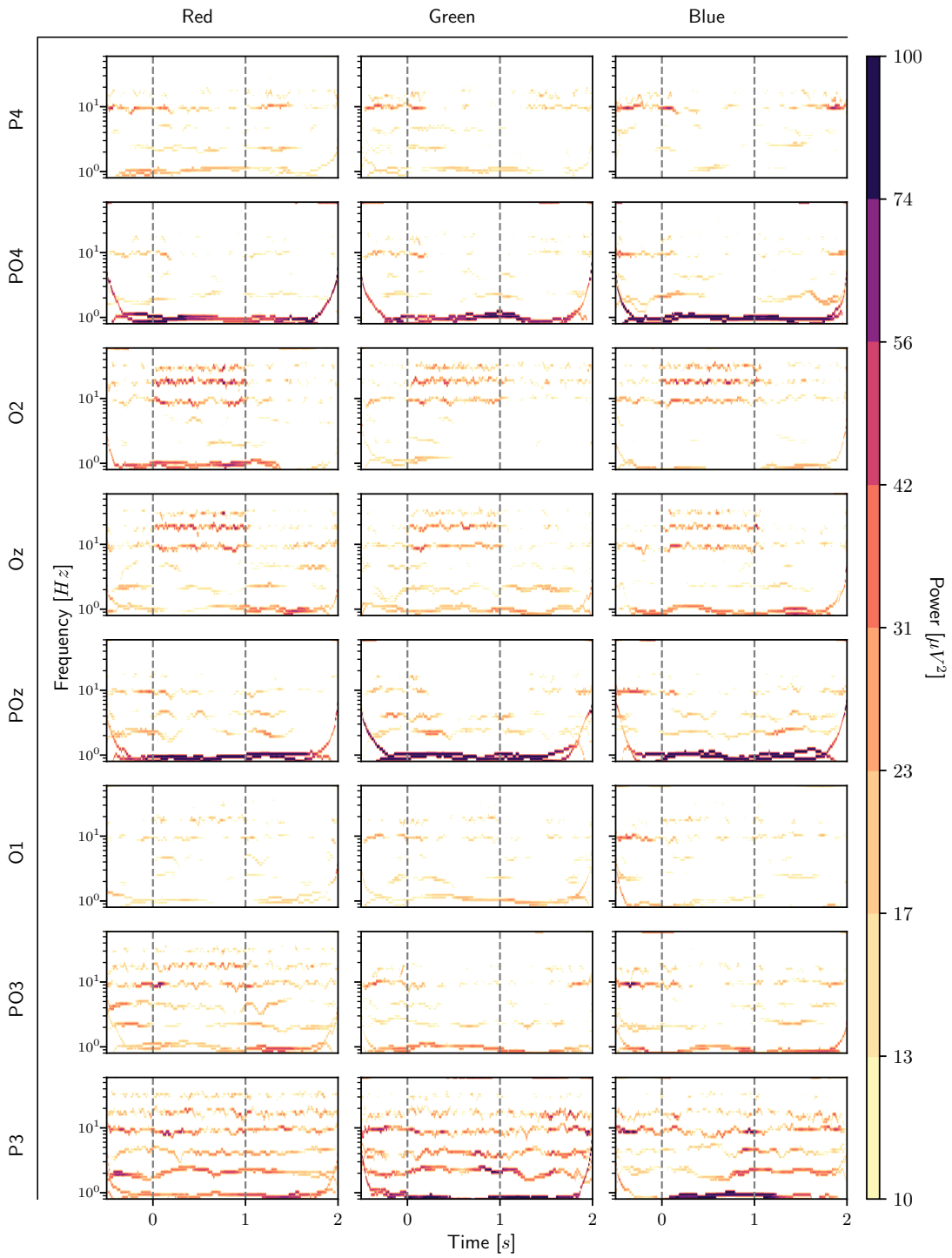

Figure A.1: Hilbert spectrum visualization for ***Subject 1***.

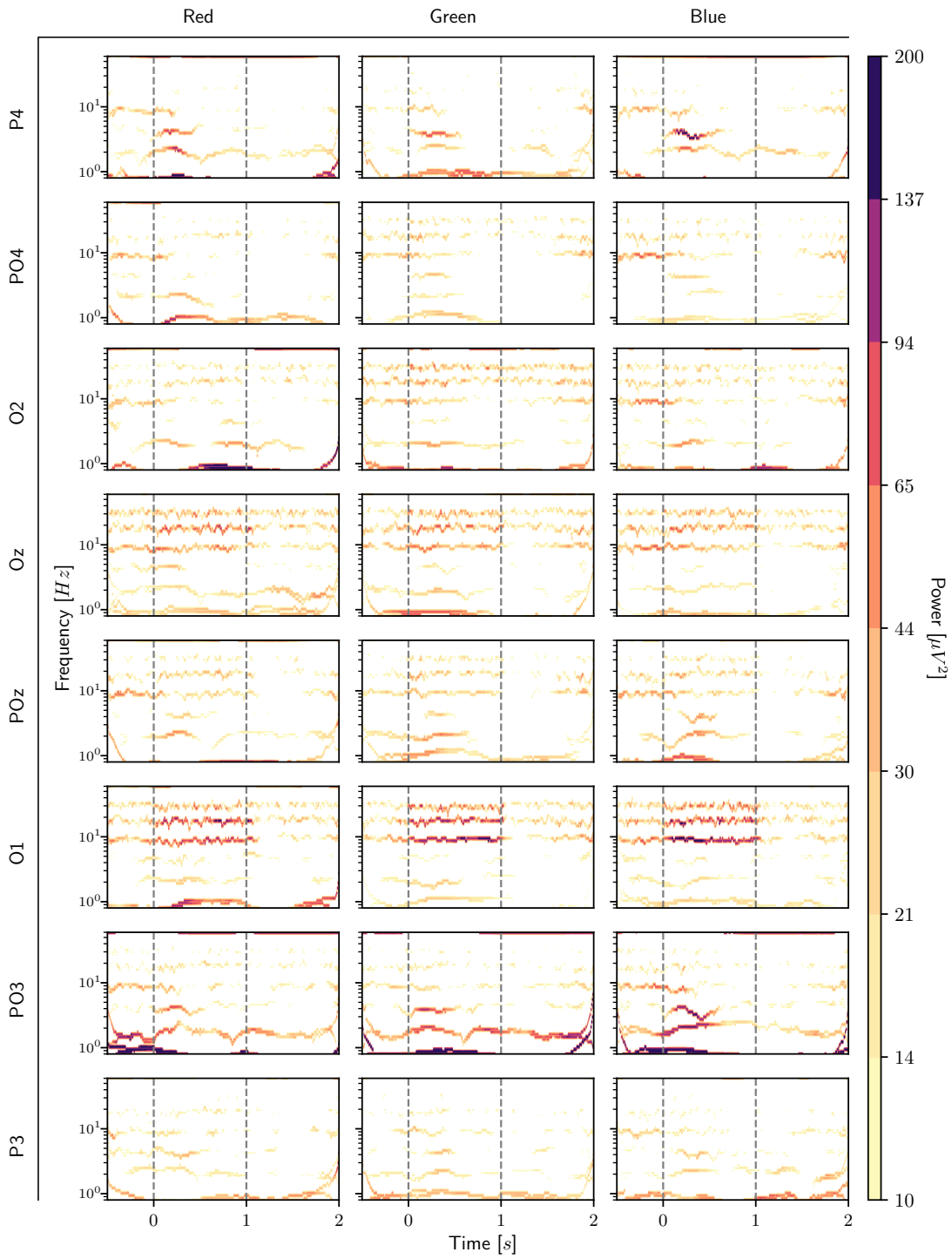

Figure A.2: Hilbert spectrum visualization for ***Subject 2***.

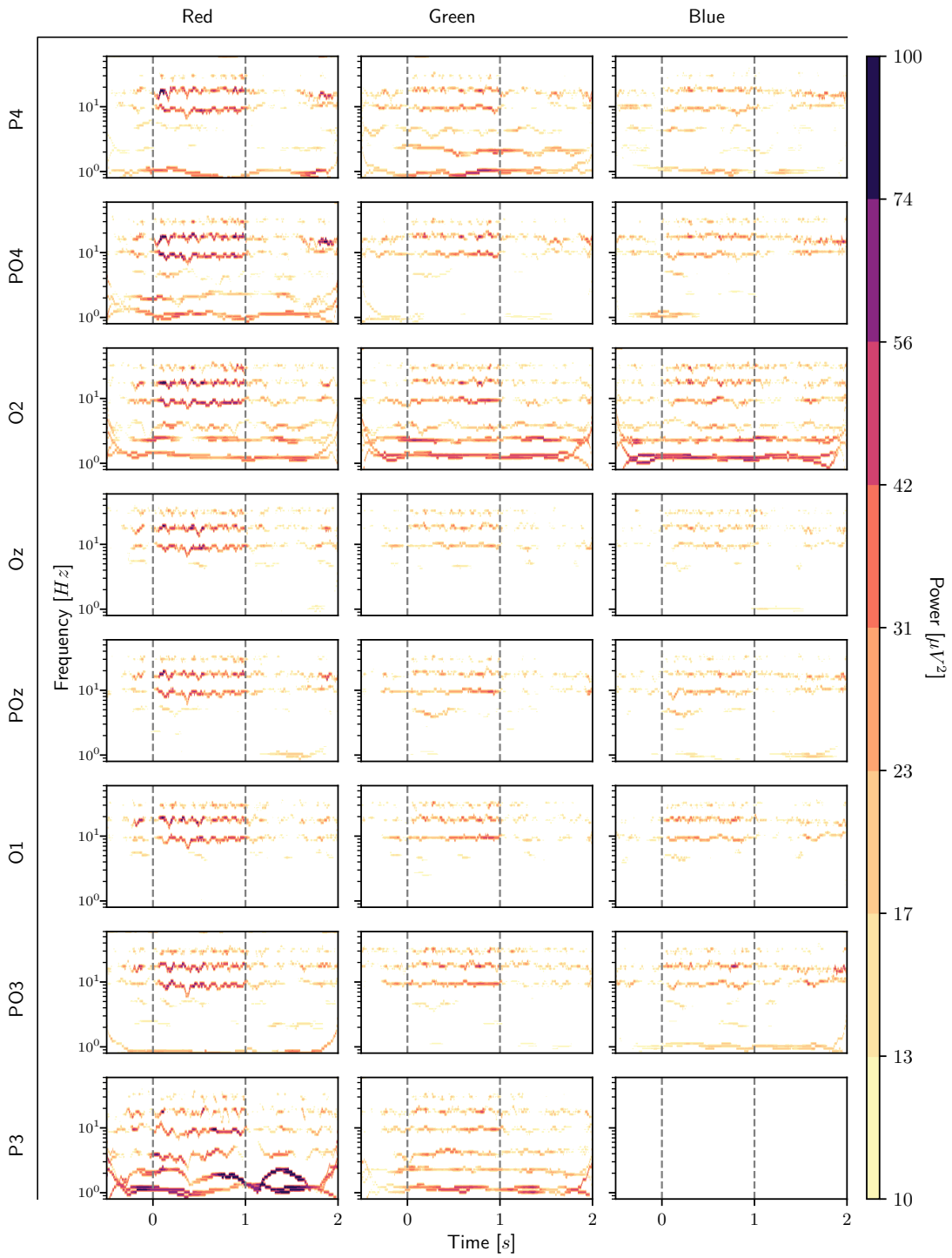

Figure A.3: Hilbert spectrum visualization for ***Subject 3***.

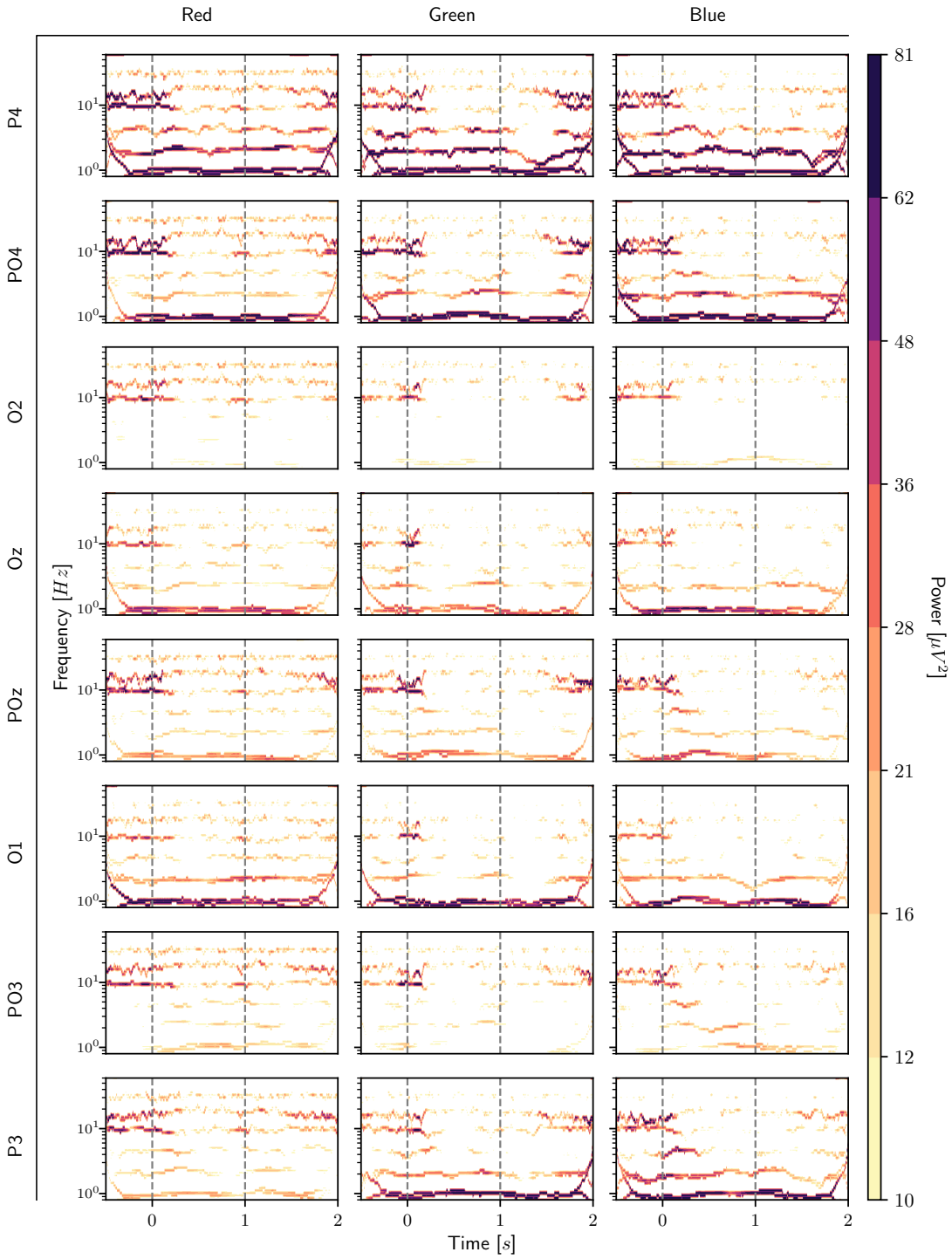

Figure A.4: Hilbert spectrum visualization for ***Subject 4***.

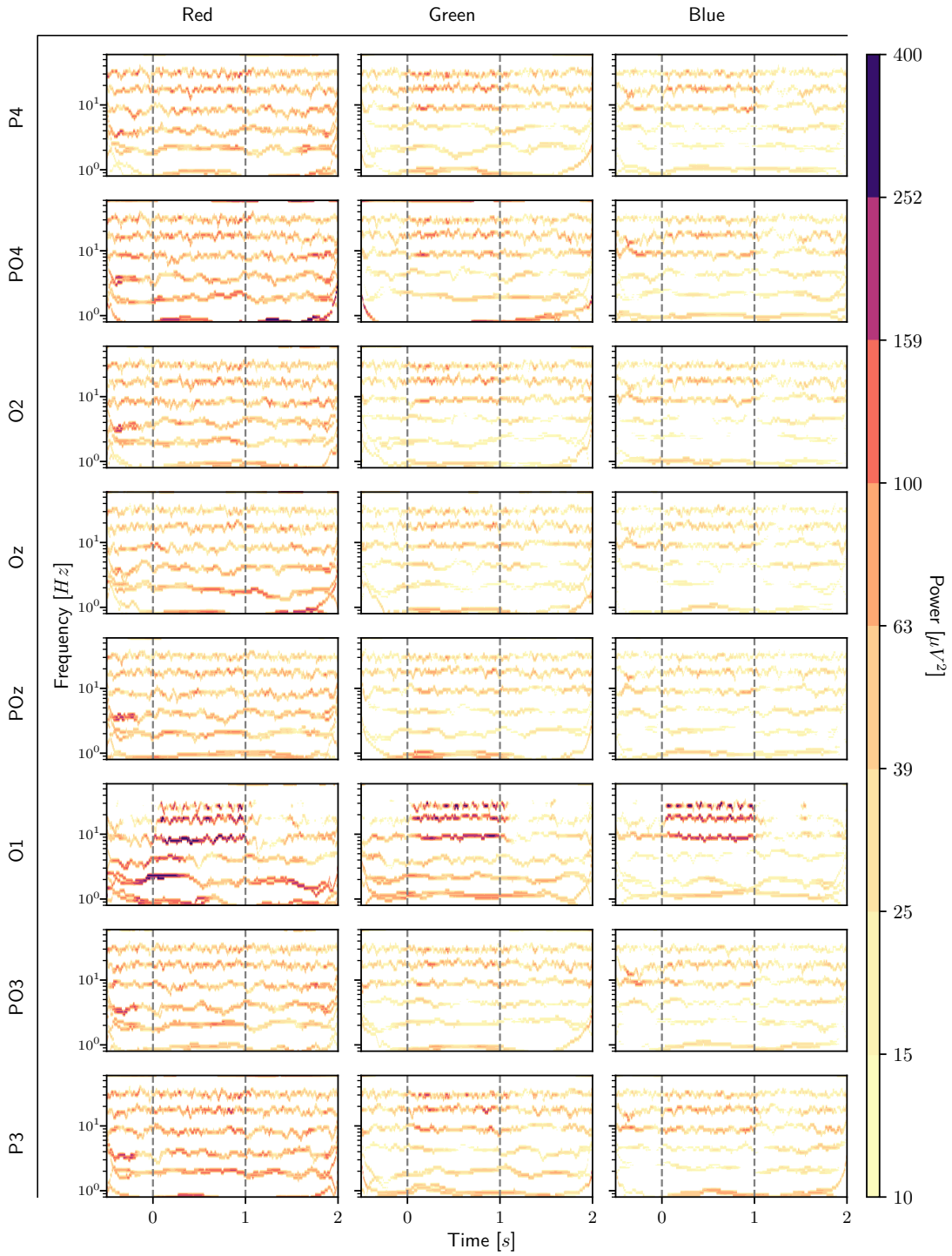

Figure A.5: Hilbert spectrum visualization for ***Subject 5***.

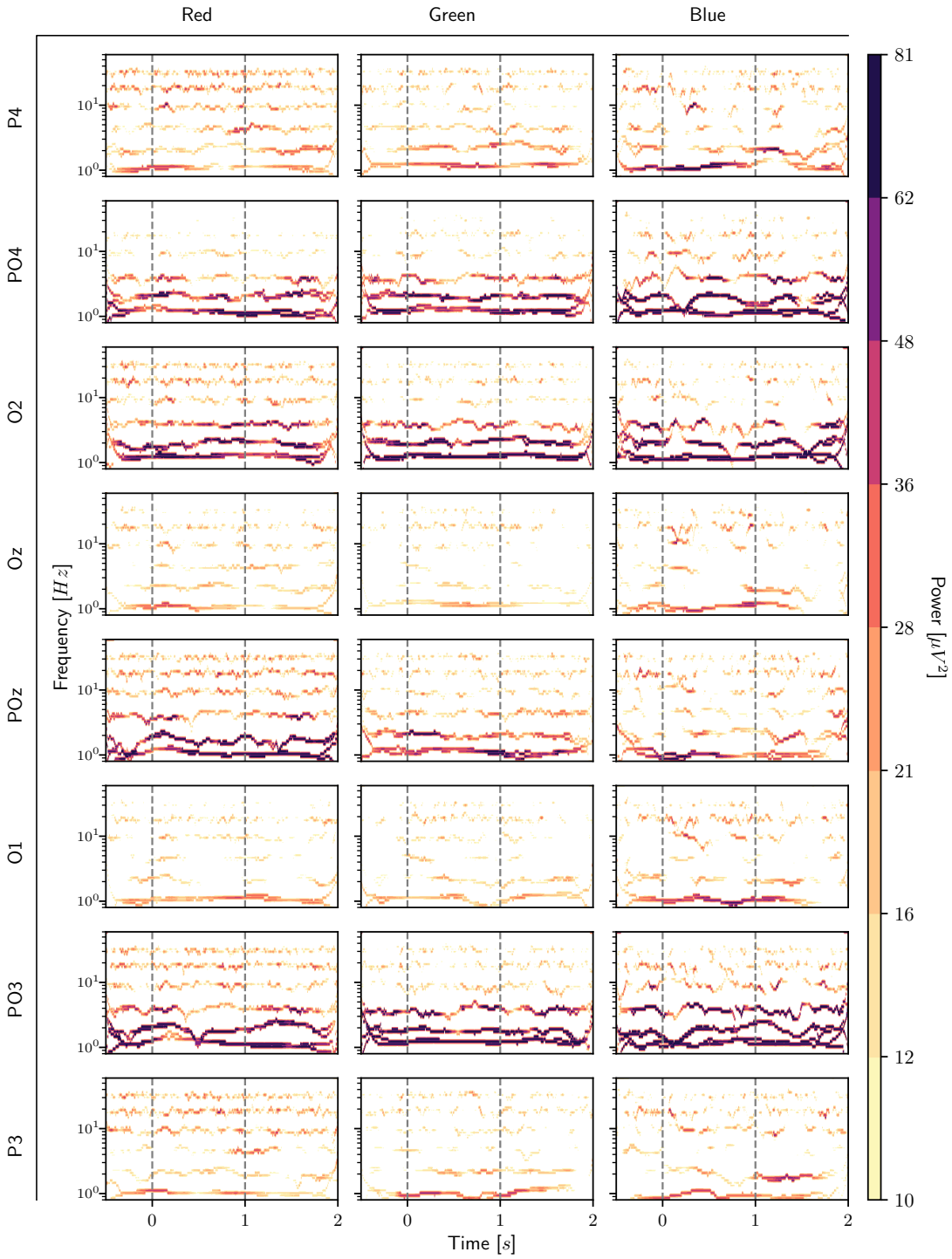

Figure A.6: Hilbert spectrum visualization for ***Subject 6***.

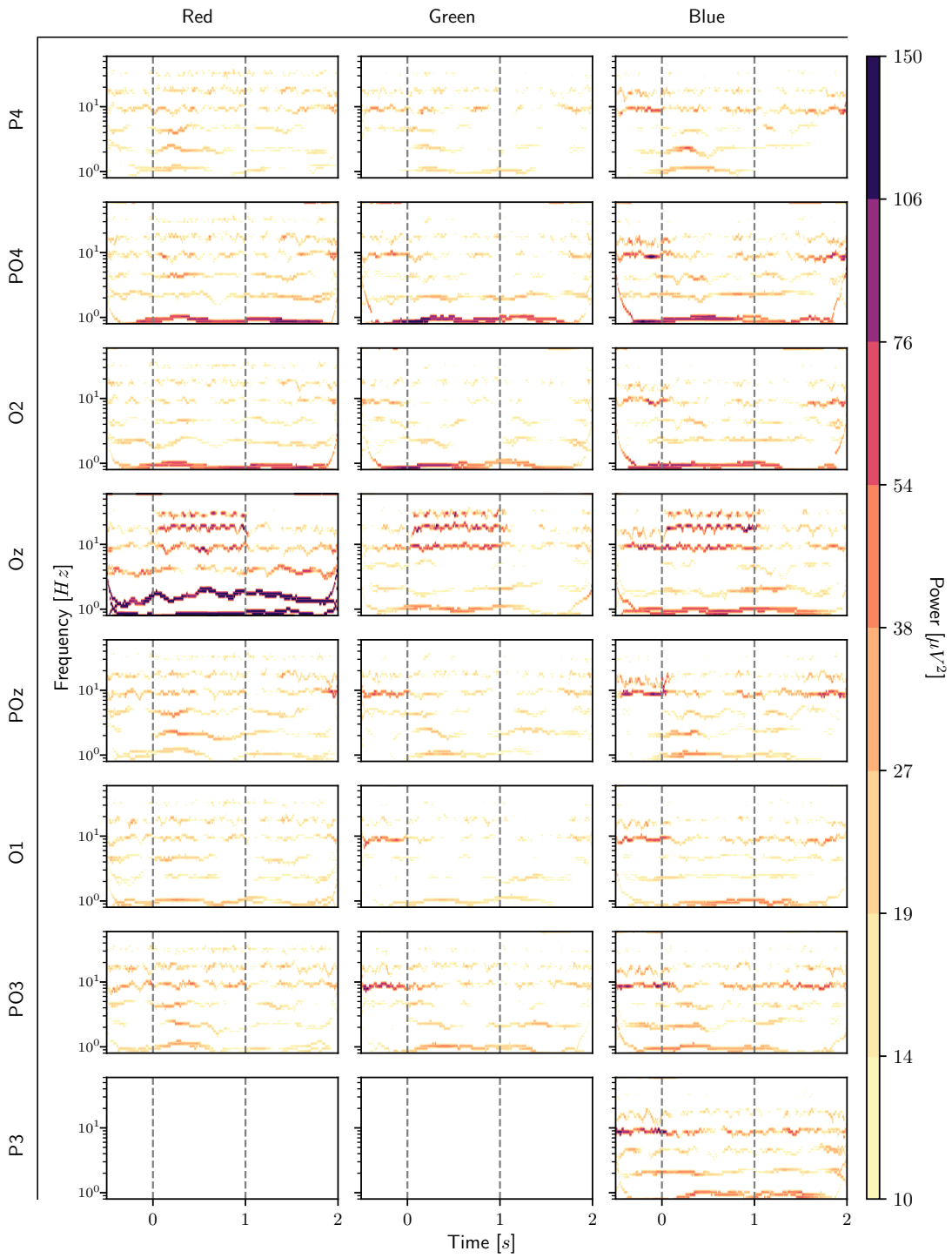

Figure A.7: Hilbert spectrum visualization for ***Subject 7***.

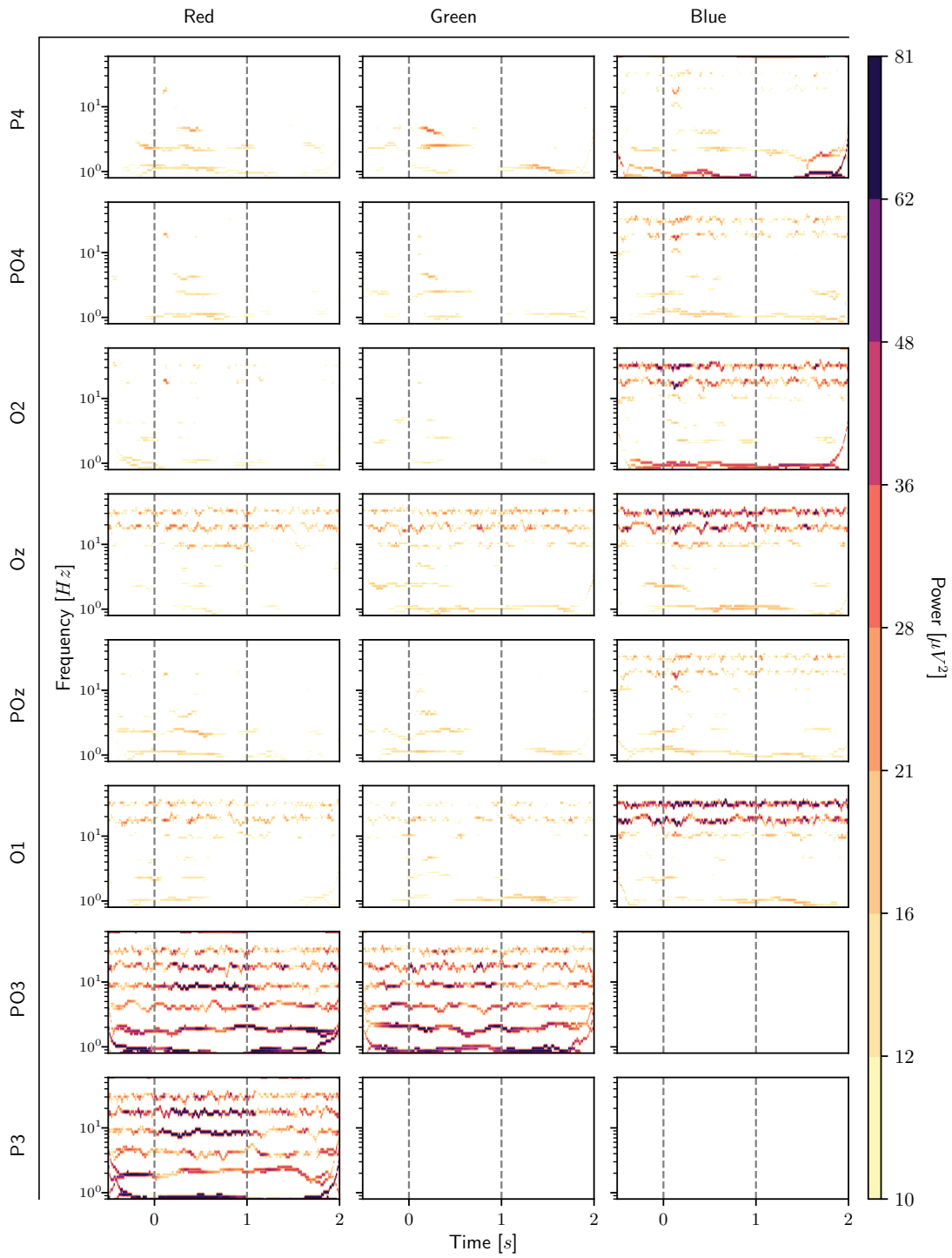

Figure A.8: Hilbert spectrum visualization for ***Subject 8***.

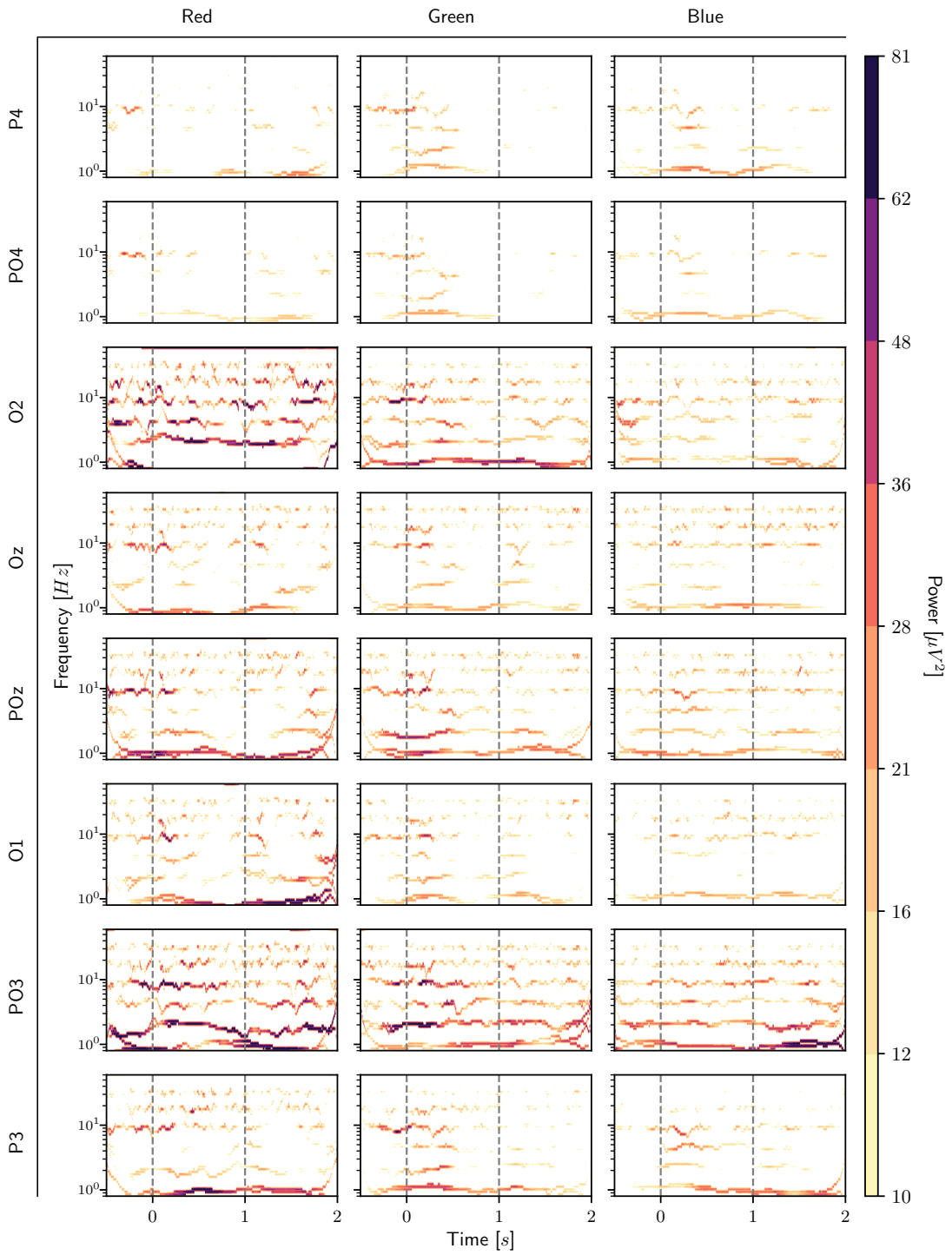

Figure A.9: Hilbert spectrum visualization for ***Subject 9***.

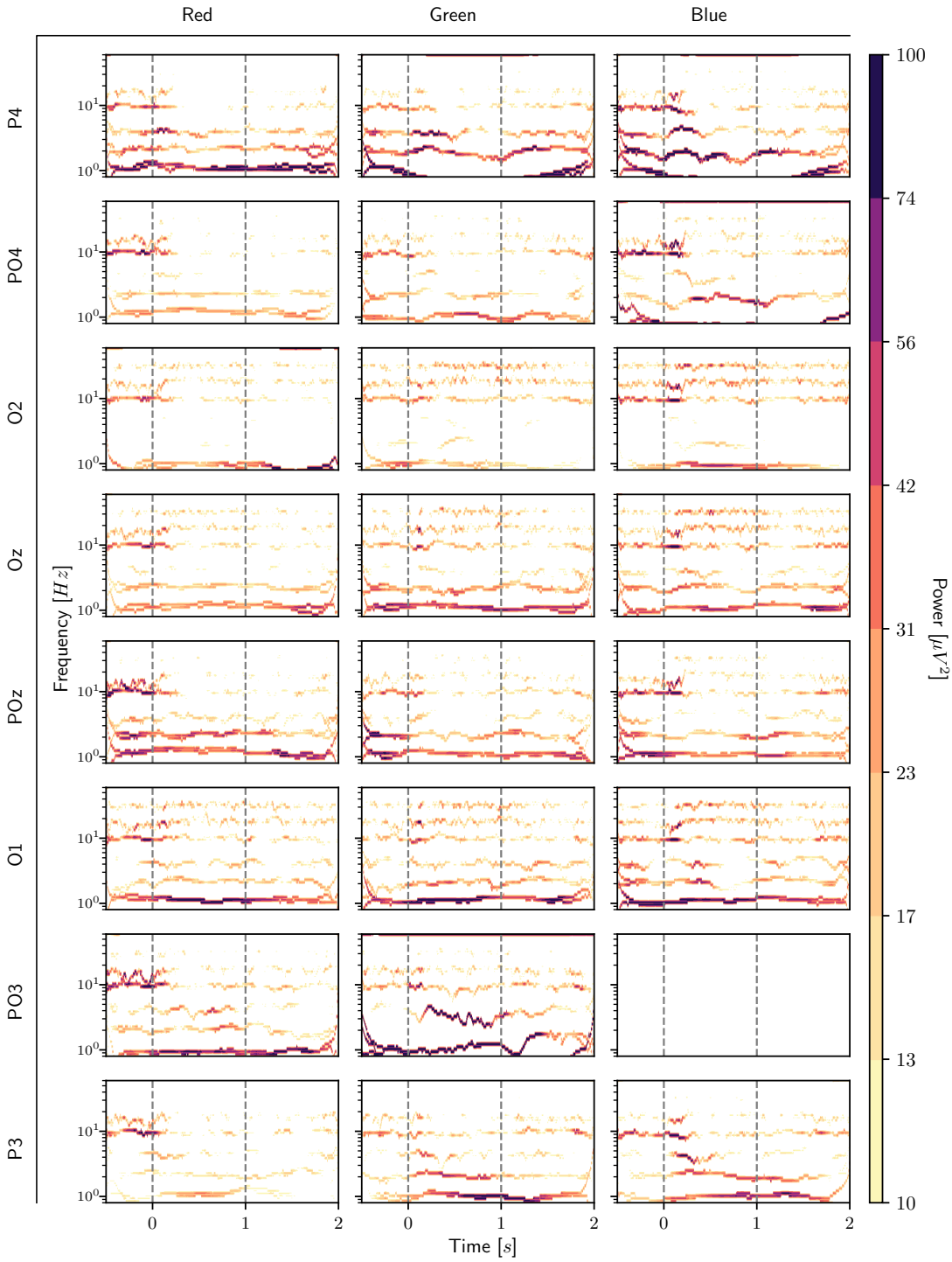

Figure A.10: Hilbert spectrum visualization for ***Subject 10***.

Appendix B

Spectral response for steady-state experiment

The following appendix contains frequency response plots, visualized by Fast Fourier Transform (FFT). The spectral information is gathered from 16 seconds of event data (marked in the corresponding colors) and 16 seconds of non-event data (marked in black). The first subplot is for the color red, the second for color green and the last for color blue.

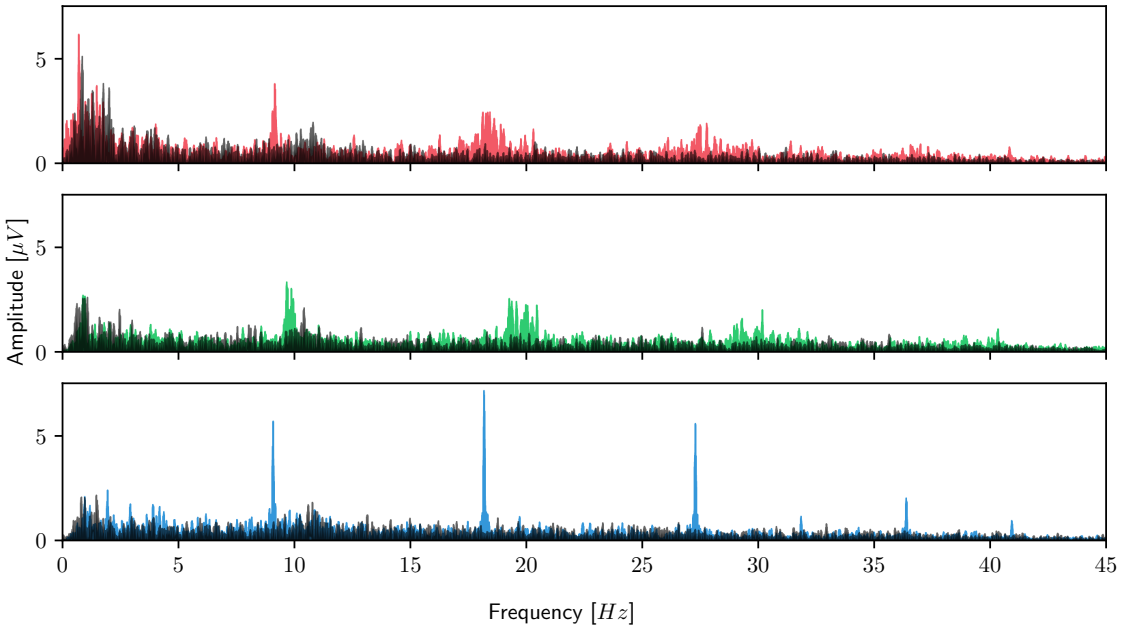

Figure B.1: Spectral information on channel ***O2*** for ***Subject 1***.

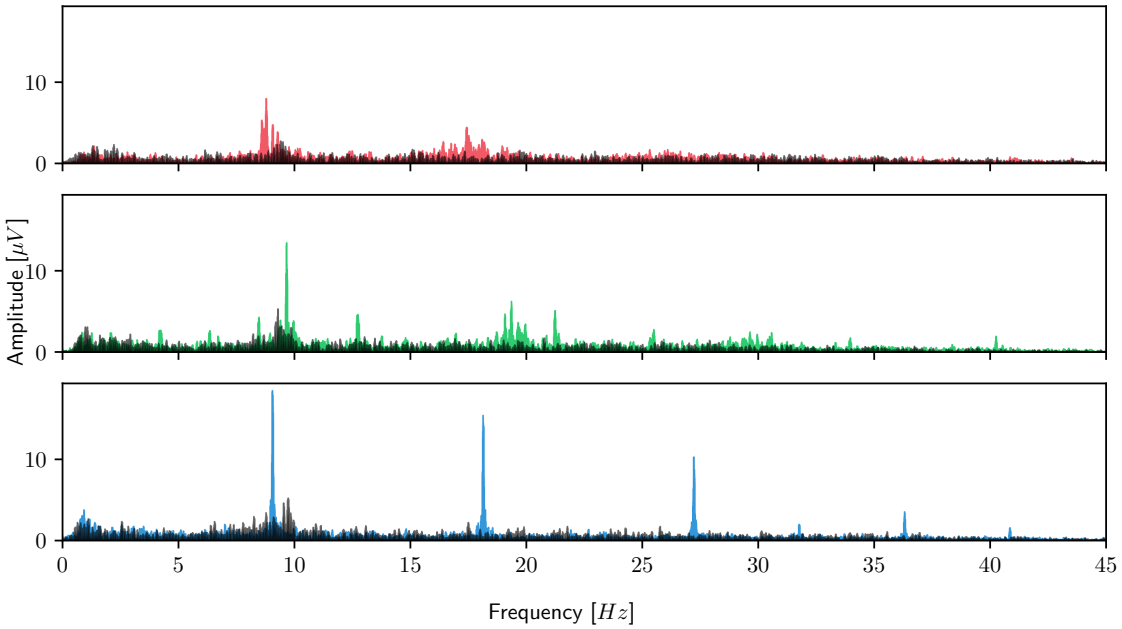

Figure B.2: Spectral information on channel ***O1*** for ***Subject 2***.

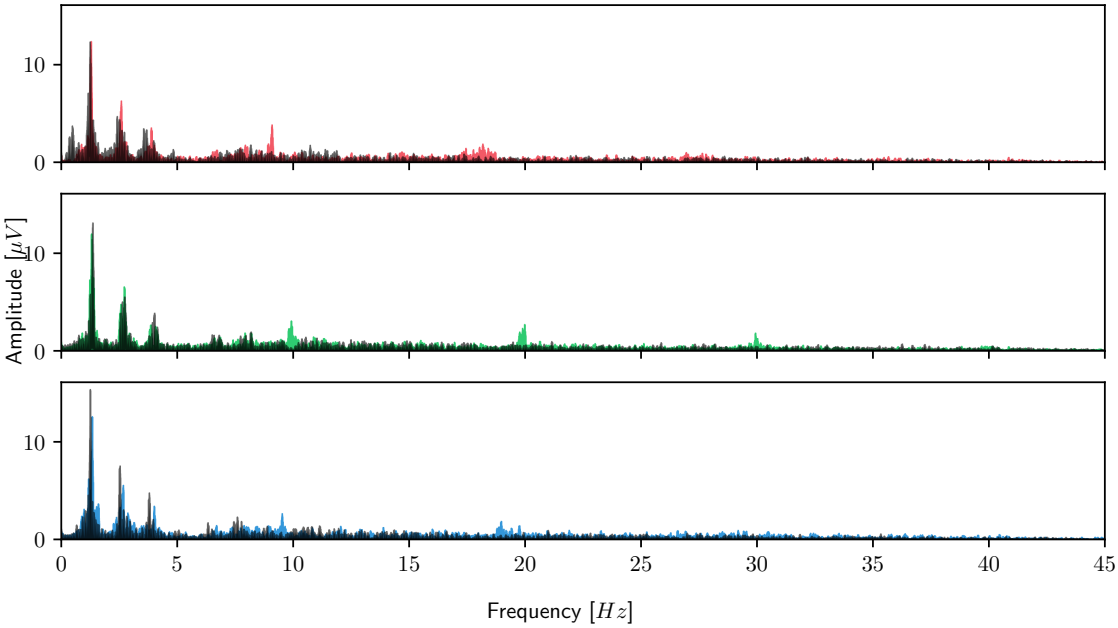

Figure B.3: Spectral information on channel ***O2*** for ***Subject 3***.

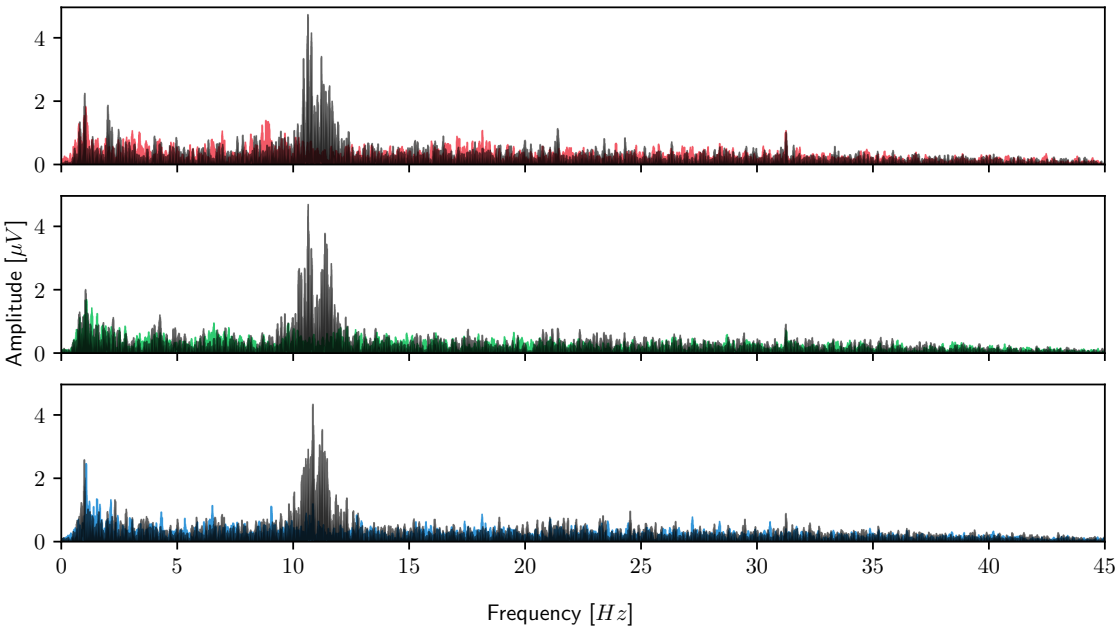

Figure B.4: Spectral information on channel ***O2*** for ***Subject 4***.

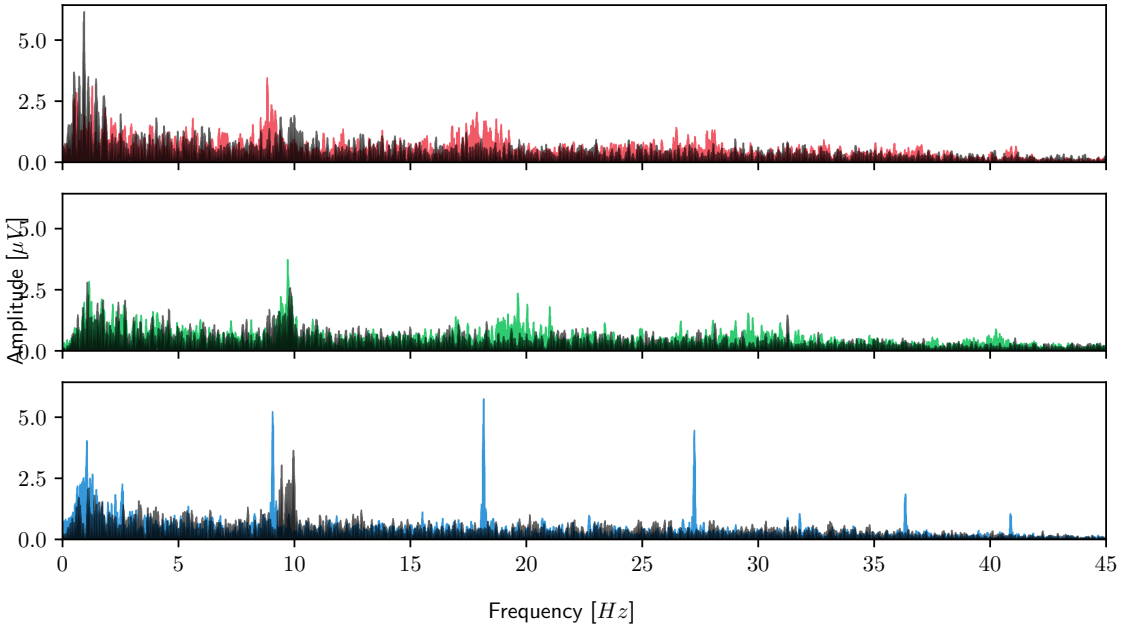

Figure B.5: Spectral information on channel ***Oz*** for ***Subject 5***.

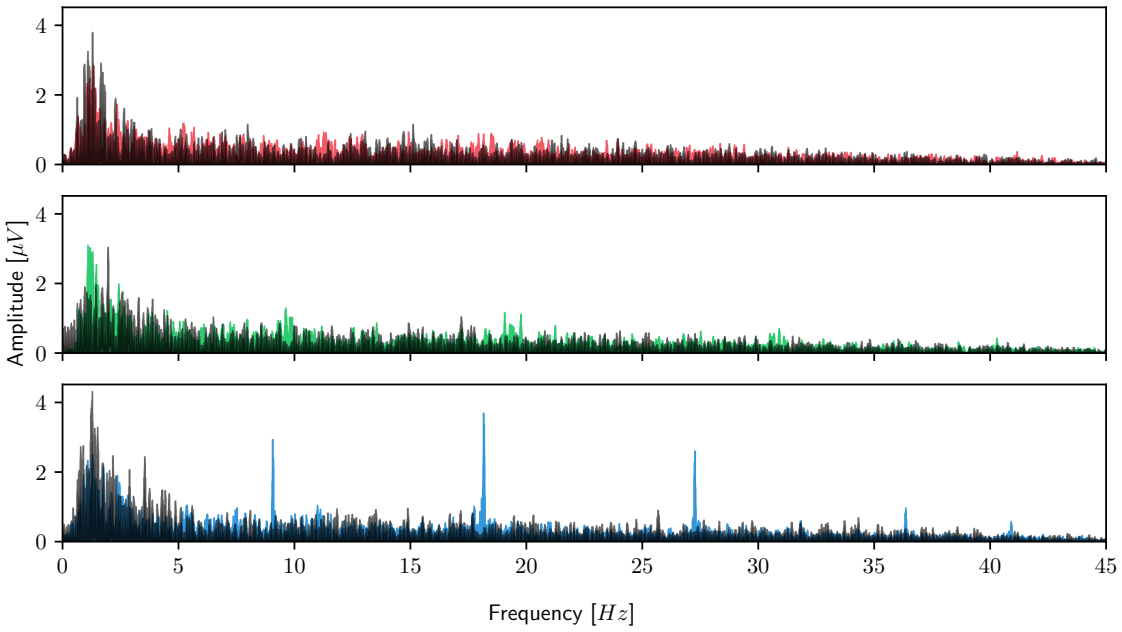

Figure B.6: Spectral information on channel ***Oz*** for ***Subject 6***.

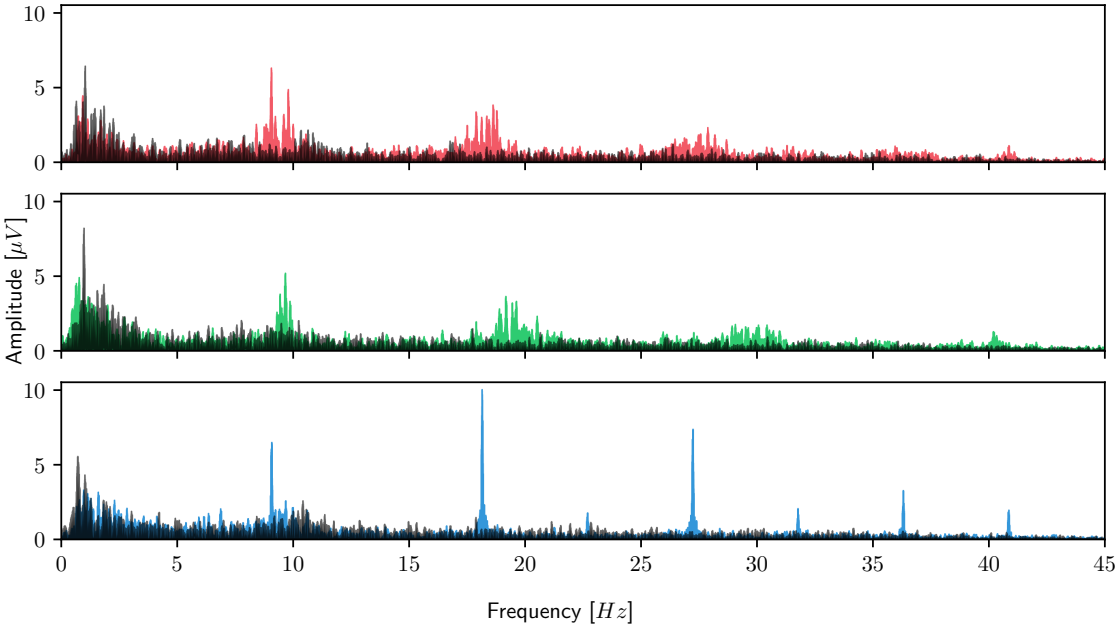

Figure B.7: Spectral information on channel ***Oz*** for ***Subject 7***.

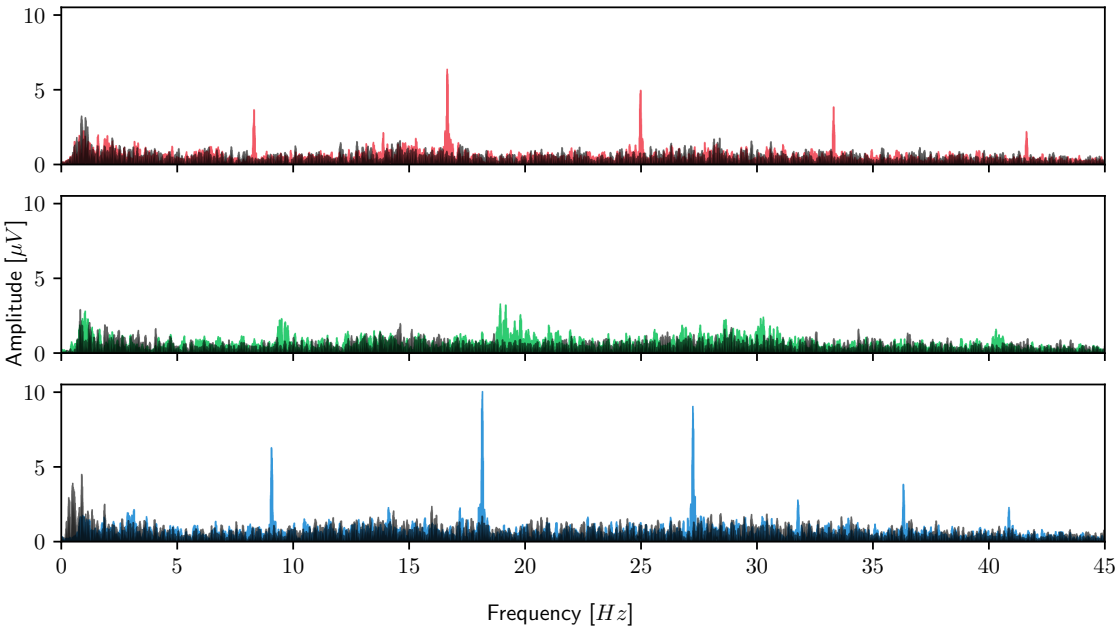

Figure B.8: Spectral information on channel ***Oz*** for ***Subject 8***.

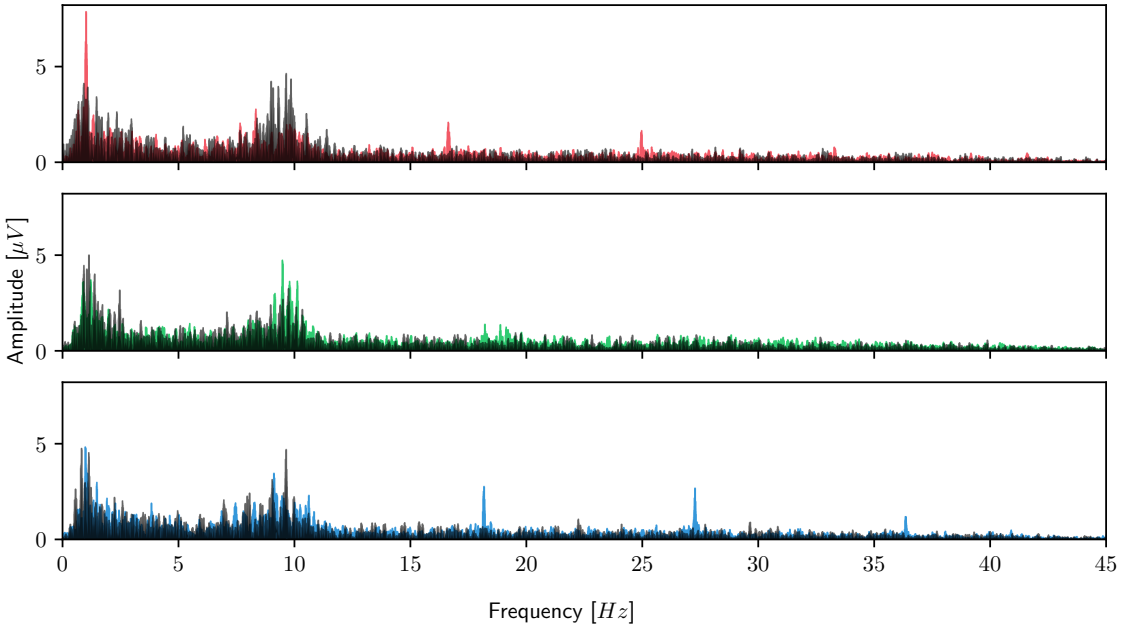

Figure B.9: Spectral information on channel ***POz*** for ***Subject 9***.

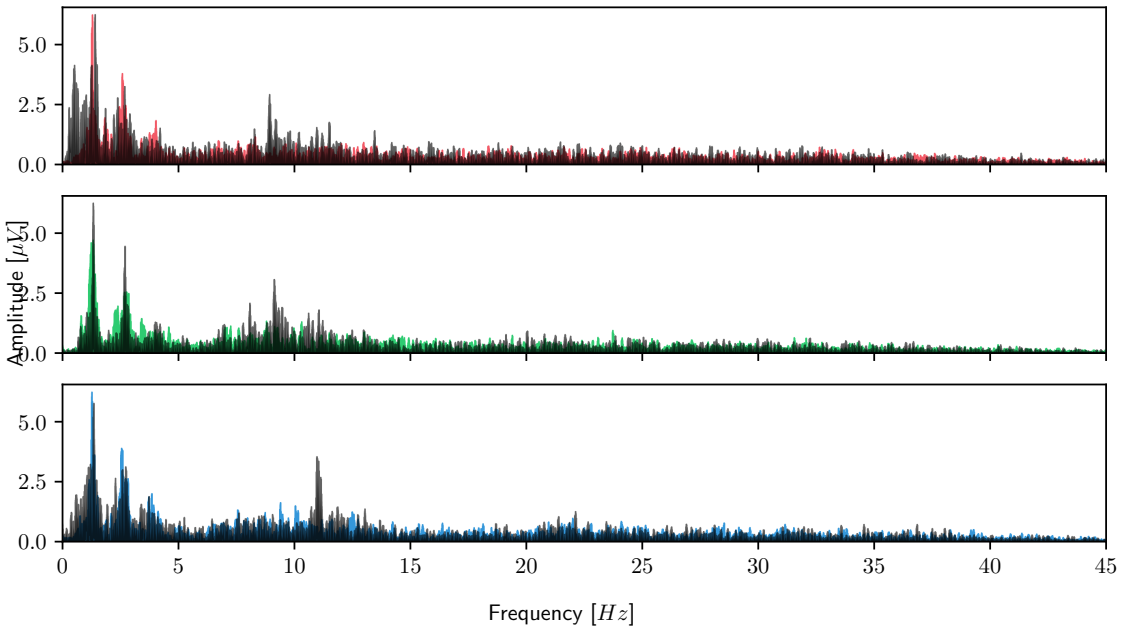

Figure B.10: Spectral information on channel ***Oz*** for ***Subject 10***.

Appendix C

Event-related power in IMF 1 and 2, per channel

The following appendix contains histogram plots, which shows difference between power during stimulus (marked in orange) and power in periods with no stimulus (marked in yellow). It includes the energy from~30Hz component and ~16Hz component, which is IMF 1 and IMF 2 respectively. The plots are presented with a distribution of all the different electrode channels and with a separate plot for each of the RGB colors. The desired level of the confidence interval is set to 95%, also represented as approximately 2σ (two times standard deviation), which is shown as a black line on top of each histogram.

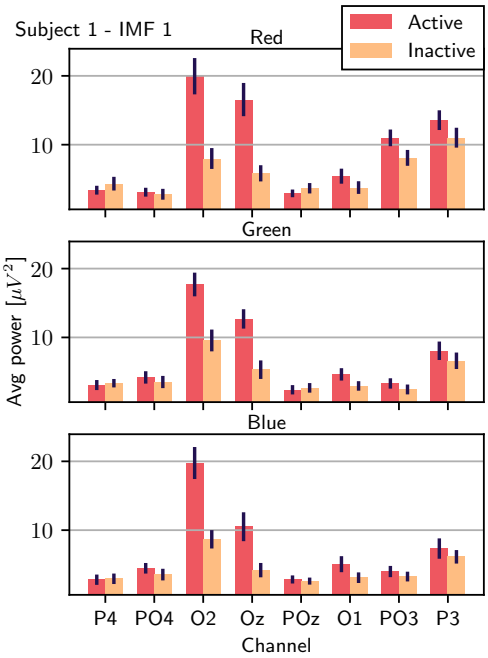

Figure C.1: Event-related power in IMF 1 for ***Subject 1***

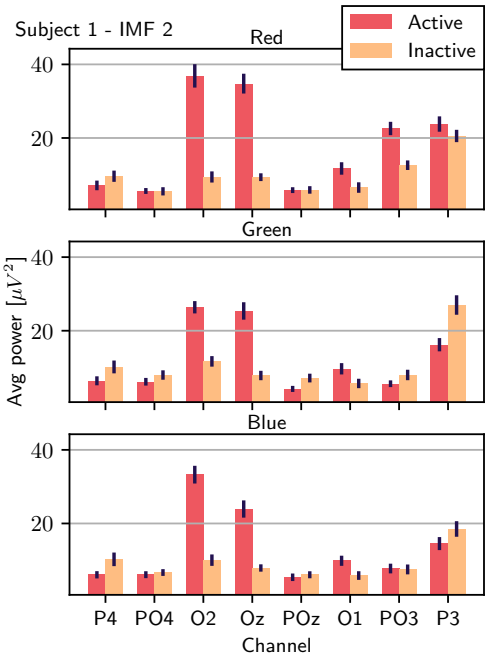

Figure C.2: Event-related power in IMF 2 for ***Subject 1***

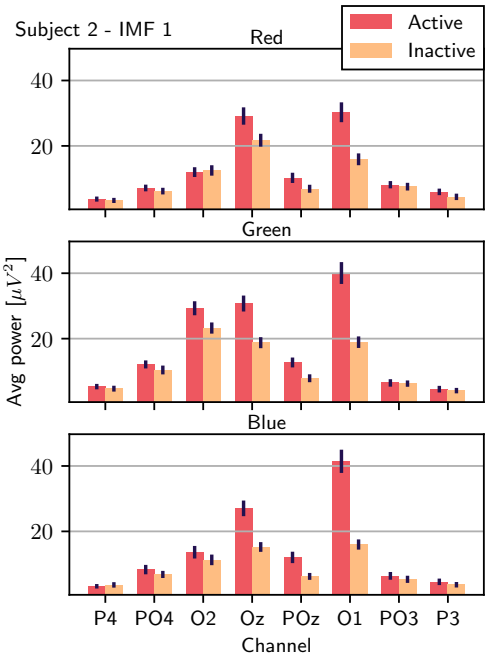

Figure C.3: Event-related power in IMF 1 for ***Subject 2***

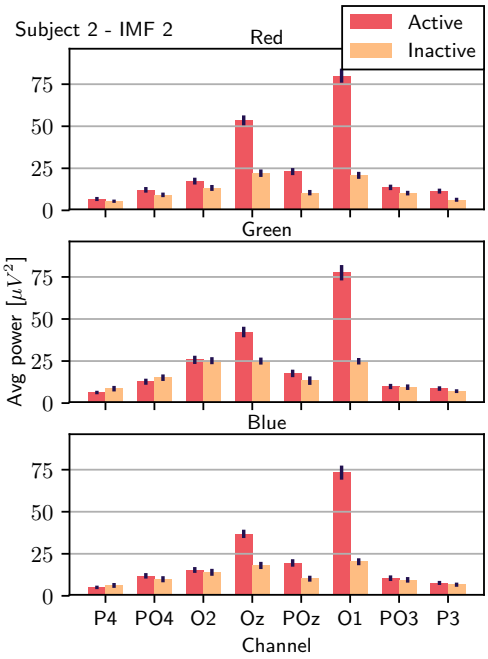

Figure C.4: Event-related power in IMF 2 for ***Subject 2***

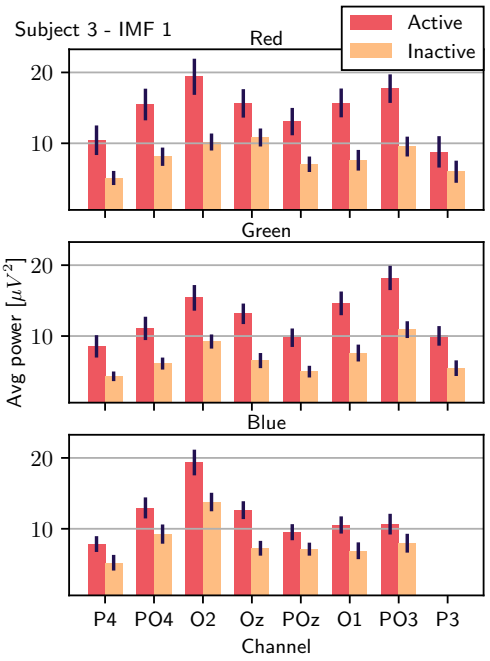

Figure C.5: Event-related power in IMF 1 for ***Subject 3***

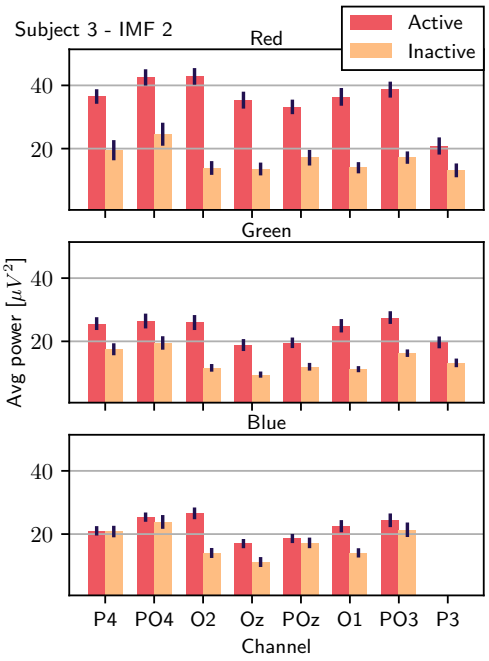

Figure C.6: Event-related power in IMF 2 for ***Subject 3***

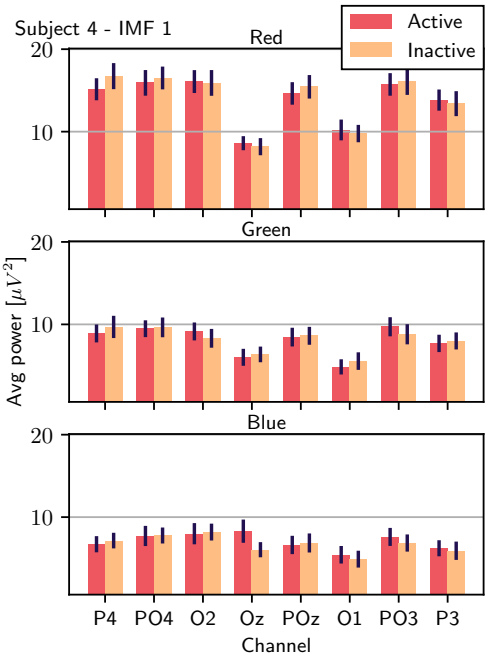

Figure C.7: Event-related power in IMF 1 for ***Subject 4***

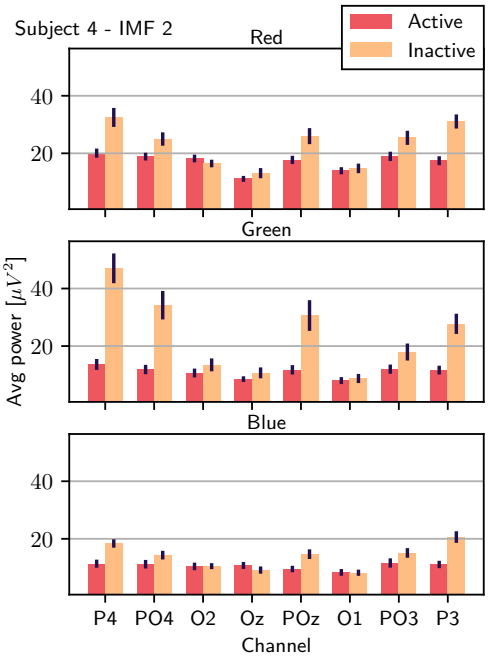

Figure C.8: Event-related power in IMF 2 for ***Subject 4***

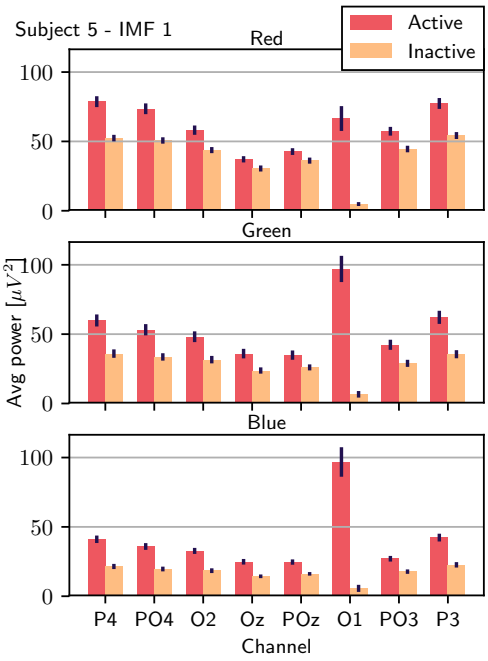

Figure C.9: Event-related power in IMF 1 for ***Subject 5***

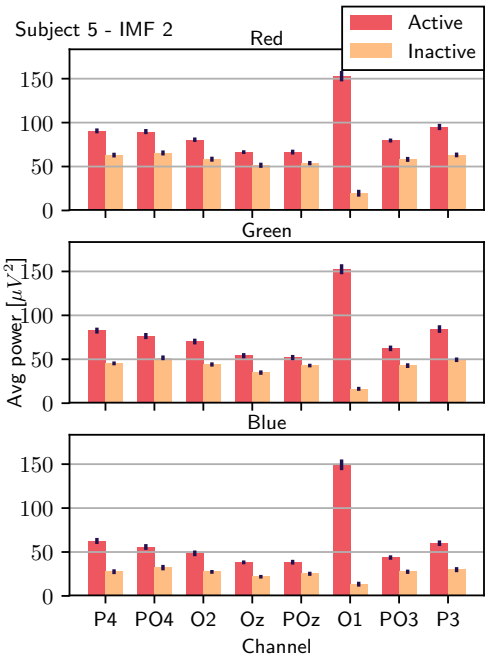

Figure C.10: Event-related power in IMF 2 for ***Subject 5***

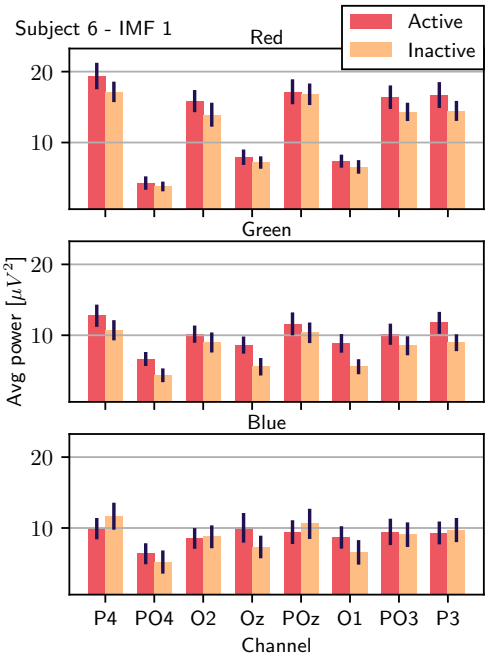

Figure C.11: Event-related power in IMF 1 for ***Subject 6***

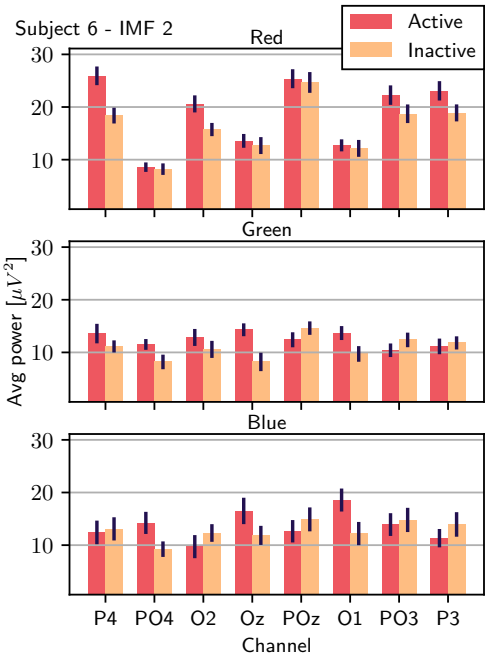

Figure C.12: Event-related power in IMF 2 for ***Subject 6***

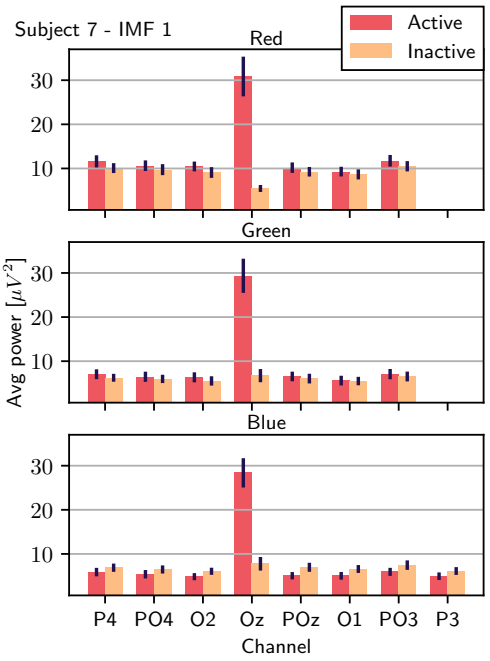

Figure C.13: Event-related power in IMF 1 for ***Subject 7***

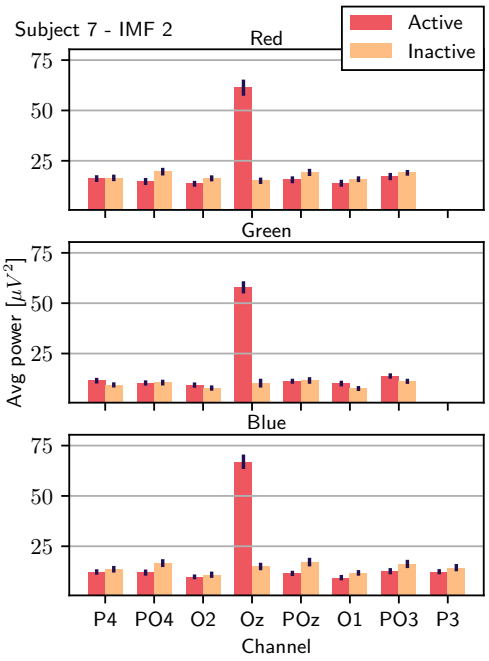

Figure C.14: Event-related power in IMF 2 for ***Subject 7***

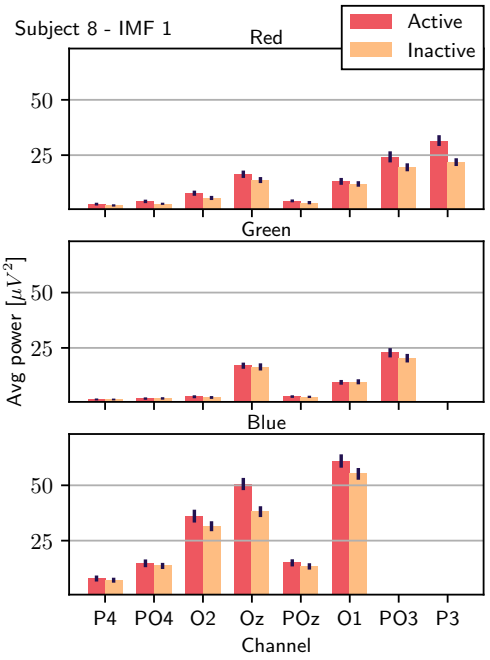

Figure C.15: Event-related power in IMF 1 for ***Subject 8***

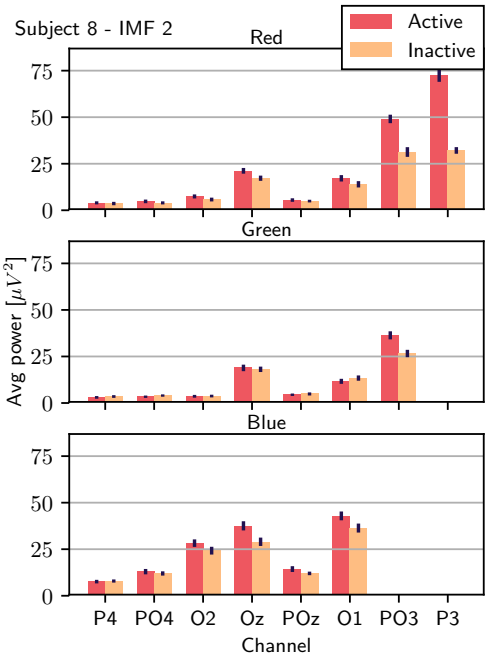

Figure C.16: Event-related power in IMF 2 for ***Subject 8***

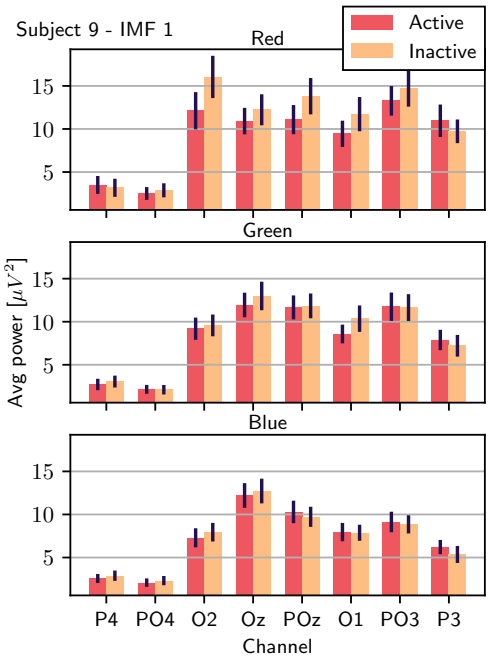

Figure C.17: Event-related power in IMF 1 for ***Subject 9***

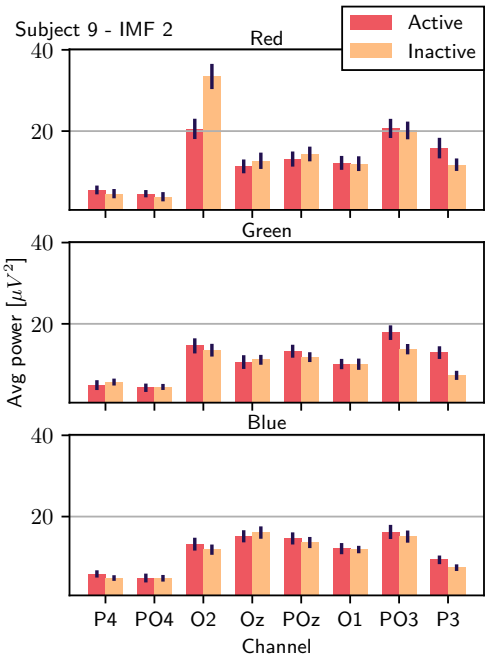

Figure C.18: Event-related power in IMF 2 for ***Subject 9***

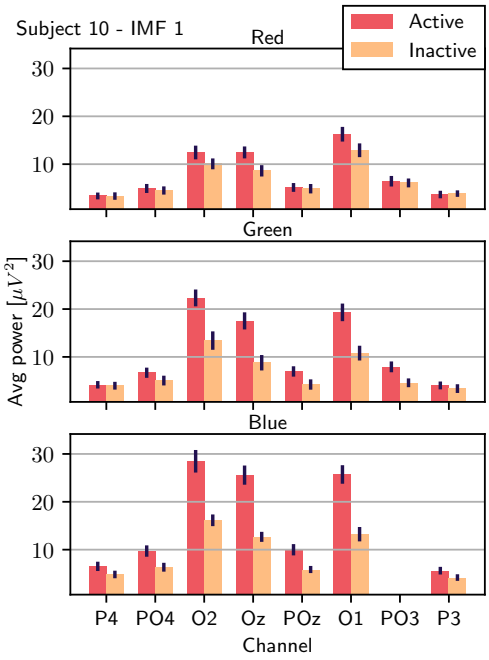

Figure C.19: Event-related power in IMF 1 for ***Subject 10***

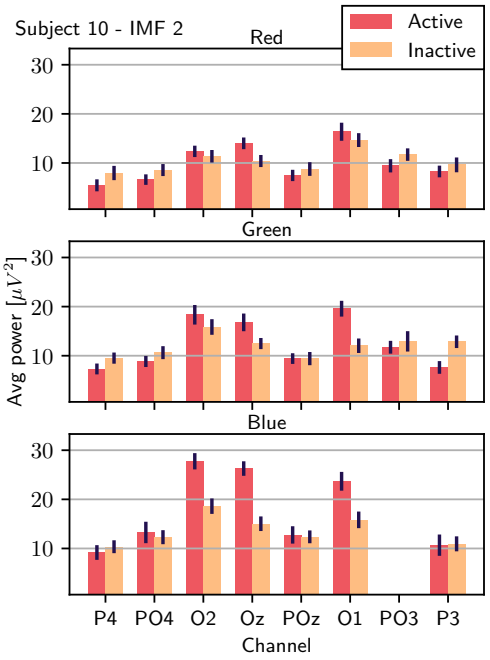

Figure C.20: Event-related power in IMF 2 for ***Subject 10***

Appendix D

Event-related power in IMF 1 and 2, time-series

The following appendix contains time-series plots, which shows the difference of power, before, during and after stimulus. The light stimuli event of 1 second starts at $t = 0.0$ *and ends at* $t = 1.0$ *and the color of the light stimuli event is given by the plot color. The plot is given as the sum of energy from ~30Hz component and ~16Hz component, which is IMF 1 and IMF 2 respectively, and then normalized. Subject 4, 6, 8 and 9 are without a statistical significant difference between active and inactive period, as seen in Appendix C, and is therefore omitted.*

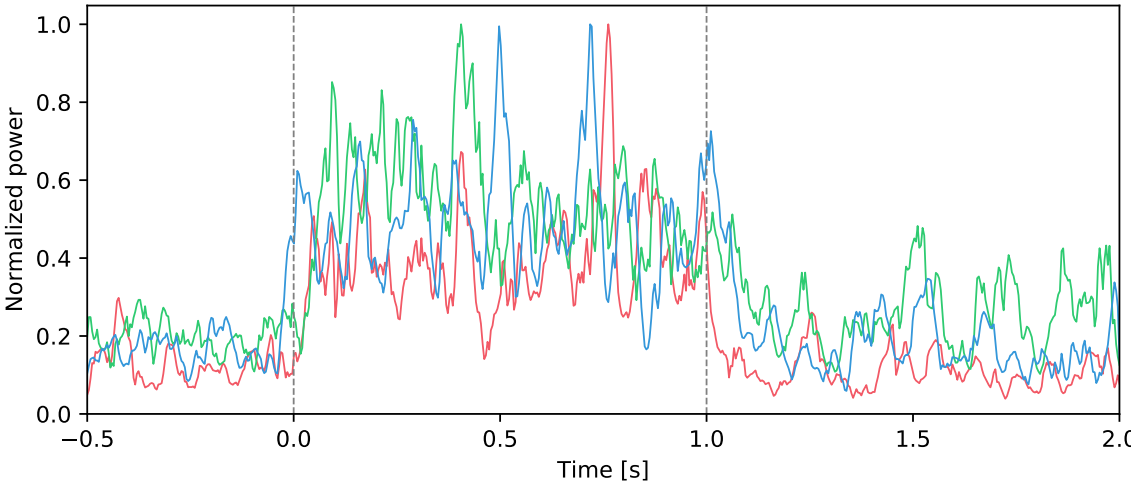

Figure D.1: Normalized power from IMF 1 and 2 on channel ***O2*** for ***Subject 1***.

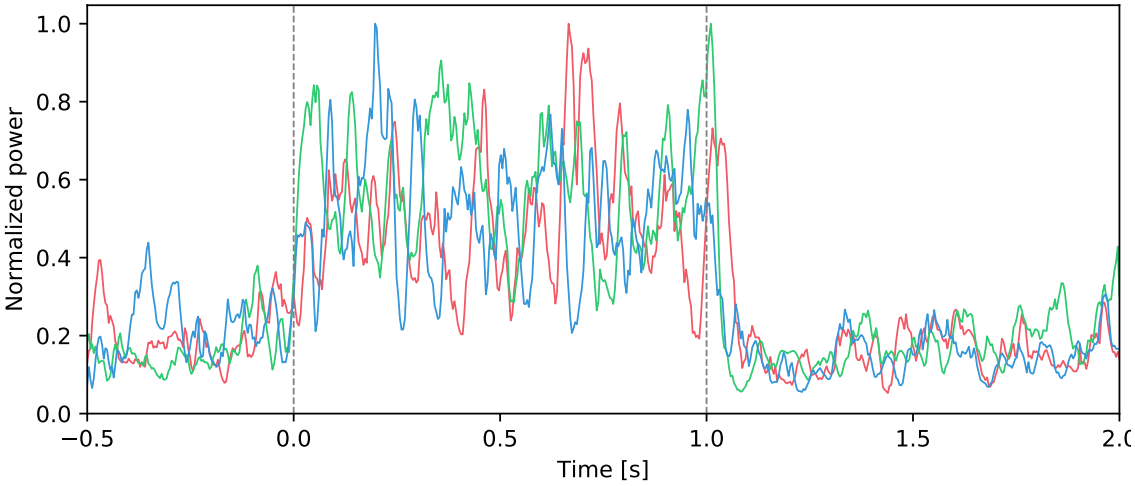

Figure D.2: Normalized power from IMF 1 and 2 on channel ***O1*** for ***Subject 2***.

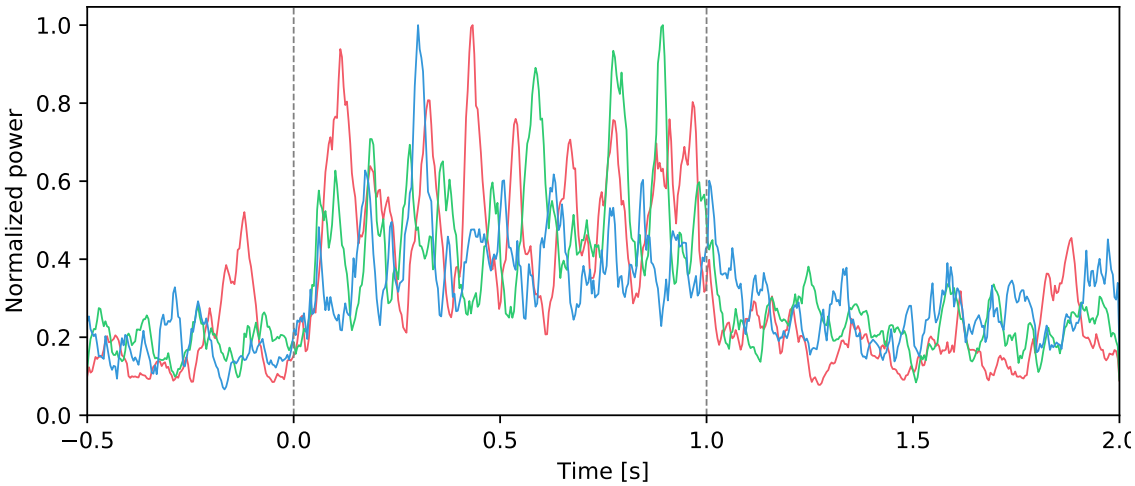

Figure D.3: Normalized power from IMF 1 and 2 on channel ***O2*** for ***Subject 3***.

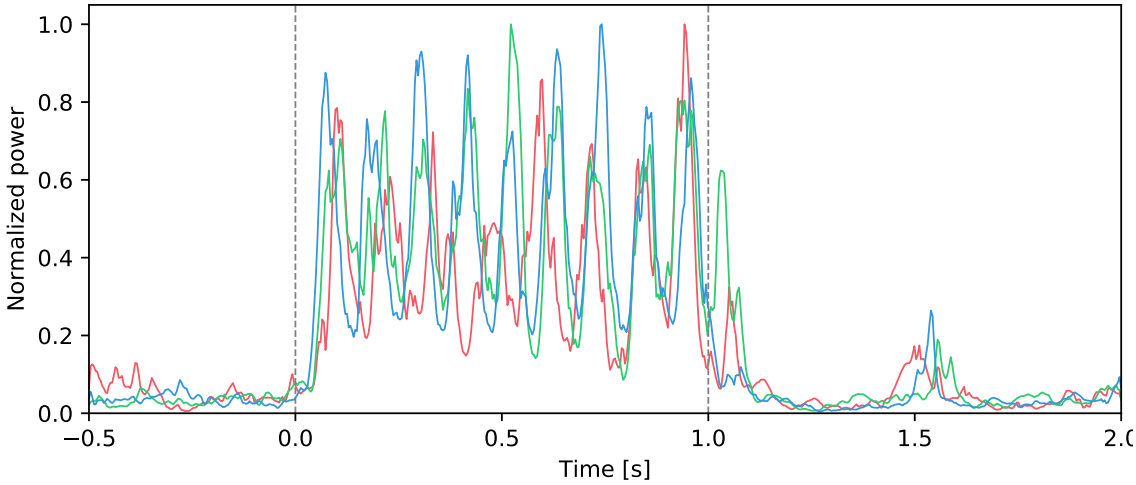

Figure D.4: Normalized power from IMF 1 and 2 on channel ***O1*** for ***Subject 5***.

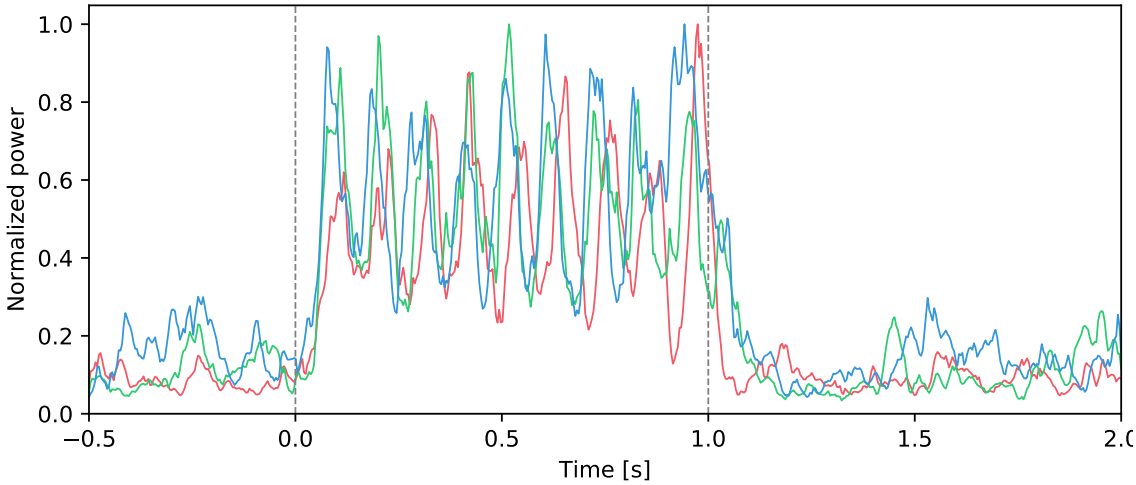

Figure D.5: Normalized power from IMF 1 and 2 on channel ***Oz*** for ***Subject 7***.

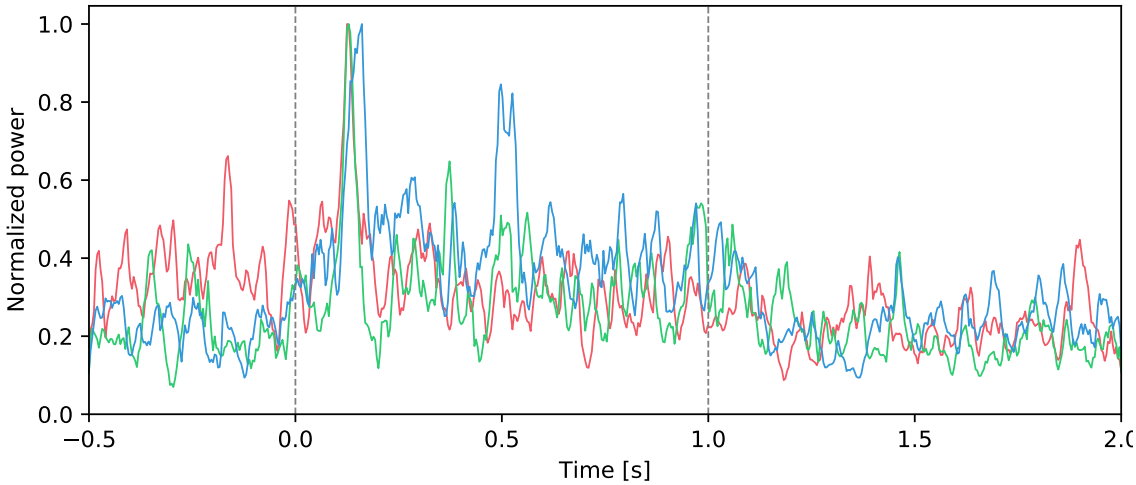

Figure D.6: Normalized power from IMF 1 and 2 on channel ***Oz*** for ***Subject 10***.

Appendix E

Acronyms

BCI Brain-Computer Interface

CNS Central Nervous System

EEG Electroencephalogram

EEMD Ensemble Empirical Mode Decomposition

EMD Empirical Mode Decomposition

ERSP Event-Related Spectral Perturbation

ERP Event-Related Potential

FFT Fast Fourier Transform

FT Fourier Transform

HHT Hilbert-Huang Transform

HSA Hilbert Spectral Analysis

HT Hilbert Transform

IDE Integrated Development Environment

IMF Intrinsic Mode Function

NDA Non-Disclosure Agreement

NTNU Norwegian University of Science and Technology

RGB Red-Green-Blue

SD Standard Deviation

SNR Signal-to-Noise Ratio

Bibliography

[1] M. C. Potter, B. Wyble, C. E. Hagmann, and E. S. McCourt, "Detecting meaning in rsvp at 13 ms per picture," *Attention, Perception, & Psychophysics*, vol. 76, no. 2, pp. 270–279, 2014. [Online]. Available: http://dx.doi.org/10.3758/s13414-013-0605-z

[2] S. Rasheed and D. Marini, "Classification of eeg signals produced by rgb colour stimuli," *Journal of Biomedical Engineering and Medical Imaging*, vol. 2, no. 5, p. 56, 2015.

[3] Worren, Fredrik. Molvær, Joar. & Molinas, Marta Maria Cabrera, "A unified real-time feature extraction and classification process for a bci based on empirical mode decomposition and support vector machine," 2016.

[4] M. Münch, G. Plomp, E. Thunell, A. Kawasaki, J. Scartezzini, and M. Herzog, "Different colors of light lead to different adaptation and activation as determined by high-density {EEG}," *NeuroImage*, vol. 101, pp. 547 – 554, 2014. [Online]. Available: http://www.sciencedirect.com/science/article/pii/S1053811914005485

[5] D. Safieddine, A. Kachenoura, L. Albera, G. Birot, A. Karfoul, A. Pasnicu, A. Biraben, F. Wendling, L. Senhadji, and I. Merlet, "Removal of muscle artifact from eeg data: comparison between stochastic (ica and cca) and deterministic (emd and wavelet-based) approaches," *EURASIP Journal on Advances in Signal Processing*, vol. 2012, no. 1, p. 127, 2012. [Online]. Available: http://dx.doi.org/10.1186/1687-6180-2012-127

[6] Paul L. Nunez and Ramesh Srinivasan., *Electric Fields of the Brain: The Neurophysis of EEG*. Oxford University Press, Inc., 2006.

[7] "Eeg recording from brain." [Online]. Available: http://www.becomeablogger.com/wp-content/uploads/2014/08/Brain-EEG.jpg

[8] H. Berger, *On the electroencephalogram of man : the 14 original reports on the human electroencephalogram*. Elsevier, 1969, vol. 28.

[9] H. Berger, *Atlas of EEG and seizure semiology*. Butterworth-Heinemann Elsevier, 2006.

[10] "Lobes of the brain." [Online]. Available: https://qbi.uq.edu.au/files/7887/QBI-brain-lobes-neuroscience.png

[11] "Visual cortex." [Online]. Available: http://images.slideplayer.com/32/9996587/slides/slide_2.jpg

[12] L. F. Nicolas-Alonso and J. Gomez-Gil, "Brain computer interfaces, a review," *Sensors*, vol. 12, no. 2, pp. 1211–1279, 2012.

[13] L. Fernando Nicolas-Alonso and J. Gomez-Gil, "Brain Computer Interfaces, a Review," *SENSORS*, vol. 12, no. 2, pp. 1211–1279, FEB 2012.

[14] L. I. Aftanasnext and S. A. Golocheikine, "Human anterior and frontal midline theta and lower alpha reflect emotionally positive state and internalized attention: high-resolution EEG investigation of meditation." *Neuroscience Letters*, vol. 310, pp. 57–60, 2001.

[15] A. Black, "The operant conditioning of central nervous system electrical activity1," ser. Psychology of Learning and Motivation, G. H. Bower, Ed. Academic Press, 1972, vol. 6, pp. 47 – 95. [Online]. Available: http://www.sciencedirect.com/science/article/pii/S0079742108603849

[16] W. Klimesch, "Eeg-alpha rhythms and memory processes." *International journal of psychophysiology : official journal of the International Organization of Psychophysiology*, vol. 26 1-3, pp. 319–40, 1997.

[17] G. Pfurtscheller and C. Neuper, "Motor imagery and direct brain-computer communication," *Proceedings of the IEEE*, vol. 89, no. 7, pp. 1123–1134, Jul. 2001. [Online]. Available: http://dx.doi.org/10.1109/5.939829

[18] K.-H. Lee, L. M. Williams, M. Breakspear, and E. Gordon, "Synchronous gamma activity: a review and contribution to an integrative neuroscience model of

schizophrenia," *Brain Research Reviews*, vol. 41, no. 1, pp. 57 – 78, 2003. [Online]. Available: http://www.sciencedirect.com/science/article/pii/S0165017302002205

[19] W. Lutzenberger, F. Pulvermüller, T. Elbert, and N. Birbaumer, *Visual Stimulation Alters Local 40-Hz Responses in Humans: An EEG-study*, 2006. [Online]. Available: https://books.google.no/books?id=tYdrnQAACAAJ

[20] M. M. Müller, A. Keil, T. Gruber, and T. Elbert, "Processing of affective pictures modulates right-hemispheric gamma band {EEG} activity," *Clinical Neurophysiology*, vol. 110, no. 11, pp. 1913 – 1920, 1999. [Online]. Available: http://www.sciencedirect.com/science/article/pii/S1388245799001510

[21] M. M. Müller, J. Bosch, T. Elbert, A. Kreiter, M. V. Sosa, P. V. Sosa, and B. Rockstroh, "Visually induced gamma-band responses in human electroencephalographic activity — a link to animal studies," *Experimental Brain Research*, vol. 112, no. 1, pp. 96–102, 1996. [Online]. Available: http://dx.doi.org/10.1007/BF00227182

[22] W. J. Freeman and B. W. van Dijk, "Spatial patterns of visual cortical fast eeg during conditioned reflex in a rhesus monkey," *Brain research*, vol. 422, no. 2, pp. 267–276, 1987.

[23] Graimann, Bernhard et.al., *Brain-Computer Interfaces : Revolutionizing Human-Computer Interaction*. Berlin/Heidelberg, DEU: Springer Berlin Heidelberg, 2010.

[24] Guger, Christoph et.al., *Brain-Computer Interface Research : A State-of-the-Art Summary*. Springer, 2013.

[25] J. Frey, "Comparison of an open-hardware electroencephalography amplifier with medical grade device in brain-computer interface applications," 2016.

[26] "Openbci overview." [Online]. Available: http://openbci.com//images/CYTON-GRAPHIC.jpg

[27] "Ultracortex mark 4." [Online]. Available: https://github.com/OpenBCI/Ultracortex/blob/master/Mark_IV/concepts/M4-June16/Photos/M4_08_D5_frame249_Realistic4%20loops.png?raw=true

[28] Jurcak, Valer et.al., "10/20, 10/10, and 10/5 systems revisited: Their validity as relative head-surface-based positioning systems," *Neuroimage*, no. 4, pp. 1600–1611, 2007.

[29] "10/10 system." [Online]. Available: http://www.mariusthart.net/downloads/eeg_electrodes_10-20.svg

[30] Norden E. Huang et.al., "The empirical mode decomposition and the hilbert spectrum for nonlinear and non-stationary time series analysis," *Proceedings of the Royal Society A: Mathematical, Physical and Engineering Sciences*, vol. 454, pp. 903–995, 1998.

[31] N. E. HUANG, Z. WU, S. R. LONG, K. C. ARNOLD, X. CHEN, and K. BLANK, "On instantaneous frequency," *Advances in Adaptive Data Analysis*, vol. 01, no. 02, pp. 177–229, 2009. [Online]. Available: http://www.worldscientific.com/doi/abs/10.1142/S1793536909000096

[32] Y. Chen, G. Zhang, S. Gan, and C. Zhang, "Enhancing seismic reflections using empirical mode decomposition in the flattened domain," *Journal of Applied Geophysics*, vol. 119, pp. 99 – 105, 2015. [Online]. Available: http://www.sciencedirect.com/science/article/pii/S0926985115001688

[33] C. Park, "A tutorial on empirical mode decomposition in brain research," in *The 18th IEEE International Symposium on Consumer Electronics (ISCE 2014)*, June 2014, pp. 1–2.

[34] N. E. Huang and Z. Wu, "A review on hilbert-huang transform: Method and its applications to geophysical studies," *Reviews of Geophysics*, vol. 46, no. 2, pp. n/a–n/a, 2008, rG2006. [Online]. Available: http://dx.doi.org/10.1029/2007RG000228

[35] Z. WU and N. E. HUANG, "Ensemble empirical mode decomposition: A noise-assisted data analysis method," *Advances in Adaptive Data Analysis*, vol. 01, no. 01, pp. 1–41, 2009. [Online]. Available: http://www.worldscientific.com/doi/abs/10.1142/S1793536909000047

[36] Liwei, Liu Geheng, Chen Feng, Qian, "The application of hilbert-huang transform in speech enhancement," vol. 5, pp. 207–210, 2010.

[37] Leela K. Gudupudi et.al., "An alternative view of loudspeaker nonlinearities using the hilbert-huang transform," *2015 IEEE Workshop on Applications of Signal Processing to Audio and Acoustics, WASPAA 2015, New Paltz, NY, USA, October 18-21, 2015*, 2004.

[38] "Openbci device." [Online]. Available: https://raw.githubusercontent.com/OpenBCI/Docs/master/assets/images/8.jpg

[39] "Rfduino host." [Online]. Available: https://raw.githubusercontent.com/OpenBCI/Docs/master/assets/images/dongle.png

[40] "Arduino uno." [Online]. Available: http://robotechshop.com/wp-content/uploads/2015/12/arduino_uno_large-comp.jpg

[41] "Rgb led strip." [Online]. Available: http://www.clasohlson.com/medias/sys_master/9479365394462.jpg

[42] Kulia, Geir, Lars Magne Lundheim, Marta Molinas, and Bjørn B. Larsen., "Investigation of distortions in microgrids," 2016.

[43] N. E. Huang and Z. Wu, "A review on hilbert-huang transform: Method and its applications to geophysical studies," *Reviews of Geophysics*, vol. 46, no. 2, pp. n/a–n/a, 2008, rG2006. [Online]. Available: http://dx.doi.org/10.1029/2007RG000228

[44] R. Deering and J. F. Kaiser, "The use of a masking signal to improve empirical mode decomposition," in *Proceedings. (ICASSP '05). IEEE International Conference on Acoustics, Speech, and Signal Processing, 2005.*, vol. 4, March 2005, pp. iv/485–iv/488 Vol. 4.

List of Figures